ABSTRACT

LI, CHAO. Petrologic and Geochemical Distinctions Along and Between Two Diabase Dike Systems in Central North Carolina. (Under the direction of Dr. R.V. Fodor.)

The Central Atlantic Magmatic Province (CAMP) is defined by circum-North Atlantic tholeiitic diabase dikes and sills emplaced with the breakup of Pangaea beginning ~200 Ma. Most petrologic studies of CAMP dikes and sills have been in southeastern North America, but not on scales small enough to determine, for example, compositional variations within long dikes, >10 km. Accordingly, to examine small-scale compositional characteristics in a portion of the CAMP, I studied 15 samples from two long, ~90 and 45 km, diabase dike systems ~40 km apart in central North Carolina for petrography, major and trace element abundances, and mineral compositions.

The two N-S trending dike systems have tholeiitic basalt compositions. Dike system 1 has 50.5 to 52.2 wt.% SiO_2, 7.8 to 3.3 wt.% MgO and 2.25 to 3.5 wt.% total alkalis, and normative quartz. System 2 has 46 to 48 wt.% SiO_2, 13.7 to 9.1 wt.% MgO and 2 to 2.5 wt.% total alkalis, and normative olivine. Overall textures are intergranular-subophitic plagioclase and clinopyroxene forming matrices (diabasic), plus minor intergranular low-Ca pyroxene and Fe-Ti oxides (+olivine, system 2). Dike system 1 samples have plagioclase phenocrysts, ~19 to 28 vol.%, mainly as glomerocrysts. Their compositions are highly calcic, ~An_{92-70}, and notable because they occur in relatively evolved samples, ~7 to 6 wt.% MgO. Dike system 2 samples are aphyric. Matrix plagioclase in system 1 is An_{80-20}, and in system 2, An_{87-48}. For both systems, clinopyroxene and low-Ca pyroxene are $Fs_{10-32}Wo_{29-42}$ and $Fs_{20-40}Wo_{8-15}$, respectively. Olivine in dike system 2 is Fo_{87-50}.

It is unlikely that dike system magmas were crustally contaminated. Dike system 1 shows no correlation between SiO_2 and crustal elements K, Rb, Th, Pb, U and light REE, and system 2 has high MgO, and low SiO_2, K, Rb, Th, Pb, U, and light REE.

Mass balancing, Rayleigh fractionation and MELTS models suggest that fractional crystallization accounts for small compositional variations within each dike system. However, mafic phenocrysts are not present in any samples. Therefore, mass balancing and MELTS for major elements only mathematically explain compositional variations and lead to inferring that mafic minerals remained at depth during parent magma crystallization.

Presence of high-Ca plagioclase in low-MgO dike system 1 samples can be due to high Ca# (e.g., ~80; Ca# = mol Ca/(Ca+Na)*100) in basaltic magma at mid-crustal pressure, $\sim 5\times10^5$ kPa. That is, higher crystallization pressures correlate with lower An. The high-An plagioclase is modeled as crystallizing along with olivine and clinopyroxene in a reservoir of high-MgO (~13 wt.%) melt. Plagioclase phenocrysts became zoned ($An_{92\text{-}70}$) as the parental melt evolved to ~7 wt.% MgO by crystallizing ~30% plagioclase + clinopyroxene + olivine. The low density of the plagioclase in the evolved melt kept it at the top of the solidification zone at the interface with remaining reservoir magma. Plagioclase as glomerocrysts in the dike is explained by convective activity in the remaining overlying reservoir that swept plagioclase grains together, plus synneusis. Eventually, glomerocryst-bearing evolved magma erupted as dike system 1.

Most trace element-abundance ratios (e.g., Ba/Nb, Zr/Hf, Th/Hf) for the two dike systems do not overlap, suggesting that the dike systems represent small-scale source heterogeneity and at least two different magmas. But consistency of trace element ratios within each dike system suggests samples from each had the same subcontinental lithospheric

source. Comparing selected trace-element ratios for the two dike systems to those representing large-scale regional NC CAMP dikes shows: (1) that the ratios for CAMP are highly variable, suggesting source heterogeneity across NC; and (2) that dike system 2 trace element ratios largely overlap NC CAMP ratios, suggesting a common source for dike system 2 and some regional dikes.

Petrologic and Geochemical Distinctions Along and Between Two Diabase Dike Systems in Central North Carolina

by
Chao Li

A thesis submitted to the Graduate Faculty of
North Carolina State University
in partial fulfillment of the
requirements for the degree of
Master of Science

Marine, Earth, and Atmospheric Sciences

Raleigh, North Carolina

2016

APPROVED BY:

_____	_____
Dr. R.V. Fodor Committee Chair	Dr. Edward F. Stoddard
_____	
Dr. Del Bohnenstiehl	

DEDICATION

This thesis is dedicated to my loved ones, for their endless love, support, and encouragement, and to the memory of my late grandfather and a great geologist, Jinsuo Wang.

BIOGRAPHY

Chao Li was born in Zhangjiakou, Hebei, China, a small city surrounded by mountains. Favorite pastimes include doing charity work for animals, drawing, and collecting old vinyls and CDs. Growing up in a family of geologists, rocks and minerals have always been his passion. His grandfather, Dr. Jinsuo Wang, shared his enthusiasm for geologic research with him. In 2012, he came to NC State University to work with Dr. Ronald Fodor for his master's project in igneous petrology and geochemistry.

ACKNOWLEDGMENTS

Foremost, I would like to express my sincere gratitude to my advisor Dr. Ron V. Fodor for the continuous support of my master's study and research, for his patience, motivation, enthusiasm, and immense knowledge. His guidance helped me in all the time of research and writing of this thesis. I could not have imagined having a better advisor and mentor. Besides my advisor, I would also like to thank the rest of my thesis committee: Dr. Edward F. Stoddard and Dr. Del Bohnenstiehl, for their encouragement and insightful comments and questions. Thank you to Mr. Jason Weinstein for providing me dike samples and thin sections, without which this study would not have gone through. Thank you also to Mr. Robert S. Jacobs of Caird Energy, Ft. Worth, TX, for providing financial assistance for obtaining thin sections and chemical analyses for this project. NCSU electron microprobe analyses were funded by a National Science Foundation instruments grant to R.V. Fodor (EAR-1255786). I would also like to thank my fellow petrologists, Ellen Craig and Michael Mohr, for the stimulating discussions, their generous help, and all the fun we have had in the past few years. Last but not the least, I would like to thank my family for giving me their unconditional love and supporting me spiritually throughout my life.

TABLE OF CONTENTS

LIST OF TABLES viii
LIST OF FIGURES ix
INTRODUCTION 1
PREVIOUS STUDIES AND PETROLOGIC INTERPRETATIONS 2
SAMPLING 5
PETROGRAPHY 9
Dike system 1 9
Dike system 2 9
ANALYTICAL PROCEDURES 15
ANALYTICAL RESULTS 15
Whole-rock compositions 16
Major Elements 16
Trace Elements 27
Mineral Compositions 35
Plagioclase 35
Pyroxene 41
Olivine 49
Fe-Ti oxide minerals 55
DISCUSSION 60
Fractional Crystallization 61
Mass Balancing 62
Rayleigh fractionation calculations 71
MELTS modeling 78
Relationship between the two dike systems 88
Crustal contamination 94
Origin of high-Ca plagioclase in evolved dike system 1 samples 102
Source area comparison for two dike systems and dike samples in broader NC 111
CONCLUSIONS 115

REFERENCES..... 119
APPENDIX..... 125

LIST OF TABLES

Table 1 Average modal compositions of samples from dike system 1 in volume percentage....11

Table 2 Whole-rock compositions (wt.% and ppm) of two dike systems in central North Carolina. For each dike system, samples are listed in the order of decreasing MgO....21

Table 3 Average compositions of representative plagioclase as phenocrysts (occurring as glomerocrysts) and as matrix, or groundmass, grains in the two dike systems in central North Carolina....37

Table 4 Average compositions of representative pyroxene in the two dike systems in central North Carolina....45

Table 5 Average compositions (wt.%) of representative olivine grains in dike system 2 in central North Carolina....51

Table 6 The most Fo-rich portions of olivines in four samples of dike system 2....54

Table 7 Average compositions of representative titaniferous magnetite (Mt), ilmenite (Ilm) and ferrian-ilmenite (Fe-ilm) in samples from two dike systems in central North Carolina....57

Table 8 Least squares mass balancing to relate most primitive sample RV-1 as parent to most evolved sample KT-1 and to tholeiitic basaltic andesite sample CL-1 in dike system 1....67

Table 9 Least squares mass balancing to relate most primitive sample ES-1 as parent to most evolved sample NC-1 and to medium-MgO composition sample CP-1 in dike system 2....68

Table 10 Least squares mass balancing to relate medium-MgO composition sample CP-1 as parent to most evolved sample NC-1 in dike system 2....69

Table 11 Least squares mass balancing to relate primitive sample C-1 (MgO ~13.86 wt.%, from Callegaro et al., 2013) as parent to relatively evolved sample RV-1 in dike system 1....70

Table 12 Rayleigh fractionation calculation[1] using (1) RV-1 as C_o and KT-1 as C_l, (2) RV-1 as C_o and CL-1 as C_l....73

Table 13 Rayleigh fractionation calculation[1] using (1) ES-1 as C_o and NC-1 as C_l, (2) ES-1 as C_o and CP-1 as C_l.....73

Table 14 Rayleigh fractionation calculation[1] using CP-1 as C_o and NC-1 as C_l.....74

Table 15 MELTS modeling for fractional crystallization of parent RV-1 (MgO ~7.76 wt.%) to daughter CL-1 (MgO ~4.28 wt.%) and KT-1 (MgO ~3.34 wt.%) under conditions with varying pressure and fO_2.....83

Table 16 MELTS modeling for fractional crystallization of parent C-1 (MgO ~13.86 wt.%, from Callegaro et al., 2013) to daughter RV-1 (MgO ~7.76 wt.%).....84

Table 17 MELTS modeling for fractional crystallization of parent ES-1 (MgO ~13.68 wt.%) to daughter CP-1 (MgO ~ 10.04 wt.%) and NC-1 (MgO ~9.08 wt.%) under conditions with varying pressure and fO_2.....85

Table 18 MELTS modeling for fractional crystallization of parent CP-1 (MgO ~10.04 wt.%) to daughter NC-1 (MgO ~9.08 wt.%).....86

Table 19 Comparisons of results from fractional crystallization relationships calculated by mass balancing and MELTS.....87

Table 20 Hybrid compositions calculated by mixing representative Rolesville batholith composition with dike system 2 compositions to compare with major and trace element compositions of some dike system 1 samples.....99

Table 21 Latitudes, longitudes and USGS 7.5-minute quadrangles for the locations of samples taken from the two dike systems in central North Carolina.....125

LIST OF FIGURES

SAMPLING

Figure 1A An overview map of the SENA dike swarms (after Callegaro et al., 2013). CAMP dikes are represented by black lines on a Late Triassic geographic reconstruction. Red square represents my study area. (Modified after Callegaro et al., 2013).....7

Figure 1B Geologic map showing the overview of the study area and sampling locations for the two dike systems. (Modified after the 1985 Geologic Map of North Carolina from North Carolina Geological Survey).....8

PETROGRAPHY

Figure 2 Representative photomicrographs of samples from two dike systems.....12

ANALYTICAL RESULTS

Figure 3 Total alkalis versus SiO_2 (TAS) diagram for the two dike systems compared to compositions of selected NC samples from Callegaro et al. (2013) and Weigand and Ragland (1970).....18

Figure 4 Normative mineralogy of dike system 1 and 2 samples are plotted on the diopside-hypersthene-olivine-quartz portion of the basalt tetrahedron of Yoder and Tilley (1962).....20

Figure 5 MgO variation diagrams for major element compositions of two dike systems compared to the compositions of North Carolina samples of Callegaro et al. (2013).....26

Figure 6 MgO variation diagrams for trace element compositions of two dike systems compared to the North Carolina samples of Callegaro et al. (2013).....30

Figure 7 Chondrite-normalized rare earth element patterns for two dike systems in central North Carolina.....33

Figure 8 Primitive-mantle normalized diagrams for two dike systems in central North Carolina.....34

Figure 9A Ternary plots for plagioclase in samples from dike system 1.....39

Figure 9B Ternary plots for plagioclase in samples from dike system 2.....40

Figure 10 Pyroxene compositions for the two dike system samples plotted as endmembers diopside, enstatite, ferrosilite, and hedenbergite (Di, En, Fs and Hd).....47

Figure 11 Forsterite (Fo) variation diagram for four samples from dike system 2.....52

Figure 12 Forsterite (Fo) versus NiO diagram for olivines in four samples of dike system 2.....53

Figure 13 TiO_2 versus total Fe as FeO in Fe-Ti oxides plotted as point-analyses.....59

DISCUSSION

Figure 14 MgO vs. Al_2O_3/CaO plot showing different fractional crystallization paths of plagioclase and clinopyroxene in the two dike systems.....66

Figure 15 Diagrams show comparison of actual and calculated daughters (KT-1 and CL-1) trace element abundances.....75

Figure 16 Diagrams show comparison of actual and calculated daughters (NC-1 and CP-1) trace element abundances.....77

Figure 17 Diagram shows comparison of actual and calculated daughter (NC-1) trace element abundances.....77

Figure 18
Selected trace element abundance ratios plots for two dike.....91

Figure 19 Selected elements enriched in continental crust versus SiO_2 in dike system 1 samples to show no correlation with increasing SiO_2, and therefore no clear case for crustal contamination.....95

Figure 20 Selected trace element-ratio plots for the two dike systems and calculated hybrid compositions suggest that dike system 1 samples are unlikely the products of dike system 2 assimilating Rolesville batholith.....101

Figure 21 Diagrams show the sequence of dike system 1 magma crystallization in a slab-shaped magma chamber.....107

Figure 22 Selected trace element abundance ratios for dike systems 1 and 2, and for samples from Callegaro et al. (2013) suggest that the two dike systems are not related to the same source, and that samples within each dike system are related to a single lithospheric source. Also, based on these ratios, the source for some dike system 2 samples may be part of the same source material that yielded some Callegaro et al. (2013) samples.....113

INTRODUCTION

The Central Atlantic Magmatic Province (CAMP) is defined by tholeiitic basalt that occurs as lavas, dikes and sills in the portions of North America, South America, Europe, and Africa that were once contiguous as part of Pangaea (e.g., Marzoli et al., 1999). Their emplacement occurred during the opening of the Atlantic Ocean as Pangaea began rifting at the time of the Triassic-Jurassic boundary (magmatism peak time ~201 Ma, range from 202 to 195 Ma; Marzoli et al., 1999; 2011; Callegaro et al., 2013). The basaltic magmas that intruded fissures are now largely present as dikes and sills near the continental margins surrounding the northern and central Atlantic Ocean. They cover a surface area over ~10^7 km^2 (Callegaro et al., 2013).

Most petrologic studies of the CAMP dikes and sills have been conducted in southeastern North America (SENA; Figure 1A) (e.g., Weigand and Ragland, 1970; Gottfried and Arth, 1985; Warner et al., 1985; McHone et al., 1987; Pegram, 1990; Warner et al., 1992; Callegaro et al., 2013). This is largely because dikes and sills in SENA have relatively high outcrop density, often occurring in swarms (Verati et al., 2005), and are accessible for sampling. Additionally, SENA is recognized as one of the CAMP regions marking the earliest break-up of Pangaea (Schlische et al., 2003). This magmatic-tectonic connection has been viewed by some as providing a good understanding of the roles of rifting and plume impingement for CAMP magmatism (e.g., McHone, 2000).

The earliest detailed studies of CAMP dikes date back to the early 1970s, as Weigand and Ragland (1970) examined SENA dike samples collected over large geographic regions and spread far from one another. Similarly, other following detailed

studies (e.g., Pegram, 1990; Callegaro et al., 2013) examined dike samples over large geographic scales. None have been done on a small scale to determine, for example, compositional variations in individual dikes and for comparing the compositions of dikes within a small geographic region (e.g., <40 km apart). Therefore, little is known about how CAMP tholeiitic dikes vary geochemically on relatively small scales, and whether any small-scale variations can be as large as the large regional geochemical variations reported (e.g., Weigand and Ragland, 1970; Pegram, 1990; Callegaro et al., 2013).

Small-scale petrologic studies can address igneous processes, such as fractional crystallization, that may have created variations within single-dike emplacements and between neighboring dikes. They can also provide information about the scale of compositional heterogeneities in the sources for large basalt provinces such as CAMP dikes. Therefore, to examine small-scale compositional characteristics in a portion of the CAMP, and to compare them with larger CAMP regions (i.e., North Carolina CAMP), I examined 15 samples from what appear to be two long, neighboring dike systems in central North Carolina for petrography, major and trace element abundances, and mineral compositions. The phrase “dike system” represents a group of dikes within a specific geographic region that have similar geochemical and petrologic characteristics, and, as in this study, occur along or close to the same north-south strike.

PREVIOUS STUDIES AND PETROLOGIC INTERPRETATIONS

The CAMP dikes in North America are often referred to as 'diabase' dikes, or, the British equivalent ‘dolerite’ dikes (e.g., Weigand and Ragland, 1970; Smith et al., 1975; Bertrand et

al., 1982; Ragland et al., 1983; Husch et al., 1984; Warner et al., 1985; Bertrand, 1991), where the adjectives diabase and dolerite refer to the almost ubiquitous intergranular/subophitic/ophitic textures of the matrices (groundmasses) that make up the dikes. The dikes of this study are texturally diabasic (or doleritic), but for the purpose of my report, I refer to my dikes as belonging to dike systems 1 and 2 according to field occurrences (Figure 1B).

One of the earliest detailed petrologic studies of diabase dikes in eastern North America was conducted by Weigand and Ragland (1970). They examined over one hundred diabase dikes and established three main compositional types: 1) olivine normative; 2) high-TiO_2 quartz normative; and 3) low-TiO_2 quartz normative. Additionally they identified one less common type: high-Fe_2O_3 quartz-normative. Olivine-normative dikes predominate in North and South Carolina, and both main types of quartz-normative dikes predominate from Nova Scotia southward to Maryland. They suggested that all three quartz-normative types can be derived from the olivine-normative type by removal of slightly different mineral assemblages (65-70% crystallization of different amounts of plagioclase, olivine and diopside). In addition, the two main quartz-normative types are not related to each other by fractional crystallization (deriving high-Ti quartz composition from low-Ti quartz composition) or by crustal contamination (mixing low-Ti quartz composition with crustal material to produce high-Ti quartz composition).

Another detailed petrologic study conducted on eastern North American dikes was by Pegram (1990), who presented isotopic compositions for SENA CAMP as Sr, Nd, and Pb isotopic ratios. Using isotopic compositions, he suggested that magmatism was due to

partial melting of enriched subcontinental lithospheric mantle, and that the tholeiitic CAMP magmas were not contaminated by continental crust (Pegram, 1990).

In another study, Warner et al. (1992) described wide ranges in rare earth element (REE) patterns and incompatible element ratios (e.g., Th/Hf, Ti/K) in tholeiitic dikes in South Carolina as representing mantle source heterogeneity. Large-scale mantle source heterogeneity had earlier been identified in other eastern North America studies (e.g., Gottfried et al., 1983; Pegram, 1990). The origin of the Pegram (1990) samples (located in North Carolina, South Carolina, Pennsylvania, New Jersey and Connecticut) requires an upper-mantle source enriched in Th, K and LREE, whereas the samples of Gottfried et al. (1983) (located in Georgia) require an upper-mantle source with relatively depleted LREE.

The most recent detailed study is by Callegaro et al. (2013) on samples from dike swarms in SENA. It includes 73 dikes from Georgia, South Carolina, North Carolina and Virginia, and three sills from Durham, North Carolina. Their study reports that SENA dikes and sills have $^{206}Pb/^{204}Pb$ ratios ~17.56 to 18.85 at 200 Ma, and $^{207}Pb/^{204}Pb$ and $^{208}Pb/^{204}Pb$ ratios all unlike those observed for CAMP basaltic dikes in other geographic regions, such as northeastern North America. The source isotopic compositions for SENA dikes and sills may therefore have been unique to the SENA area (Callegaro et al., 2013).

The prevalent hypotheses for the origin of the CAMP are: a) sublithospheric plume impingement to cause flood basalt magmatism (e.g., Wilson, 1997; Marzoli et al., 1999; Janney and Castillo, 2001); and b) magmatism unrelated to a mantle plume(s) that led to Central Atlantic flood basalt magmatism (e.g., Holbrook and Kelemen, 1993; Bertrand, 1991; McHone, 2000; Coltice et al., 2007). Advocates for the plume model claim that the

large volumes of melt related to CAMP produced over a short interval, <10 m.y., likely required involvement of a mantle plume or plume-head (Marzoli et al., 1999; Janney and Castillo, 2001). Radial orientation of some CAMP dikes (Janney and Castillo, 2001) is consistent with a plume origin.

Proponents of a non-plume origin for the CAMP argue that the associated magmatism is widespread and noncentralized in origin (Holbrook and Kelemen, 1993), and that there is little correlation between rapid, major pulse magmatism and the breakup of Pangaea at the Triassic-Jurassic boundary (McHone, 2000). Also, there is no hotspot or linear volcanic chain in the central Atlantic region recognized as linked to the CAMP in time and space (McHone, 2000). Coltice et al. (2007) proposed a non-plume model that shows partial melting in the subcontinental lithosphere under Pangaea could be induced solely by continental aggregation, without the involvement of plume.

SAMPLING

My study is on diabase dikes in central North Carolina (Figure 1A). One of the dikes is particularly long, up to ~120 km, as mapped by Reising and Stoddard (2006). They identified this dike as extending from central Johnston County to the Virginia border, and having intruded the Rolesville batholith and other granitoid country rocks. The dike trends about N15°W, curving to a N-S direction near Rolesville, and then to approximately N10°E north of Henderson. Reising and Stoddard (2006) described the dike as having plagioclase phenocrysts in sizes up to 2 cm, and containing two pyroxenes with high and low Ca.

For this study, I sampled the Reising and Stoddard (2006) dike at seven locations from Middleburg to Clayton, North Carolina (Figure 1B-1). I also sampled eight locations along another apparent subparallel dike extending from Durham southward to Cary, North Carolina (Figure 1B-2). These two dike systems are ~40 km apart. The approximate N-S orientations of my sampled dike systems are consistent with the overall ~N to S orientations of dike swarms in NC (e.g., Callegaro et al., 2013; Figure 1A). Because most dike systems in central NC are in approximate north to south orientations, I believe that my sample locations represent two dike systems within the many dike systems known to be present in NC.

My samples from the easternmost dike (dike system 1) represent a N-S distance of ~90 km (Figure 1B-1). The dike is observed as a stream outcropping ~20 m wide at its location near Middleburg (Figure 1B-1). Most of the samples are from outcroppings or from boulders that are weathering remnants of the original dike. The second dike (dike system 2) is ~45 km long (Figure 1B-2) and ~40 km west of the dike system 1, largely as boulder accumulations of original dike outcroppings (Figure 1B-2). Because this dike system passes through some Durham and Wake county construction sites and through the Research Triangle Park, some sample locations are now covered and no longer accessible (e.g., sample CP-1; Figure 1B-2).

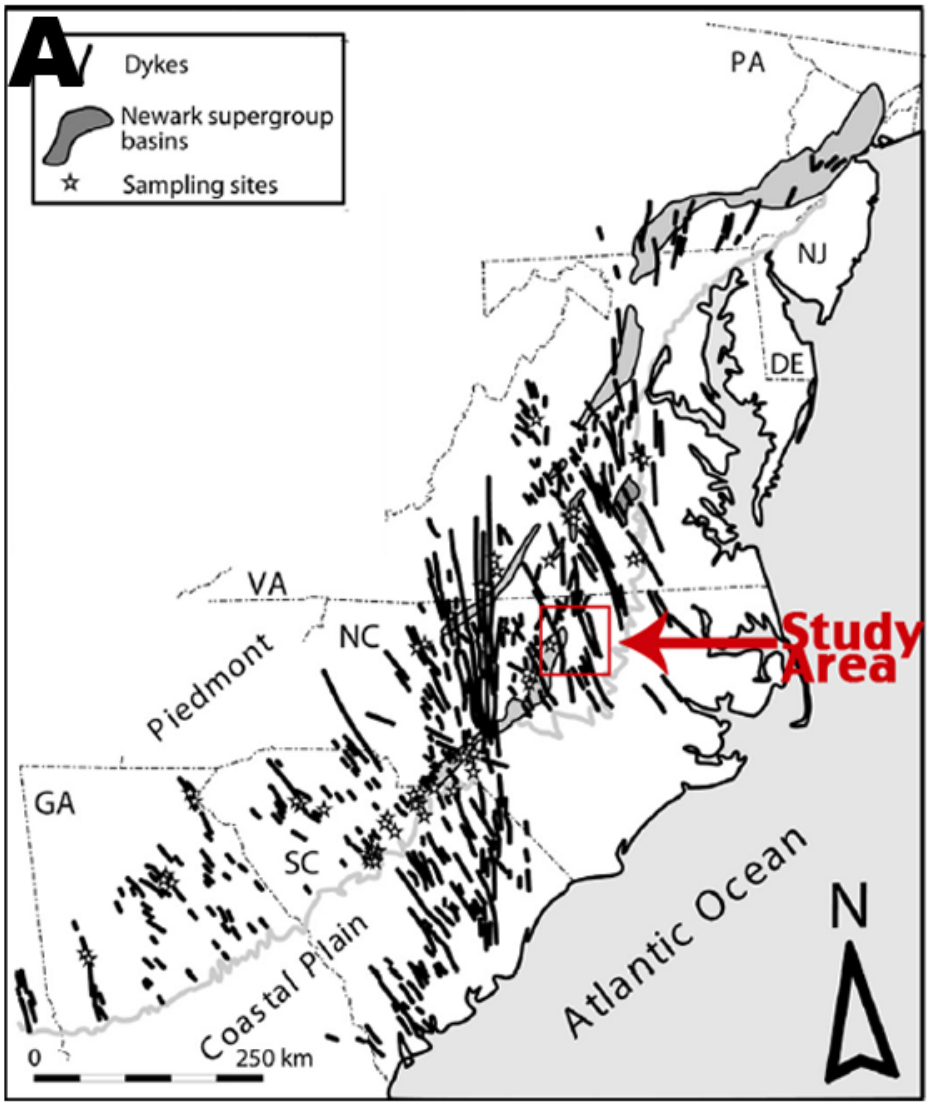

Figure 1A. An overview map of the SENA dike swarms (after Callegaro et al., 2013). CAMP dikes are represented by black lines on a Late Triassic geographic reconstruction. Red square represents my study area. (Modified after Callegaro et al., 2013)

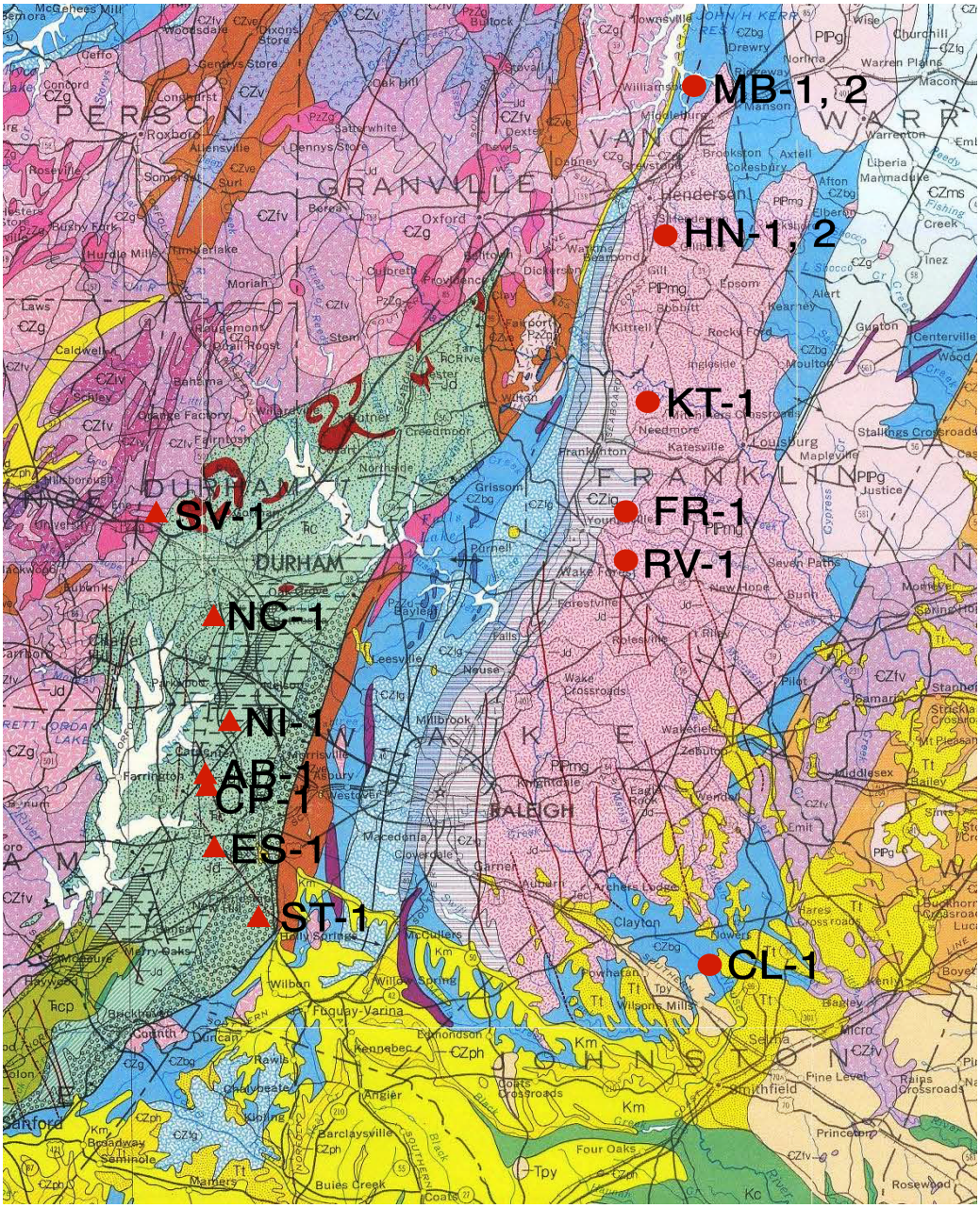

Figure 1B. Geologic map showing the overview of the study area and sampling locations for the two dike systems: number 1 shown by sampling sites on eastern side of map, and number 2 shown by sampling sites on the western side. The sample locations are plotted on a portion of the geologic map of North Carolina (North Carolina Geological Survey, 1985)

PETROGRAPHY

Dike system 1

All samples from dike system 1 are plagioclase-phyric, where plagioclase phenocrysts range from ~2 to 6 mm in size and occupy volumes as low as 1.6% to as great as to 27% (Table 1). The phenocrysts are most often intergrown as clusters, or glomerocrysts, that are ~4 to 7 mm in size (Figure 2 A, B), and less commonly as individual grains (Figure 2 C). The remaining portions of the plagioclase-phyric dike system 1 samples are aphyric matrices composed mainly of clinopyroxene grains, generally ~0.5 to 1 mm, but in one case ~2 mm, in intergranular, ophitic and subophitic (diabasic) textural relationships with plagioclase laths ~0.5 to 1 mm (Figure 2 A, D, E, F), Modal analyses show that the plagioclase:clinopyroxene ratios in these matrices are ~1.5 to 5 (Table 1).

Small grains ~0.1 mm of low-Ca pyroxene, both orthopyroxene and pigeonite (as determined by microprobe analyses), are also part of the matrix intergranular textures at ≤2.6 vol.% (Table 1), as are ~0.5 to 0.7 mm sized Fe-Ti oxide grains, ~1.7 to 3.7 vol.% (Figure 2F). Finally, ~1 to 4 vol.% interstitial altered glass and secondary alteration products, largely chlorite ~0.3 to 0.5 mm, are present. Local areas of granophyric texture were reported for dike system 1 by Reising and Stoddard (2006), but this texture was not observed in this study.

Dike system 2

Samples from dike system 2 are aphyric, having diabasic textures that exhibit intergranular, ophitic and subophitic relationships between largely plagioclase and clinopyroxene, but also include olivine, low-Ca pyroxene (orthopyroxene and pigeonite as determined by microprobe analyses), and Fe-Ti oxides. Plagioclase and clinopyroxene in these samples vary from 0.5 to 2.5 mm, creating a range in overall intergranular-texture from medium to coarse (Figure 2 G-L). Olivine, visually estimated during thin section examinations to be at ~5 to 10 vol.%, is smaller, ~0.1 to 0.8 mm, and subrounded in form (Figure 2 I-K). Besides occurring in an intergranular texture, olivine occurs as small inclusions in plagioclase (e.g., Figure 2 I, K). The low-Ca pyroxenes are ~0.1 mm in size and present at ≤2 vol%. The Fe-Ti oxides are ~0.1 to 0.5 mm and occupy ~1 to 5 vol.% of these samples.

Table 1. Average modal compositions of samples from dike system 1 in volume percent.

	RV-1	MB-2	FR-1	HN-2	HN-1	KT-1
plagioclase-P	19.6	25.2	24.1	26.7	14.6	1.6
plagioclase-M	44.3	48.2	41.7	39.6	50.5	63.7
clinopyroxene	30.2	22.3	27.4	27.9	27.1	27.4
low-Ca pyroxene	2.6	1.3	2.6	2.3	2.2	1.7
altered glass and alteration products	1.4	1.3	1.6	1.4	1.9	1.9
Fe-Ti oxides	1.9	1.7	2.6	2.1	3.7	3.7

P: Phenocryst
M: Matrix

Figure 2. Representative photomicrographs of samples from two dike systems. All are in cross-polarized light except panel F, which is in plane-polarized light. All scale bars are 1 mm. **A)** A glomerocryst of several plagioclase phenocrysts, from ~3 to 6 mm, in dike system 1 sample MB-2. Large grain at top center is darker near its margin due to compositional zoning. Small clinopyroxene grain is included within the glomerocryst. **B)** Glomerocryst of plagioclase phenocrysts, 2 to 7 mm, in dike system 1 sample FR-1. **C)** A large plagioclase phenocryst (~5 mm) in dike system 1 sample CL-1. **D)** Overall intergranular and subophitic matrix made largely of clinopyroxene and plagioclase laths plus minor Fe-Ti oxides in dike system 1 sample FR-1. **E)** Relatively large clinopyroxene grain (~4 mm) in ophitic and subophitic relationship with plagioclase laths making up part of the matrix of dike system 1 sample HN-1. **F)** Plane-polarized view of KT-1 to show a concentration of Fe-Ti oxide grains in part of the matrix composed mainly of plagioclase laths and clinopyroxene. **G)** Dike system 2 sample AB-1 has plagioclase laths and clinopyroxene in intergranular and minor subophitic relationships. **H)** Dike system 2 sample NC-1 shows largely plagioclase laths and clinopyroxene in intergranular relationship. **I)** Dike system 2 sample ES-1, the most MgO-rich in this study, shows plagioclase laths and clinopyroxene in intergranular relationship. Small amounts of olivine are also present, such as the three small subrounded grains near the center of photo (labeled; one as an inclusion in plagioclase). **J)** Subrounded olivine grain (center; ~0.8 mm) among intergranular clinopyroxene and plagioclase making up dike system 2 sample CP-1. **K)** Two anhedral olivine grains (center, ~0.6 mm; lower right, ~0.3 mm) are enclosed by plagioclase and partially enclosed by augite, showing the sequence of crystallization. **L)** Intergranular texture of dike system 2 sample SV-1, finer grained than other dike system 2 samples (panels G to K).

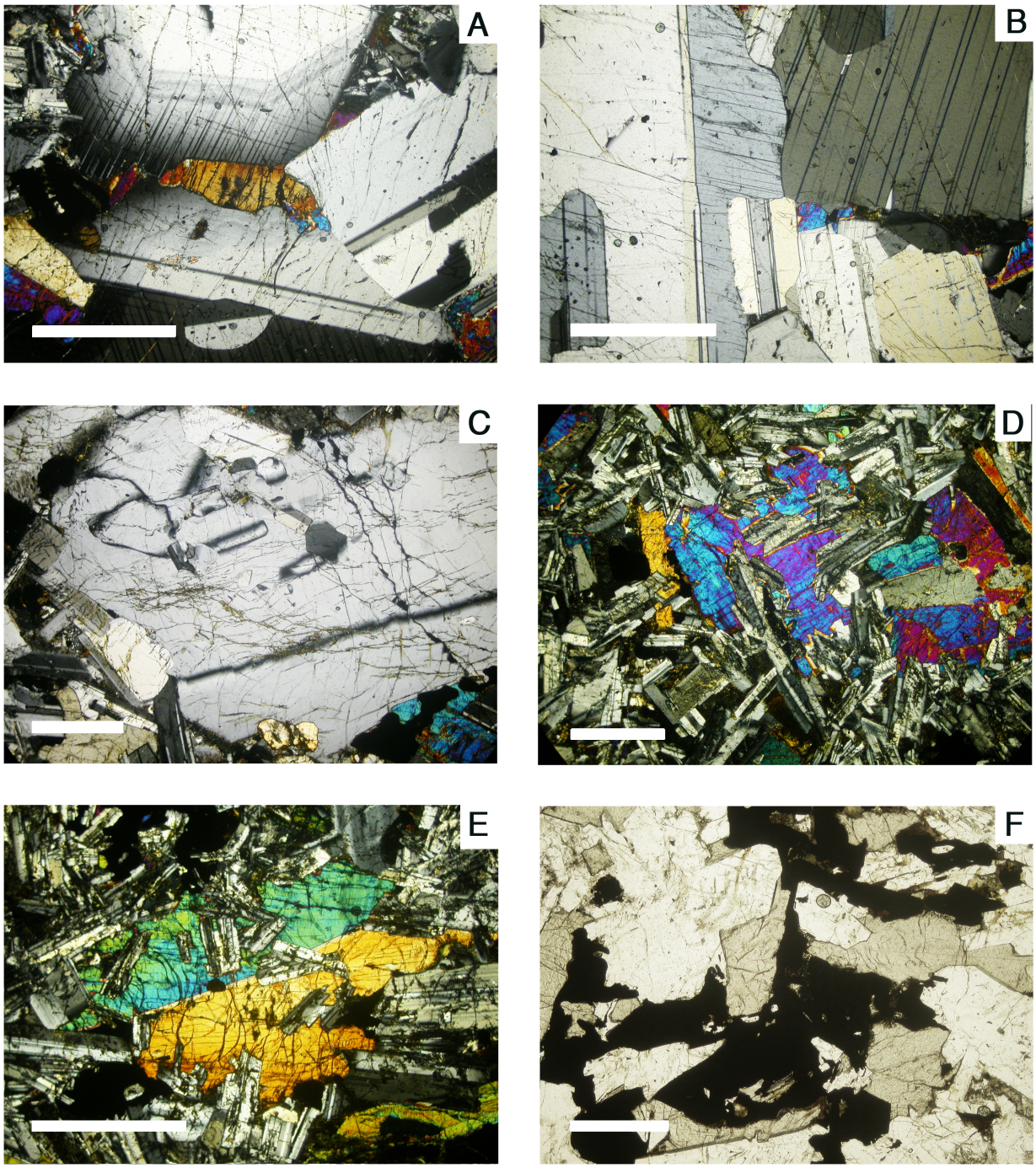
A
B
C
D
E
F

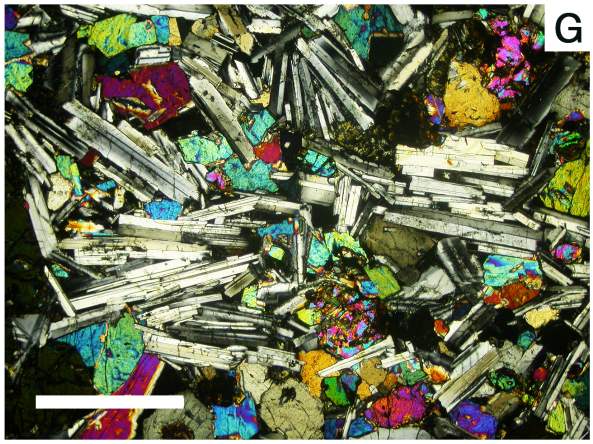
G

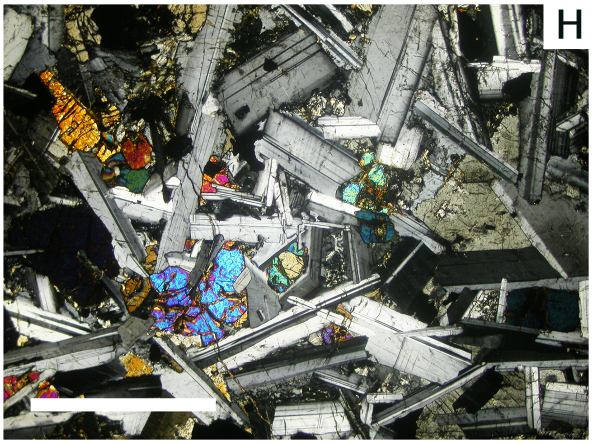
H

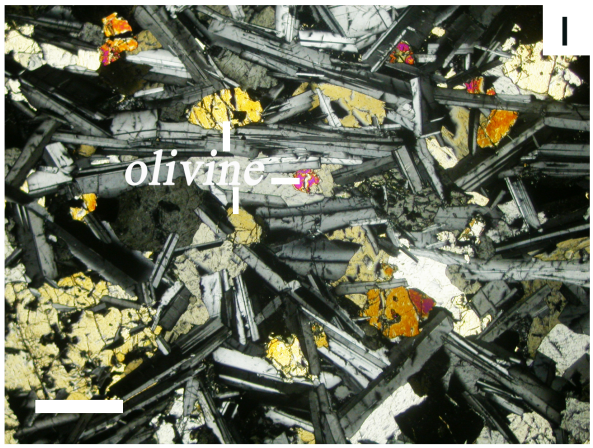
I
olivine

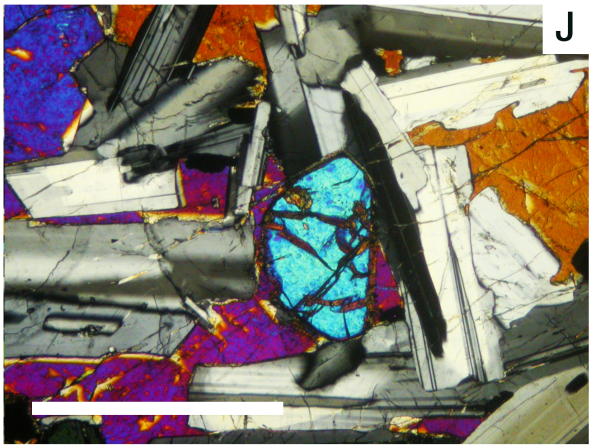
J

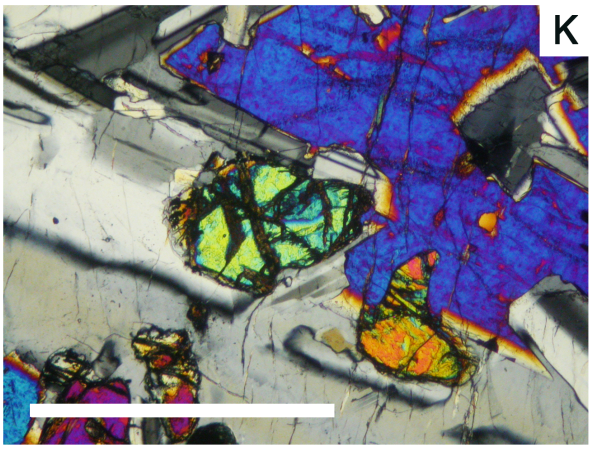
K

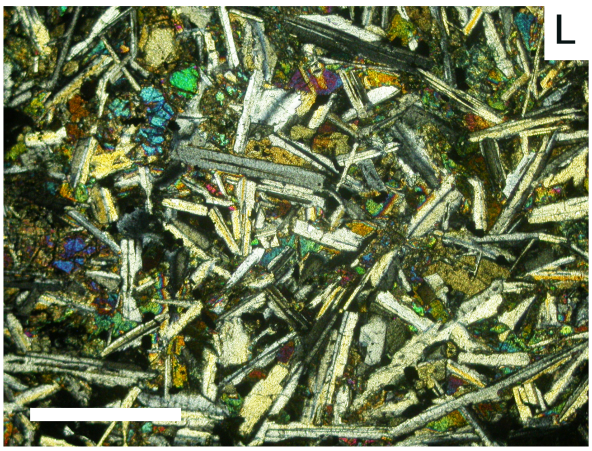
L

ANALYTICAL PROCEDURES

Samples were coarsely crushed (mm-cm in size) in a mechanical jaw crusher and then ground to powder in a shatterbox. Loss-on-ignition was determined by weight difference after 1,000 °C ignition of powders. Major-element abundances were determined using X-ray fluorescence spectrometry, and trace element abundances were determined by ICP-MS. Both types of analyses were made at Acme Analytical Lab, Vancouver, BC. Compositions of plagioclase, clinopyroxene, low-Ca pyroxene, olivine and Fe-Ti oxide minerals were determined using an ARL-SEMQ electron microprobe at North Carolina State University. Reference standards were olivine, clinopyroxene, orthopyroxene, feldspars, ilmenite, chromite, all provided by the Smithsonian Institute, and for Ni in olivine, a Ni-doped diopside was used. Operating conditions were 15 KeV accelerating voltage at 0.015 μA sample current. A 1–2 μm electron beam was used at 10-second count times per spot for peaks and backgrounds.

ANALYTICAL RESULTS

The whole-rock major and trace element compositions of fifteen samples from the two dike systems are presented in Table 2. Eight of the samples were analyzed for mineral compositions (Tables 3, 4, 5, 6).

Whole-rock compositions

Major Elements

Eight samples of dike system 1 (Middleburg to Clayton, NC; Figure 1B) and seven samples of dike system 2 (Durham to Cary, NC; Figure 1B) are plotted on a SiO_2 versus Na_2O+K_2O diagram (TAS) (Figure 3). The reference line for Hawaiian tholeiitic and alkalic basalt cpmpositions in the TAS diagram shows that all dike samples have tholeiitic basalt compositions except one from dike system 1 that is transitional to tholeiitic basaltic andesite. Dike system 1 ranges in SiO_2 from 50.5 to 52.2 wt.% over a relatively large range in total alkalis, from 2.3 to 3.5 wt.%. Dike system 2 has lower SiO_2, from 46 to 48 wt.%, but over a smaller range in total alkalis, from 2 to 2.5 wt.%. There is a gap in SiO_2 between the two systems of ~2.5 wt.%.

Both dike-system compositions are compared in Figure 3 to those of previously analyzed dike samples from North Carolina (e.g., Weigand and Ragland, 1970; Callegaro et al., 2013). Samples of Callegaro et al. (2013) both fill the SiO_2 gap between the two dike systems and overlap the SiO_2 of both dike systems (Figure 3). Some of the lower SiO_2 samples of Callegaro et al. (2013) have slightly lower total alkalis than dike system 2 samples. Three samples of Weigand and Ragland (1970) exceed the SiO_2 contents of dike

system 1, but overlap the alkali contents of dike system 1. The composition of one sample of Weigand and Ragland (1970) corresponds to those of dike system 2.

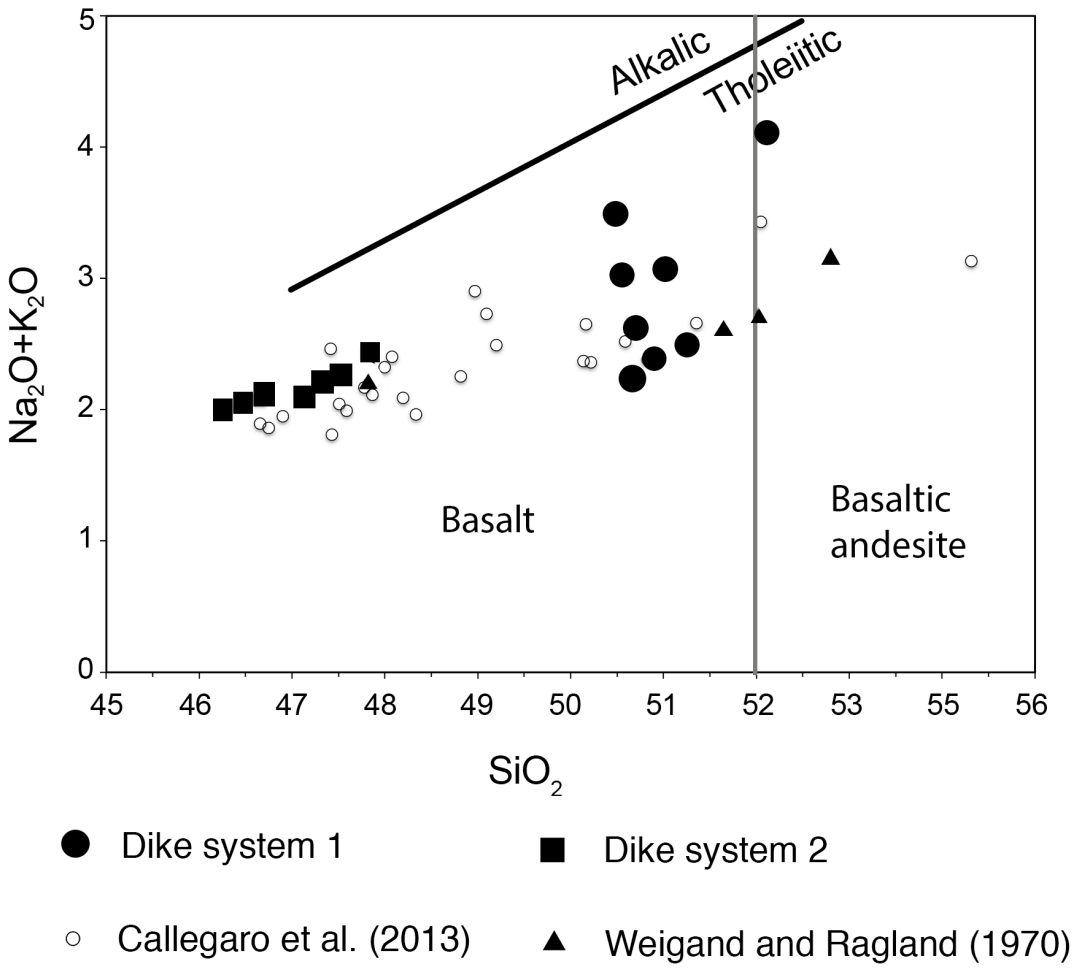

Figure 3. Total alkalis versus SiO_2 (TAS) diagram for the two diabase dike systems compared to compositions of selected NC dike samples from Callegaro et al. (2013) and Weigand and Ragland (1970). Data in wt.%. TAS diagram after Le Bas et al. (1986). The alkalic-tholeiitic line is from Macdonald and Katsura (1964) for Hawaiian basalts.

Normative mineralogy for the two dike systems is plotted in Figure 4 on the base of a basalt tetrahedron. Samples from dike system 1 are quartz-normative, and those from dike system 2 are olivine-normative. Samples from Callegaro et al. (2013) are also olivine-normative and quartz-normative. In terms of SiO_2, all dike system 1 samples overlap Callegaro et al. (2013) samples, while dike system 2 samples plot apart by their strongly ol-normative mineralogy (Figure 4). For the Weigand and Ragland (1970) study, the sample with the lowest SiO_2 is olivine-normative basalt and falls among dike system 2 samples. The three relatively SiO_2-rich Weigand and Ragland (1970) samples are quartz-normative and overlap dike system 1 samples.

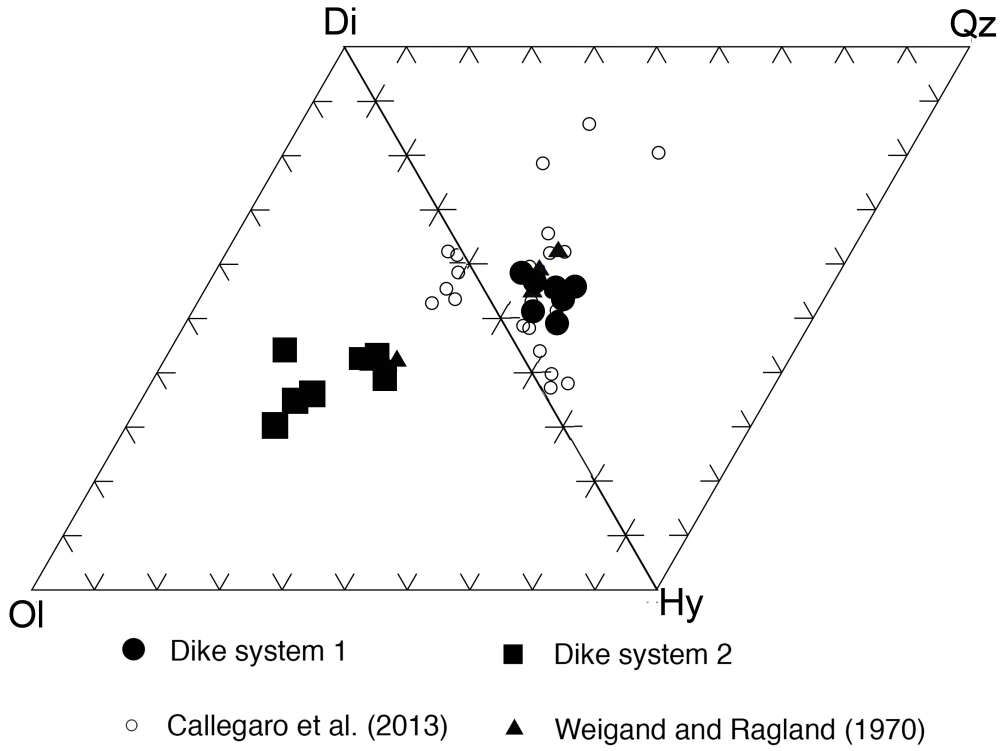

Figure 4. Normative mineralogy of diabase dike system 1 and 2 are plotted on the diopside-hypersthene-olivine-quartz portion of the basalt tetrahedron after Yoder and Tilley (1962). Dike samples from Weigand and Ragland (1970) and Callegaro et al. (2013) are plotted for comparison.

Table 2. Whole-rock compositions (wt.% and ppm) of two diabase dike systems in central North Carolina. For each dike system, samples are listed in the order of decreasing MgO.

	Dike System 1								Dike System 2						
	RV-1	MB-1	MB-2	FR-1	HN-2	HN-1	CL-1	KT-1	ES-1	AB-1	ST-1	CP-1	SV-1	NI-1	NC-1
SiO_2	50.65	51.22	50.83	50.70	50.63	51.01	52.12	50.51	46.30	46.50	46.66	47.12	47.34	47.49	47.83
TiO_2	0.62	0.72	0.68	0.76	0.92	1.01	1.05	1.21	0.47	0.48	0.61	0.49	0.71	0.70	0.70
Al_2O_3	16.58	15.08	17.32	17.47	17.47	17.23	17.94	18.40	14.90	14.30	14.87	18.19	16.71	16.74	17.19
Fe_2O_3	9.94	12.32	9.86	10.45	11.47	12.09	10.15	12.36	12.42	12.50	12.55	9.38	11.86	11.62	11.44
MnO	0.17	0.21	0.17	0.16	0.18	0.18	0.16	0.16	0.18	0.18	0.18	0.14	0.19	0.18	0.17
MgO	7.76	7.42	6.53	5.93	5.10	5.06	4.28	3.34	13.68	13.25	12.44	10.04	9.48	9.37	9.08
CaO	11.70	10.42	11.87	11.79	10.77	10.57	9.56	10.06	9.86	10.07	10.23	12.15	11.04	11.22	11.19
Na_2O	2.01	2.16	2.11	2.24	2.36	2.41	3.00	2.89	1.84	1.87	1.97	1.95	2.04	2.09	2.17
K_2O	0.31	0.41	0.31	0.43	0.70	0.70	1.17	0.63	0.22	0.23	0.15	0.21	0.22	0.20	0.31
P_2O_5	0.06	0.09	0.07	0.08	0.10	0.11	0.13	0.12	0.07	0.07	0.07	0.05	0.08	0.08	0.08
Total	99.80	100.05	99.75	100.01	99.70	100.37	99.56	99.68	99.94	99.45	99.73	99.72	99.67	99.69	100.16
L.O.I	0.34	0.49	0.28	0.64	0.63	0.58	0.49	0.54	0.10	0.09	0.57	0.45	0.88	0.49	0.14
Mg#	63.2	57.0	59.3	55.5	49.5	47.9	48.1	37.3	70.8	70.0	68.6	70.2	63.8	64.0	63.6
Rb	9.8	13.2	10.0	14.3	34.1	28.8	33.8	13.6	2.3	3.0	2.9	2.6	3.5	3.4	4.5
Sr	134	140	139	158	172	210	215	251	92.0	96.0	98.0	135	133	131	160
Ba	91.0	140	91.0	97.0	158	259	318	152	163	159	116	91.0	156	107	138
Zr	42.6	59.6	44.7	58.9	76.2	78.5	114	86.8	38.9	39.9	42.3	31.2	54.0	50.6	43.0
Y	20.5	24.2	17.9	22.1	24.3	29.0	31.8	27.4	16.0	17.7	19.1	15.3	23.7	23.6	21.9
Nb	2.2	3.1	2.4	2.6	3.9	4.1	8.3	4.7	1.5	1.5	1.7	1.3	2.0	1.8	2.2
Ni	70.7	62.1	49.1	47.9	43.0	45.3	53.3	29.9	466	458	413	266	226	235	198

Table 2. Continued.

Cr	210	163	179	156	104	87.0	40.0	28.0	523	523	541	312	273	278	204
Sc	42.1	43.7	39.7	42.2	38.7	40.0	35.2	33.3	34.9	40.4	38.4	37.3	45.8	45.6	38.5
V	248	252	255	262	270	315	298	334	172	188	197	162	233	230	216
La	4.8	7.0	5.6	6.0	8.1	9.1	13.9	8.5	4.0	4.1	4.1	3.1	4.9	5.1	5.2
Ce	10.9	16.1	12.5	14.2	17.9	20.1	30.4	18.9	9.1	9.5	9.2	7.6	10.9	11.6	11.0
Pr	1.4	2.0	1.5	1.8	2.3	2.4	3.9	2.4	1.1	1.3	1.3	0.9	1.5	1.5	1.5
Nd	5.8	8.7	7.2	8.0	10.1	11.1	16.3	11.0	4.7	5.5	6.1	4.8	6.1	7.4	6.9
Sm	1.8	2.8	2.1	2.1	2.7	3.2	3.6	2.8	1.4	1.6	1.9	1.6	2.0	2.0	1.9
Eu	0.7	0.9	0.8	0.9	0.9	1.0	1.3	1.2	0.4	0.5	0.6	0.6	0.8	0.8	0.8
Gd	2.7	3.5	2.8	3.5	4.3	4.7	4.3	3.9	1.4	2.4	2.6	2.3	3.4	2.8	3.2
Tb	0.4	0.5	0.5	0.6	0.7	0.7	0.8	0.7	0.4	0.4	0.4	0.3	0.5	0.6	0.5
Dy	3.4	4.1	3.7	4.0	4.6	5.2	5.8	4.7	2.8	3.0	3.5	2.9	4.1	3.8	3.9
Ho	0.7	0.8	0.8	0.9	0.9	1.0	1.1	1.1	0.6	0.6	0.7	0.6	0.9	0.9	0.8
Er	2.0	2.6	2.2	2.6	3.0	3.3	3.8	3.5	2.1	2.1	2.2	1.8	2.8	3.1	2.4
Tm	0.4	0.4	0.3	0.4	0.4	0.5	0.6	0.5	0.3	0.3	0.3	0.3	0.4	0.4	0.4
Yb	2.2	2.9	2.1	2.7	2.9	3.4	3.8	3.4	2.1	2.0	2.5	1.9	2.8	3.1	2.7
Lu	0.3	0.4	0.3	0.4	0.4	0.5	0.6	0.5	0.3	0.3	0.4	0.3	0.5	0.5	0.4
Hf	1.2	1.8	1.4	1.6	2.0	2.1	3.0	2.4	1.1	1.2	1.3	0.9	1.5	1.4	1.1
Th	1.0	1.6	1.2	1.5	1.9	2.0	2.6	2.1	0.2	0.2	0.2	0.2	0.3	0.3	0.4
Ta	0.2	0.2	0.2	0.2	0.3	0.3	0.6	0.3	<0.1	0.1	<0.1	<0.1	0.1	<0.1	0.1
Pb	2.1	3.6	2.4	2.9	3.3	3.8	4.6	4.3	1.7	2.7	4.2	1.2	1.5	1.6	1.8
U	0.3	0.4	0.3	0.4	0.5	0.5	0.5	0.5	<0.1	<0.1	<0.1	<0.1	<0.1	<0.1	<0.1

Mg# = [(MgO/40.3)/(MgO/40.3+ Fe_2O_3*0.81/71.85)]*100

LOI = loss-on-ignition; represents volatile loss during sample ignition to 1000°C.

The major element compositions are illustrated in MgO variation diagrams (Figure 5). Eight samples from Middleburg to Clayton (dike system 1; Figure 1B) and seven samples from Durham to Cary (dike system 2; Figure 1B) collectively form two distinct MgO compositional groups, from 7.8 to 3.3 wt.% for dike system 1 and from 13.7 to 9.1 wt.% for dike system 2 (SiO_2 vs. MgO panel; Figure 5). The low-MgO dike system 1 corresponds to its relatively high SiO_2, ~50.5 to 52.1 wt.%, and the high-MgO dike system 2 relates to lower SiO_2, ~46.3 to 47.8 wt.%.

Dike system 1 has essentially constant SiO_2 over its MgO range, and CaO trends positively with MgO. Other major elements, Al_2O_3, TiO_2, P_2O_5, K_2O, and Na_2O, have negative correlations with MgO. The Fe_2O_3 data are rather scattered. For dike system 2, SiO_2, CaO, Al_2O_3, and Na_2O all have weak to moderate inverse correlations with MgO, and other major elements, TiO_2, P_2O_5, K_2O, and Fe_2O_3, are generally scattered over the MgO range. One sample, CP-1, stands apart from the other samples by having notably lower Fe_2O_3 (~9.5 wt.%) and P_2O_5 (~0.05 wt.%), and higher Al_2O_3 (~18.2 wt.%) and CaO (~12.2 wt.%).

When comparing the two dike systems, the lowest MgO (<5 wt.%) dike system 1 samples have generally higher TiO_2, P_2O_5, K_2O and Na_2O than any of the high-MgO (>10 wt.%) dike system 2 samples. Specifically, the highest values for major elements in dike system 1 are from 1.8 to 4.7 times higher than in dike system 2 samples (dike system 1 highest / dike system 2 lowest; Figure 5). But overall, the two dike systems essentially form continuous major element trends across the MgO range of ~13 to 3 wt.% (Figure 5).

The two dike systems are compared to the major element compositions of North Carolina dike samples from Callegaro et al. (2013). Dike system 1 samples are within the compositional fields of Callegaro et al. (2013) except for those lower in MgO (<5 wt.%) than reported by Callegaro et al. (2013). Nearly all dike system 2 major element abundances are within the compositional fields of Callegaro et al. (2013).

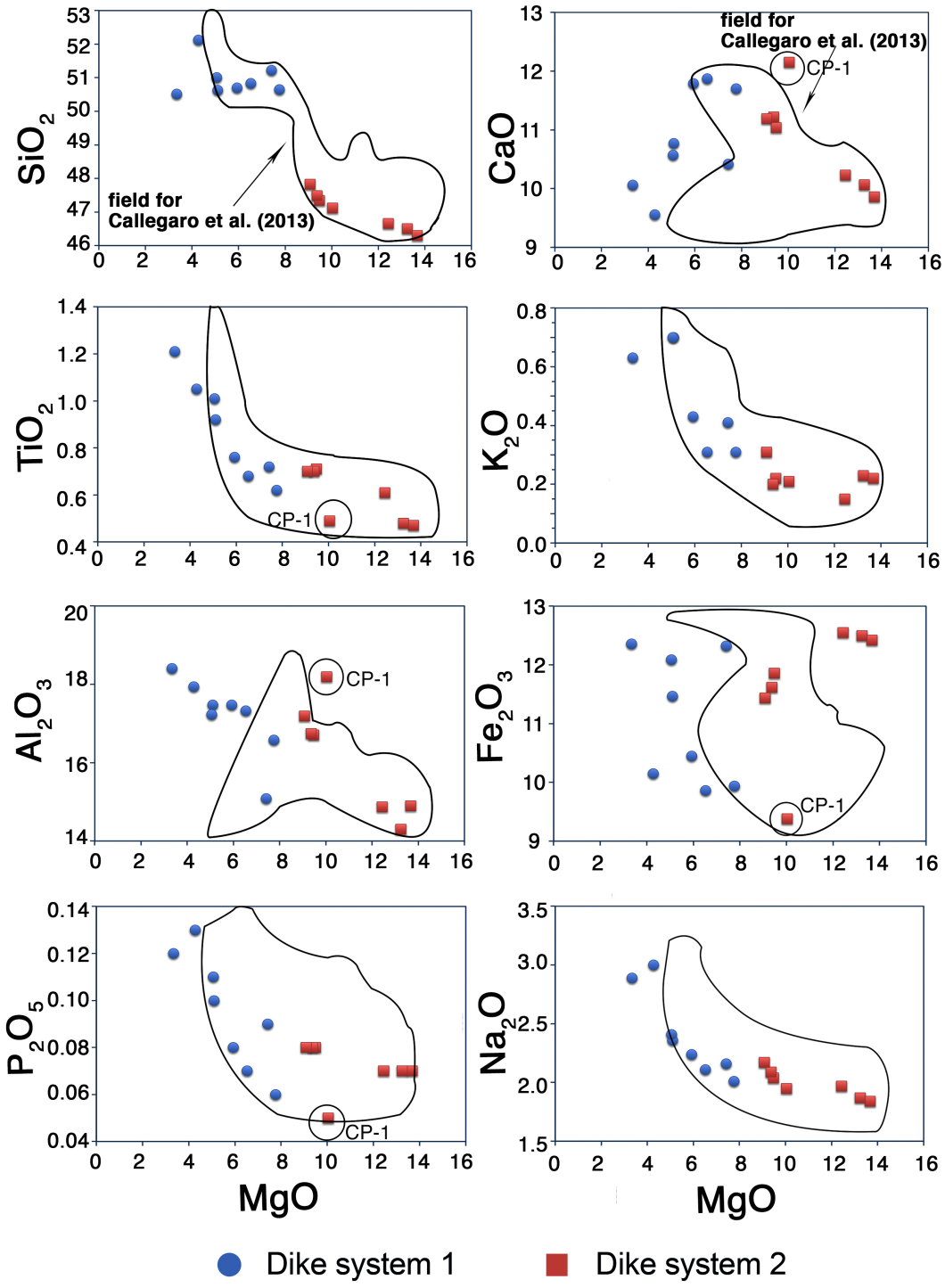

Figure 5. MgO variation diagrams for major element compositions of two diabase dike systems compared to the compositions of North Carolina samples of Callegaro et al. (2013) represented by the encircled field. Data plotted as wt.%.

Trace Elements

Trace element abundances for samples from the two dike systems are plotted in MgO variation diagrams (Figure 6) and listed in Table 2. An important observation is that the high-MgO, olivine-normative samples of dike system 2 have notably lower abundances of incompatible elements than the samples of dike system 1, as was observed for incompatible major elements TiO_2, P_2O_5, K_2O, and Na_2O (Figure 5).

Abundances for LILE (large-ion lithophile elements) Sr, Rb and Ba in the two dike systems are relatively low (e.g., Sr ~90 to 250 ppm, Rb ~2 to 34 ppm, Ba ~100-150 ppm), consistent with other reported tholeiitic dike compositions (e.g., Weigand and Ragland, 1970; Bertrand, 1991; Marzoli et al., 2011). Sr abundances form a generally increasing trend across the ~14 to 3 wt.% MgO range for the two dike systems combined, where dike system 1 samples have the highest concentrations (Figure 6). However, this inverse correlation (with MgO) is flat in the region of ~8 to 9 wt.% MgO where dike system 2 MgO values transition to those of dike system 1 (Figure 6). Rb abundances are relatively constant for dike system 2, ~2 to 4 ppm, but higher and in two clusters for dike system 1, where the highest values, 29 to 34 ppm. Ba abundances create a generally flat, scattered trend between ~90 to 160 ppm across the two dike systems, except for two dike system 1 samples that are comparatively high, ~ 250 to 300 ppm (Figure 6).

The HFSE (high field strength elements) La, Zr, Nb, Th, and Hf all show relatively low-abundance, flat trends for dike system 2 samples across their MgO of ~14 to 9 wt.% MgO. In the more evolved (lower MgO) dike system 1 samples, abundances for most HFSE appear to transition from dike system 2 at ~8 wt.% MgO to slightly increasing

concentrations through to ~ 3 wt.% MgO (Figure 6). Th abundances, however, show a gap between the two dike systems (Figure 6). Y abundances are more scattered than other HFSE, but generally increase as MgO decreases throughout the two dike systems combined (Figure 6).

The abundances of compatible elements Ni and Cr have similar trends, where both decrease with decreasing MgO across the two dike systems. In detail, Cr displays a continuum between dike systems 1 and 2, while Ni shows a compositional gap of over 100 ppm between the two dike systems (Figure 6). The abundances of transition metals Sc and V are more complex. Sc abundances in dike system 1 display strong compatibility, forming a positive linear trend as MgO increases, while Sc abundances in dike system 2 are scattered (Figure 6). The V-abundance trend is similar to those for incompatible elements such as Sr and La, which form inverse continuous trends across the ~14 to 3 wt.% MgO range for the two dike systems combined, where dike system 1 samples have the highest concentrations (Figure 6).

The trace element compositions for the two dike systems are compared to those for North Carolina samples from Callegaro et al. (2013). For all trace elements, dike system 2 samples and the higher-MgO (~6 to 7 wt.%) dike system 1 samples largely overlap the compositional fields of Callegaro et al. (2013). However, the Callegaro et al. (2013) samples that have MgO overlapping dike system 1 MgO abundances do not display the strong Sc correlation with MgO that dike system 1 samples collectively demonstrate (Figure 6).

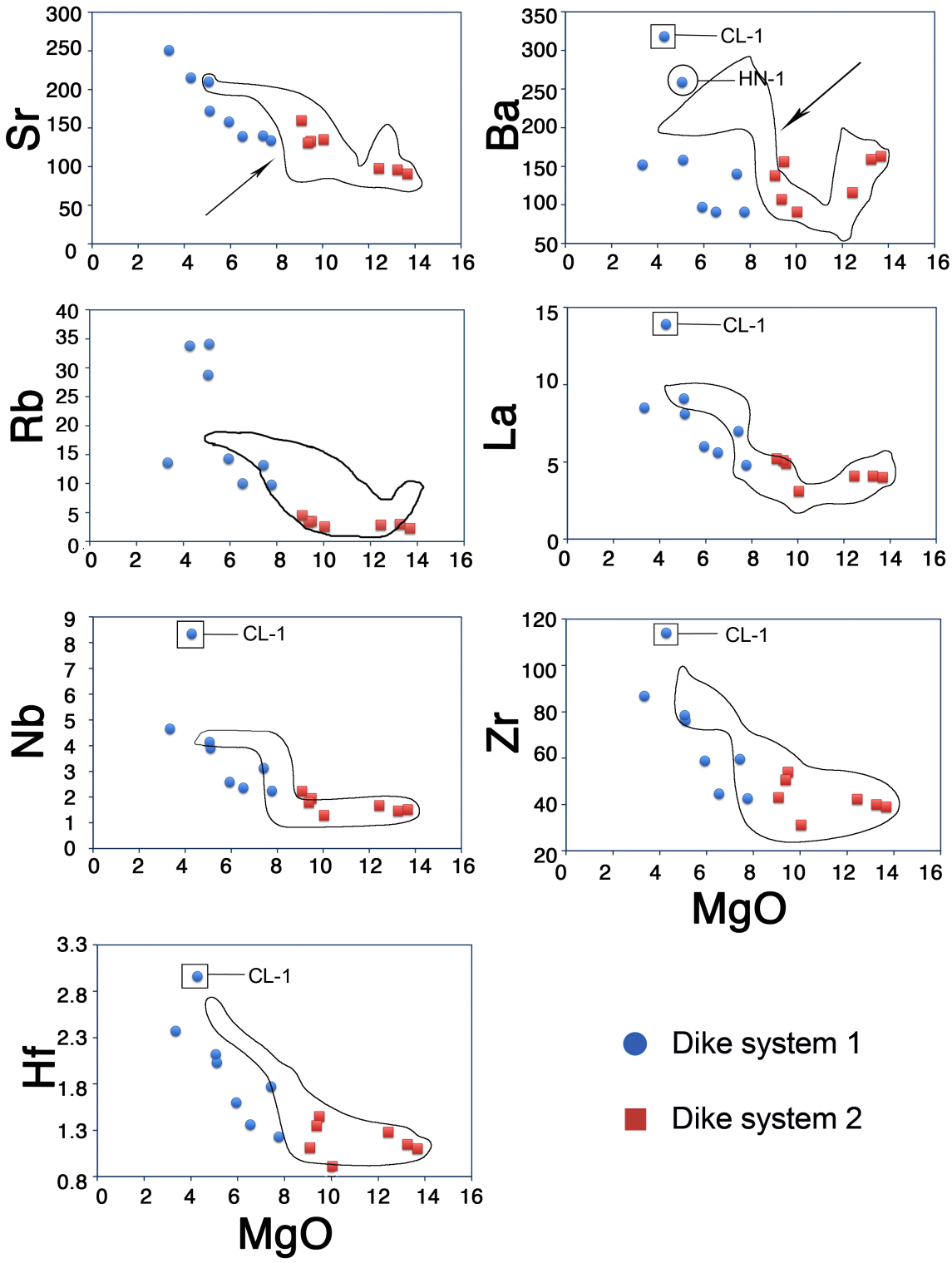

Figure 6. MgO variation diagrams for trace element compositions of two diabase dike systems compared to the North Carolina samples of Callegaro et al. (2013) represented by the encircled field. Trace element data plotted in ppm according to petrographic group as shown.

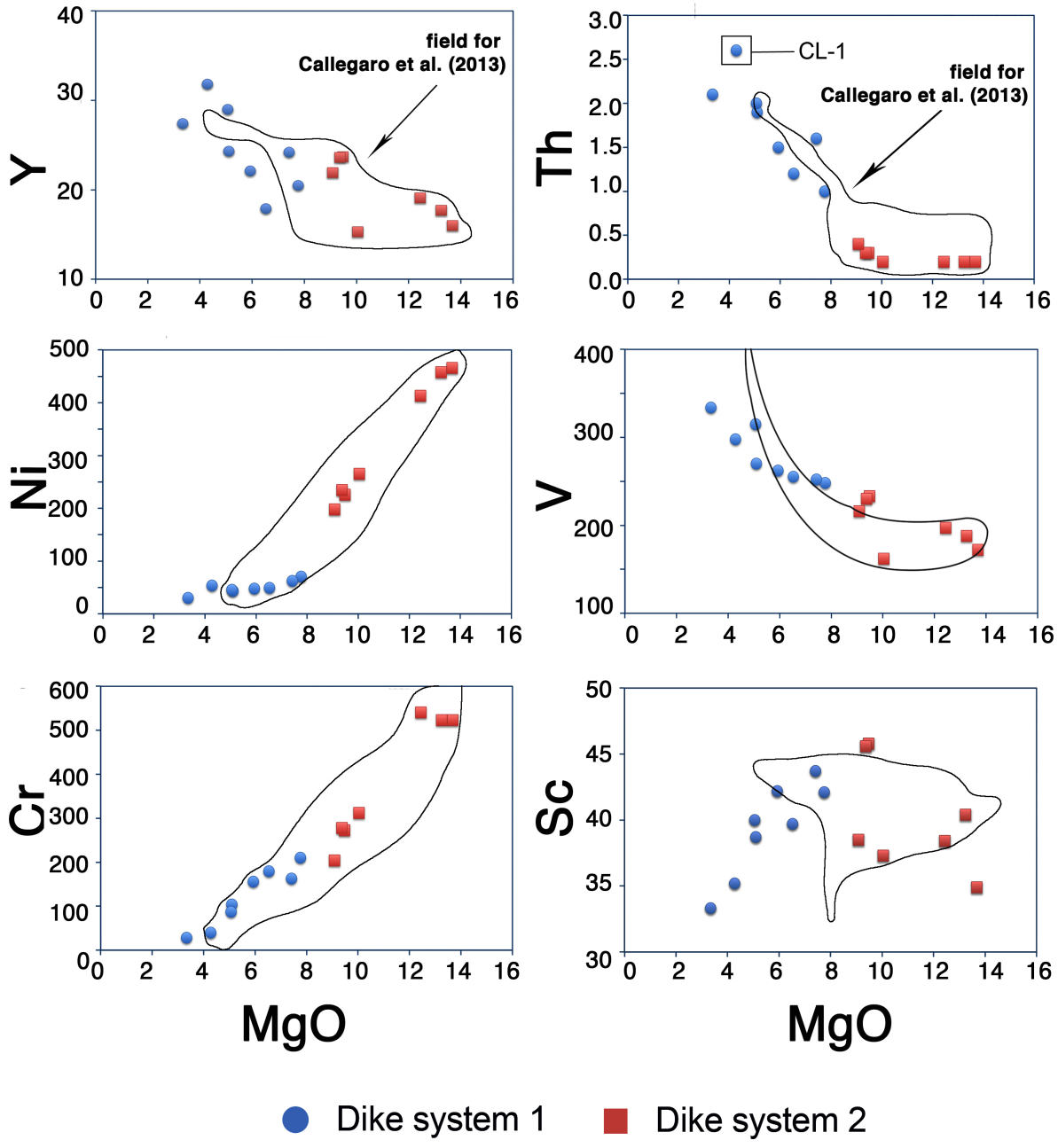

Figure 6. (Continued) MgO variation diagrams for trace element compositions of two diabase dike systems compared to the North Carolina samples of Callegaro et al. (2013) represented by the encircled field. Trace element data plotted in ppm according to petrographic group as shown.

The chondrite-normalized rare-earth element (REE) patterns for all samples are illustrated in Figure 7. The patterns for dike system 1 have moderate enrichment of the light rare earth elements (LREE) where $(La/Sm)_n$=1.6-2.25. The tholeiitic basaltic andesite sample CL-1 has LREE enrichment that exceeds those of the other samples (~$(La/Sm)_n$=2.25). The patterns for dike system 2 are close to flat and have lower LREE enrichment, ~$(La/Sm)_n$=1.11-1.75. Sample CP-1 has among the lowest concentrations of REE and essentially no LREE enrichment (~$(La/Sm)_n$=1.11). Consistent with the groupings for incompatible elements in MgO variation diagrams (Figure 6), some of the dike system 2 patterns plot lower than those for system 1 (Figure 7).

The primitive-mantle normalized patterns are in Figure 8. In general, dike system 1 shows Nb, Ta, P and Ti negative anomalies and relatively high enrichments in Rb and Ba, similar to what is observed for some other CAMP rocks (e.g., Merle et al., 2011; Ghatak and Basu, 2012; Callegaro et al., 2013). Primitive mantle patterns for dike system 2 samples are lower than patterns for dike system 1 samples, with exception of Ba. The relatively lower patterns are expected from the trace elements plots in Figure 6. Dike system 2 patterns also show negative anomalies for Nb, Ta (when detectable), P, and Ti, as dike system 1 patterns do. But they have a pronounced negative anomaly for Th that dike system 1 samples do not display. Ba stands apart in dike system 2 patterns because its abundances are elevated compared to neighboring incompatible elements in the patterns, Rb and Th. Otherwise, Ba values in both dike system 1 and 2 samples are similar (Figure 6).

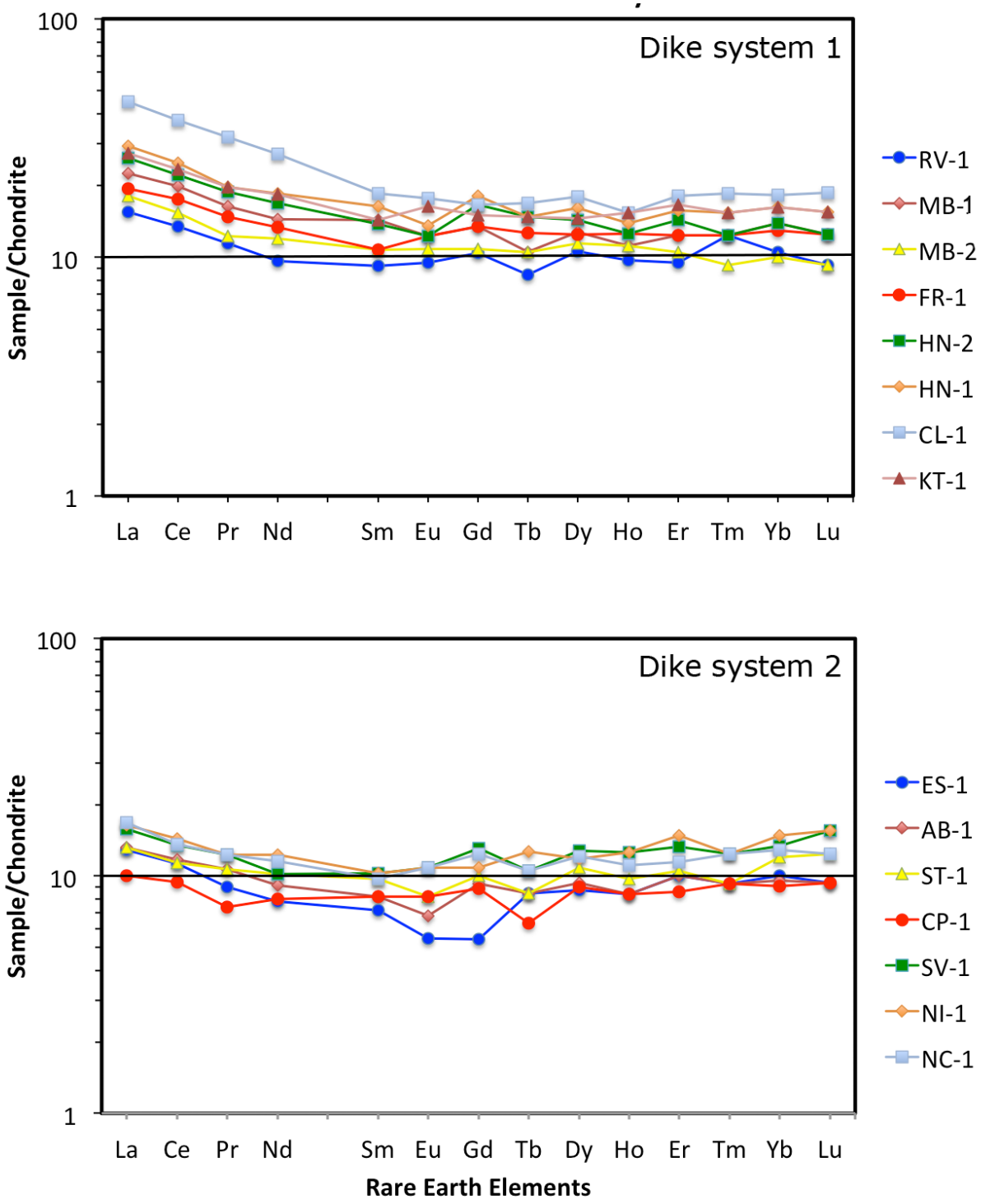

Figure 7. Chondrite-normalized rare earth element patterns for two diabase dike systems in central North Carolina. Dike system 1 is quartz-normative, dike system 2 is olivine-normative. Chondrite normalizing values are from Masuda et al. (1973).

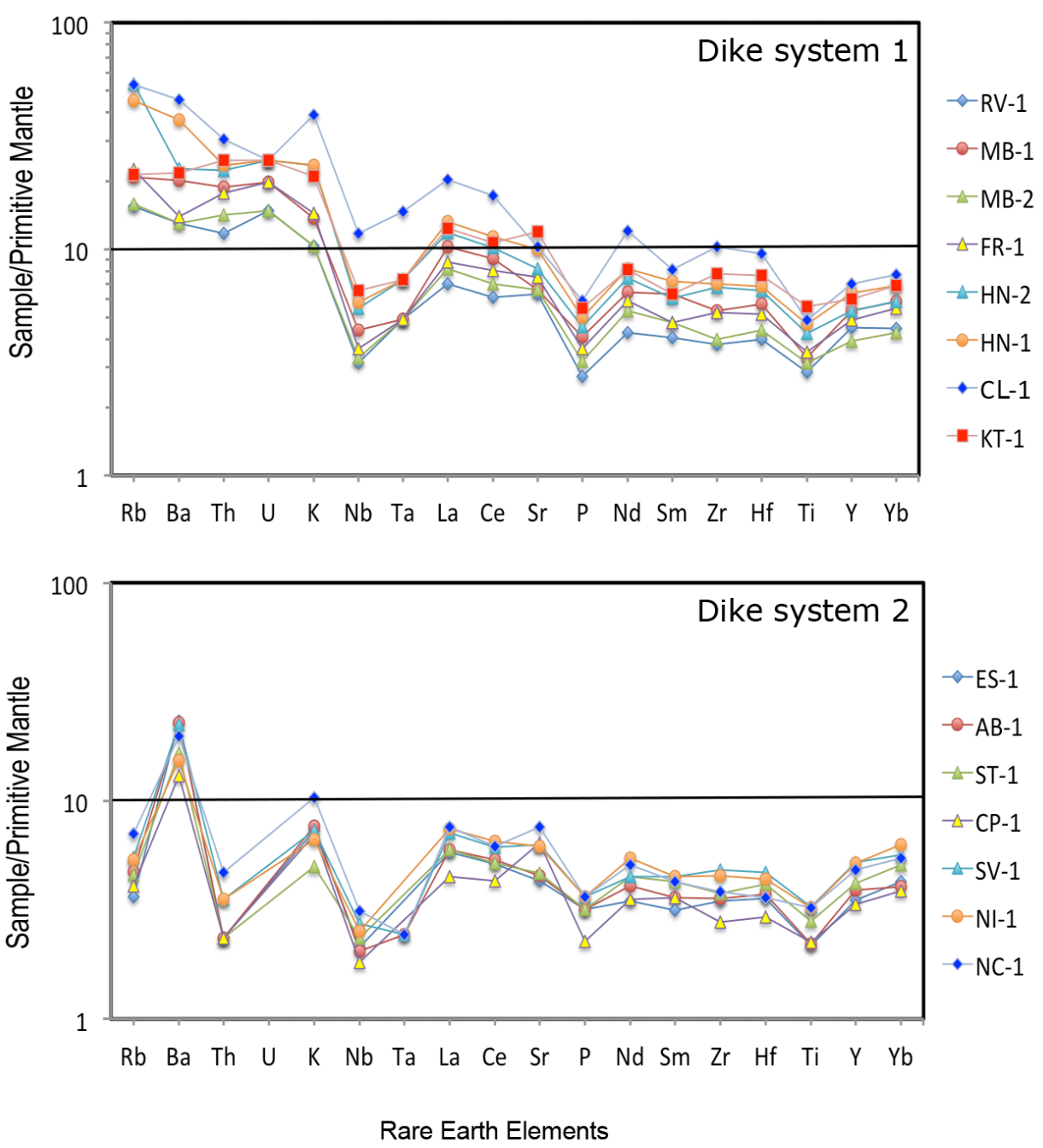

Figure 8. Primitive-mantle normalized diagrams for two diabase dike systems in central North Carolina. Normalizing values are from McDonough and Sun (1995). U abundances in dike system 2 samples are below detection limit and therefore no data points are shown.

Mineral Compositions

Plagioclase

As discussed previously in the petrography section, all dike system 1 samples have large plagioclase grains as phenocrysts, and the phenocrysts mainly occur as glomerocrysts (Figure 2A, B and C). Average compositions for representative plagioclase grains are in Table 3, and endmembers are plotted in An-Ab-Or ternary diagrams in Figure 9. In dike system 1, the cores of some phenocrysts in two samples (MB-2 and FR-1) have the most calcic compositions observed, from calcic bytownite to anorthite (~An_{80-92}). In the cores of phenocrysts in three other samples (HN-1, CL-1 and KT-1), the most calcic compositions observed are sodic bytownite compositions (~An_{70-75}) (Figure 9A). In all samples, the phenocrysts were observed to be zoned individually, having rims slightly less calcic than cores, ~An_{50-70}, to rims notably more sodic, ~An_{35-40} (Figure 9A).

Surrounding the plagioclase glomerocrysts are matrix plagioclase grains in intergranular to subophitic textures with clinopyroxene (Figure 2D and E). These plagioclase-matrix compositional ranges have strong overlap with phenocryst compositions (Figure 9A). They overlap all but the calcic cores in each sample (Figure 9A). The matrix grains are largely more sodic than the phenocrysts, and collectively display wide compositional ranges. For example, FR-1 plagioclase matrix is sodic bytownite to calcic oligoclase (~An_{76-22}). Other samples have more concentrated plagioclase-matrix compositions, ranging from sodic bytownite to sodic andesine (~An_{70-40}) (Table 3; Figure 9A).

The dike system 2 samples have plagioclase occurring only as a network of laths in intergranular to subophitic textures with clinopyroxene. Their compositional ranges are small, calcic bytownite that extends by zoning to sodic labradorite (~An_{85-50}), except sample NC-1, which has the most sodic compositions, ranging from calcic bytownite to sodic andesine (~An_{84-38}) (Table 3; Figure 9B).

For comparison, Callegaro et al. (2013) reported plagioclase phenocrysts (no size or textural relationship provided) in their many NC and SC dikes studied as having compositions ~An_{89-48}. This plagioclase An range overlaps those observed in the samples from both dike systems 1 and 2, ~An_{92-20} and ~An_{85-38}, respectively (Figure 9A and B).

Table 3. Average compositions of representative plagioclase as phenocrysts (PC, occurring as glomerocrysts) and as matrix (groundmass, GM) grains in the two diabase dike systems in central North Carolina.

	Dike system 1									
	MB-2		FR-1		HN-1		CL-1		KT-1	
	PC	GM	PC	GM	PC	GM	PC	GM	PC	GM
SiO_2	47.4	51.1	45.8	53.5	50.3	52.5	51.0	52.7	52.6	53.7
Al_2O_3	33.8	30.8	35.1	29.2	31.5	29.5	29.6	29.5	28.6	28.5
FeO	0.63	0.97	0.46	0.87	0.65	1.3	0.71	0.88	0.77	0.79
CaO	16.1	13.1	17.5	10.8	14.3	12.4	12.7	10.9	11.9	10.9
Na_2O	2.4	4.1	1.5	5.2	3.4	4.5	3.9	4.9	4.5	4.8
K_2O	0.07	0.17	0.02	0.33	0.12	0.22	0.21	0.37	0.22	0.25
Total	100.39	100.09	100.38	99.89	100.27	100.38	98.14	99.25	98.56	98.99
An	78.5	63.4	86.6	52.7	69.7	59.9	63.4	53.9	64.2	54.8
Or	0.41	1.1	0.11	1.9	0.7	1.2	1.3	2.1	1.0	1.5

	Dike system 2							
	ES-1		AB-1		CP-1		NC-1	
	GM-1	GM-2	GM-1	GM-2	GM-1	GM-2	GM-1	GM-2
SiO_2	49.2	49.1	50.1	50.3	50.6	49.6	54.9	53.2
Al_2O_3	33.2	32.4	32.4	30.7	31.6	32.3	28.4	29.6
FeO	0.61	0.59	0.76	0.92	0.86	0.84	0.86	1.3
CaO	16.1	15.4	14.9	15.1	14.6	15.3	12.1	13.1
Na_2O	2.4	2.4	2.7	2.4	2.9	2.8	4.2	3.3
K_2O	0.07	0.06	0.11	0.11	0.19	0.12	0.35	0.27
Total	101.58	99.99	100.97	99.39	100.75	100.99	100.81	100.68

Table 3. Continued

An	78.3	77.4	74.8	77.4	72.3	74.9	59.9	67.5
Or	0.40	0.40	0.61	0.60	1.2	0.70	2.1	1.7

Each column is an average of 8-17 points analyzed per grain.
PC = plagioclase phenocrysts occurring as glomerocrysts.
GM = plagioclase as laths that form intergranular/subophitic networks (matrix to plagioclase glomerocrysts in dike system 1 samples).

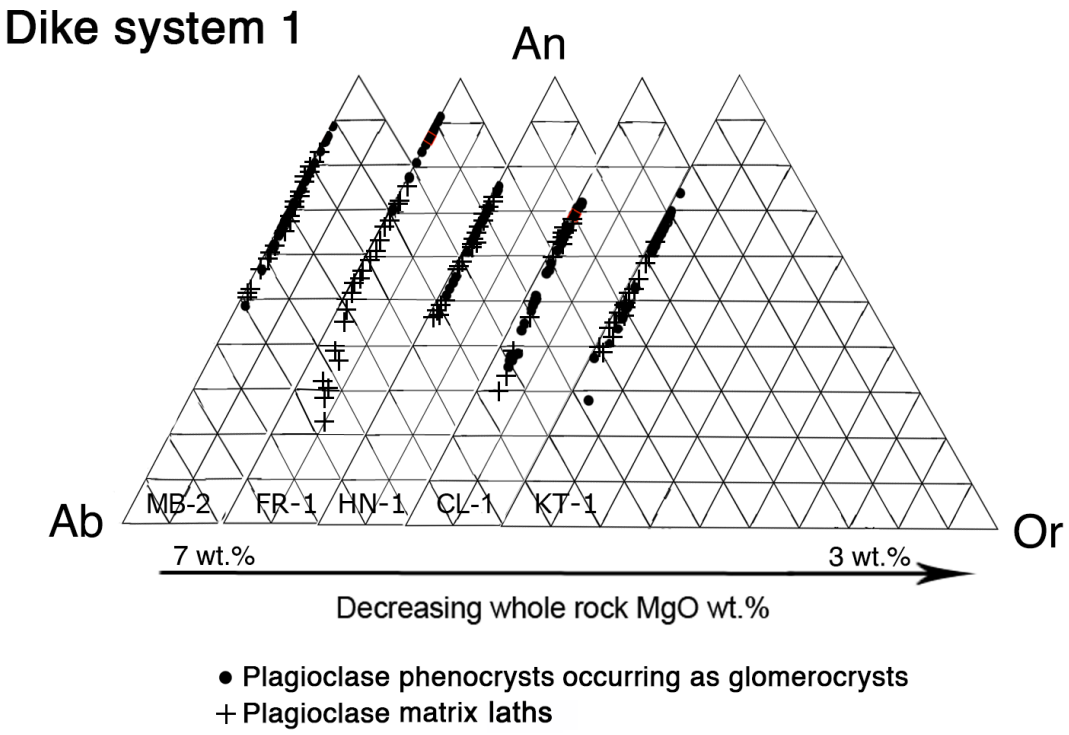

Figure 9A. Plagioclase compositions for dike system 1 samples plotted as endmembers anorthite, albite, and orthoclase (An, Ab, Or). Each plotted point represents an analyzed point in phenocrysts and matrix grains. The ternary diagrams are plotted in order (left to right) of decreasing host-rock MgO to demonstrate the general relationship between plagioclase An and their host compositions. Namely, highest An plagioclase compositions are in samples with MgO, ~7 to 6 wt.%, and lowest An compositions are in lower, more evolved MgO samples (~5 to 3 wt%).

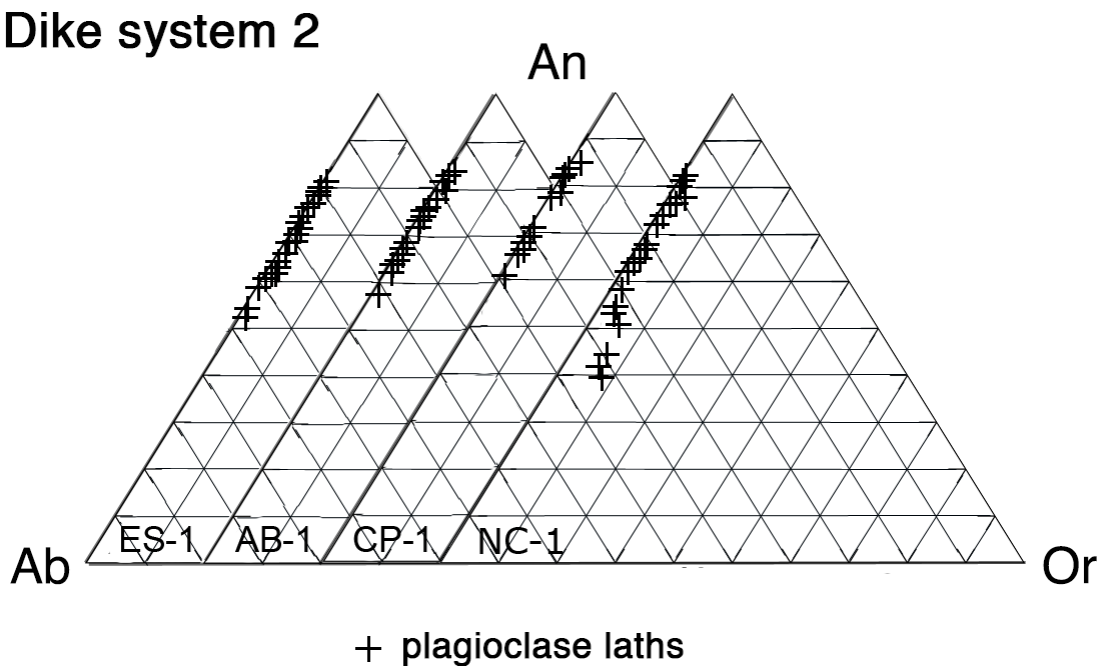

Figure 9B. Plagioclase compositions for dike system 2 samples plotted as endmembers anorthite, albite, and orthoclase (An, Ab, Or). Each plotted point represents an analyzed point in plagioclase laths that are in intergranular/subophitic textures with clinopyroxene. There is no correlation between whole rock MgO (~13 to 9 wt.%) and plagioclase An. All samples show similar An compositions and ranges.

Pyroxene

Average compositions for representative pyroxene grains are in Table 4, and Fs, Wo, and En endmembers are plotted in quadrilaterals in Figure 10. Both dike systems have clinopyroxene and low-Ca pyroxene only as matrix grains in intergranular, ophitic and subophitic textural relationships with plagioclase laths (Figure 2 D-L).

Clinopyroxene

Dike system 1 samples have clinopyroxene compositions ~Fs_{10-32}, where the range expressed represents normal compositional zoning in individual grains (Figure 10). In some samples, such as MB-2 and HN-1, the compositional range can represent two or more zoned grains with distinctly different average compositions (Table 4). The Figure 10 data points, overall, demonstrate relatively similar Fs ranges for all samples, ~Fs_{10-32}.

Across the Fs range observed, Wo has a relatively tight range, ~Wo_{30-38} (Figure 10). Clinopyroxene Wo has a generally flat correlation with Fs, with exception of that in KT-1 (lowest MgO, ~3 wt.%), where it has a slightly positive trend with increasing Fs toward hedenbergite (Figure 10).

The Cr_2O_3 in the dike system 1 clinopyroxenes shows some relationship with whole-rock MgO and Mg#s. Namely, the high-Mg# (~81.1) clinopyroxene in MB-2 (Mg# 59.3) has relatively high Cr_2O_3, ~0.3 wt.%, whereas other lower-Mg# (<75) clinopyroxenes in more evolved samples (e.g., lower MgO and Mg#) have Cr_2O_3 just above detection limits (Table 4).

Three dike system 2 samples (ES-1, CP-1 and NC-1) have clinopyroxenes with limited compositional ranges, ~$Fs_{10-19}Wo_{38-42}$. Only sample AB-1 has clinopyroxene compositions outside that range. It has Wo that decreases to <30 mol% towards subcalcic augite, ~$Fs_{10-26}Wo_{28-42}$ (Figure 10). All samples have clinopyroxenes with Mg#s within a narrow range, ~78 to 81, whereas the whole-rock MgO and Mg#s respectively range from 9 to 13 wt.% and from 63 to 70 (Tables 2 and 4).

Dike system 2 clinopyroxenes have higher Wo, ~40-42 mol%, compared to clinopyroxene in dike system 1 (generally ~Wo_{35}), and slightly higher Al_2O_3, ~2 to 4.1 wt.% compared to clinopyroxene in dike system 1, ~1.7 to 2.4 wt.% (Table 4). Dike system 2 clinopyroxene also has higher Cr_2O_3 (~0.3 to 0.9 wt.%) than dike system 1 clinopyroxene (Figure 10; Table 4), which correlates with the higher Mg#s in both dike system 2 clinopyroxene (~78 to 81; Table 4) and host rocks (~63.6 to 70.8; Table 2).

Unlike clinopyroxene Mg# and Cr_2O_3, the higher CaO and Al_2O_3 cannot be directly attributed to the more primitive characteristics of dike system 2 samples. Similar compositional distinctions for clinopyroxenes in South Carolina CAMP dikes were noted by Warner et al. (1985; 1992), who showed that among olivine-normative dikes, both a subcalcic augite trend (decreasing Wo) and a ferroaugite trend (increasing Fs and Wo) are present as observed in dike systems 2 and 1 samples, respectively (Figure 10). But their explanation to relate the ferroaugite trend to samples with greater normative olivine do not apply here, as my ferroaugite-trending samples (dike system 1) are quartz normative. It appears more likely that the ferroaugite trend reflects higher Fe/Mg in dike system 1 samples (Table 2). The small differences in Wo between the two systems probably relate to

clinopyroxene equilibration temperatures. That is, Wo in clinopyroxene of two-pyroxene systems increases with decreasing equilibrium temperature as shown long ago in P-T experiments on pyroxenes (e.g., Boyd and Schairer, 1964; Lindsley, 1983).

Low-Ca pyroxene

The small, sparse (~1.3 to 2.6 vol%) low-Ca pyroxene grains in dike system 1 samples are mainly orthopyroxene (~$Fs_{15}Wo_{8}$) transitioning to pigeonite (~$Fs_{25\text{-}50}Wo_{10\text{-}15}$) (Figure 10). In sample HN-1, there is a weak correlation for slightly increasing Wo in low-Ca pyroxene attending slightly decreasing Wo in coexisting clinopyroxene (Figure 10), a relationship expected for high-Ca and low-Ca pyroxene systems (e.g., Lindsley, 1983).

The low-Ca pyroxenes in dike system 2 show a relationship with coexisting clinopyroxenes in which they are Fs-richer. That is, the low-Ca pyroxenes have 15-20 mol% more Fs than their coexisting clinopyroxenes, such that, for example, ES-1 has pigeonite ~$Fs_{35}Wo_{13}$ and clinopyroxene that is largely ~$Fs_{10\text{-}15}Wo_{45}$ (Figure 10). No low-Ca pyroxene was observed in sample AB-1, in which clinopyroxene is zoned toward low-Ca augite, $Fs_{25}Wo_{28}$ (Figure 10).

Pyroxenes in the study of Callegaro et al. (2013) are mainly clinopyroxene phenocrysts (no size or textural relationship provided) with compositions of $Fs_{9\text{-}30}Wo_{36\text{-}42}$. Their Fs component is similar to the clinopyroxenes in the two dike systems, whereas the two dike systems have slightly wider clinopyroxene-Wo ranges: dike system 1 ~$Fs_{10\text{-}32}Wo_{29\text{-}}$

$_{39}$, and dike system 2 ~$Fs_{9\text{-}25}Wo_{28\text{-}42}$ (Table 4). No matrix clinopyroxene compositions were reported by Callegaro et al. (2013). Also, they described orthopyroxene as infrequent, and did not provide orthopyroxene compositional data (Callegaro et al., 2013).

Table 4. Average compositions of representative pyroxene in the two diabase dike systems in central North Carolina.
CPX = clinopyroxene, LCP = low-Ca pyroxene

							Dike 1							
	MB-2				FR-1		HN-1				CL-1		KT-1	
	CPX	CPX	LCP	LCP	CPX	LCP	CPX	CPX	LCP	LCP	CPX	LCP	CPX	LCP
SiO_2	52.3	51.3	52.4	54.0	52.9	52.9	53.3	51.4	52.7	51.5	50.9	53.2	51.1	52.4
TiO_2	0.26	0.38	0.21	0.19	0.31	0.19	0.26	0.40	0.21	0.29	0.56	0.19	0.49	0.24
Al_2O_3	2.4	1.7	1.0	0.99	2.2	1.3	1.8	1.6	0.97	1.3	2.3	0.99	1.7	1.2
Cr_2O_3	0.32	0.04	0.05	0.17	0.02	0.01	0.06	0.01	0.01	0.02	0.01	0.02	0.01	0.01
FeO	7.6	13.1	22.3	16.3	10.3	18.1	11.3	17.9	19.4	21.9	11.3	15.4	16.5	16.9
MnO	0.23	0.33	0.48	0.37	0.28	0.40	0.32	0.48	0.59	0.68	0.36	0.47	0.47	0.43
MgO	18.3	16.2	19.8	24.2	18.1	22.9	17.1	13.5	22.5	19.1	16.4	24.1	12.2	21.9
CaO	17.1	15.7	4.5	4.3	16.1	4.7	16.4	14.4	4.4	5.7	17	4.1	16.5	5.1
Na_2O	0.19	0.17	0.01	0.02	0.12	0.01	0.15	0.12	0.01	0.02	0.23	0.01	0.15	0.01
Total	98.68	98.9	100.8	100.6	100.4	100.7	100.6	99.6	100.8	100.52	98.93	98.51	99.2	98.2
Mg#	81.1	68.7	61.3	72.6	75.8	69.3	73.0	57.4	67.4	60.9	72.1	73.6	56.9	69.8
Fs	12.3	21.2	35.6	25.1	16.3	27.8	18.1	29.6	29.8	34.7	18.1	24.2	27.9	27.1
Wo	35.3	32.3	9.1	8.5	32.5	9.3	33.5	30.6	8.7	11.7	34.9	8.3	35.6	10.4
En	52.4	46.5	55.3	66.4	51.2	62.9	48.4	39.8	61.5	53.6	47.0	67.5	36.5	62.5

Table 4. Continued

Dike 2

	ES-1		AB-1		CP-1		NC-1	
	CPX	LCP	CPX	LCP	CPX	LCP	CPX	LCP
SiO_2	51.6	50.9	52.2	52.1	53.3	53.7	51.8	52.6
TiO_2	0.37	0.21	0.34	0.50	0.27	0.31	0.48	0.41
Al_2O_3	2.9	0.61	4.1	1.6	2.1	0.82	3.5	0.82
Cr_2O_3	0.44	0.01	0.89	0.01	0.38	0.01	0.26	0.01
FeO	7.8	21.5	6.8	14.9	6.9	17.5	7.9	20.7
MnO	0.22	0.67	0.15	0.50	0.17	0.46	0.21	0.65
MgO	16.3	18.6	16.3	15.4	17.6	24.4	15.8	18.9
CaO	18.9	6.1	19.3	14.1	19.1	3.4	18.3	3.9
Na_2O	0.28	0.01	0.23	0.26	0.28	0.01	0.24	0.01
Total	98.88	98.54	100.2	99.4	100.02	100.55	98.55	98.13
Mg#	78.8	60.7	81.0	64.8	82.0	71.3	78.1	61.9
Fs	12.8	34.4	11.2	24.7	11.1	26.7	13.4	34.9
Wo	39.6	12.5	40.9	29.8	39.1	6.8	39.3	8.5
En	47.6	53.1	47.9	45.5	49.8	66.5	47.3	56.6

Each column is a representative average of 3-13 points analyzed per grain.

Mg# = [(MgO/40.3)/(MgO/40.3+ FeO/71.85)]*100

Figure 10. Pyroxene compositions for the two diabase dike system samples plotted as endmembers diopside, enstatite, ferrosilite, and hedenbergite (Di, En, Fs and Hd). Each plotted point represents an analyzed point, and 6-13 points were analyzed per grain for 2-4 pyroxene grains per sample.

Dike system 1

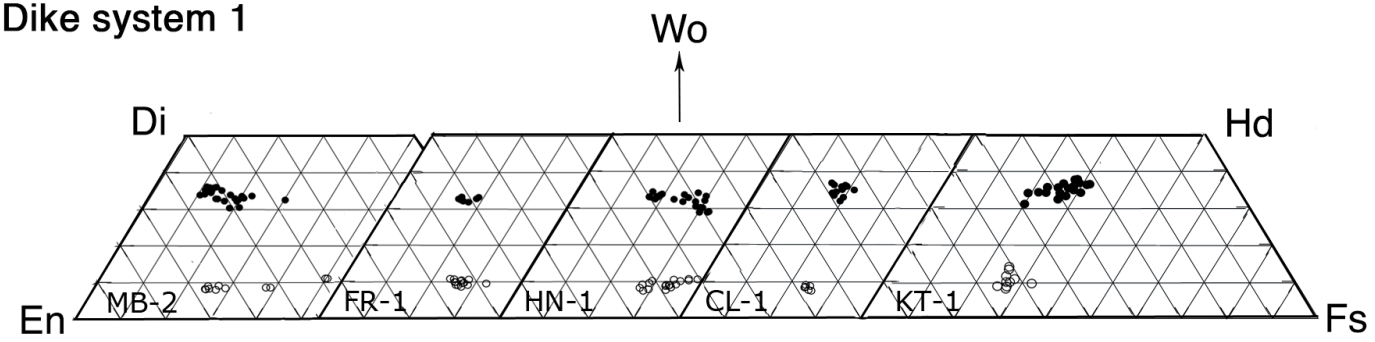

● clinopyroxene ○ low-Ca pyroxene

Dike system 2

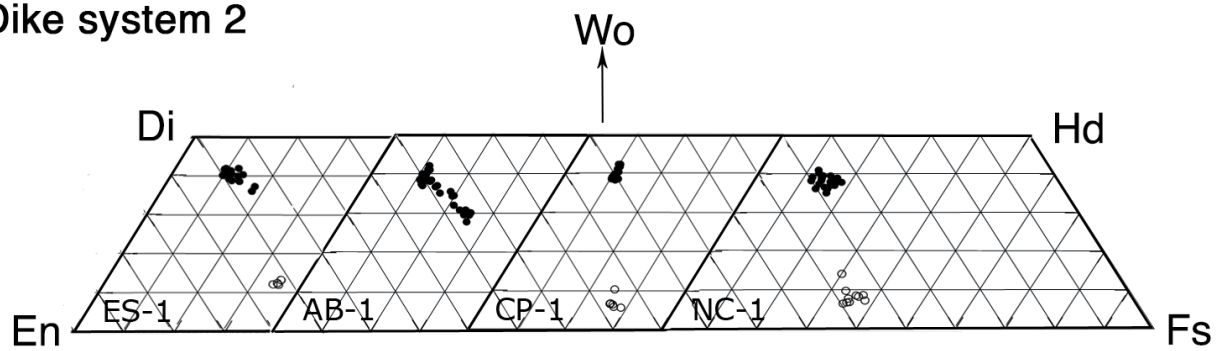

● clinopyroxene ○ low-Ca pyroxene

Olivine

Average compositions for representative olivine grains in dike system 2 are listed in Table 5, and are plotted in Figure 11 as Fo (forsterite endmember) for individual points. The four examined samples have olivine only as matrix grains that are in intergranular to subophitic textures with clinopyroxene and plagioclase laths (Figure 2-I and J). Three to four grains were analyzed in each of four samples. Three dike system 2 samples have olivine with relatively high Fo core areas, ~Fo_{81-87}, coexisting with grains that have overall lower Fo, ~Fo_{60-80} (Table 5; Figure 11). All olivine rims have lower Fo relative to cores, some as low as 52 to 55 mol% (Figure 11). In the fourth sample (CP-1), ~Fo_{70-74} was the only composition observed (Table 5; Figure 11).

Figure 12 shows the positive correlation between Fo and NiO. The highest NiO is about 0.4 wt% in the >Fo_{80} olivine, and lowest NiO is <0.05 wt.% in <Fo_{60} olivine.

The most Fo-rich core compositions observed for each grain were used to evaluate whether the olivine cores were in equilibrium with liquid compositions represented by their whole-rock compositions. The olivine compositions used are the most Mg-rich analytical points observed in olivine in each sample, and their corresponding FeO/MgO K_Ds are listed in Table 6. An olivine-liquid FeO/MgO partitioning coefficient of $K_D = 0.3 \pm 0.03$ represents olivine/liquid equilibrium (Roeder and Emslie, 1970). Based on this standard, olivine in sample AB-1 with $K_D \approx 0.35$ and sample NC-1 with $K_D \approx 0.33$ (Table 6) crystallized from liquid compositions close to those of their host rocks. High FeO/MgO partition coefficients in samples CP-1 and ES-1 ($K_D \approx 0.83$ and 0.53, respectively; Table 6) suggest that they

crystallized from melt compositions more evolved (lower MgO) than their host rocks (e.g., during late-stage matrix crystallization).

Olivine compositions from the study of Callegaro et al. (2013) both overlap those for dike system 2 samples and extend to higher and lower Fo compositions, ~Fo_{89-48}. However, Callegaro et al. (2013) stated that their olivine grains are phenocrysts, whereas dike system 2 olivines are small matrix grains (Figure 2-I and J).

Table 5. Average compositions (wt.%) of representative olivine grains in dike system 2 in central North Carolina.

	Dike system 2							
	NC-1		CP-1		ES-1		AB-1	
	1	2	1	2	1	2	1	2
SiO_2	35.7	37.9	37.4	37.7	36.1	37.9	35.1	37.8
FeO	36.5	17.1	25.3	24.5	29.8	19.4	34.6	17.2
MnO	0.61	0.27	0.44	0.45	0.56	0.33	0.61	0.28
MgO	28.4	43.1	35.9	37.9	32.5	41.7	28.6	44.1
CaO	0.15	0.34	0.17	0.16	0.31	0.29	0.32	0.36
NiO	0.07	0.31	0.12	0.15	0.12	0.25	0.12	0.31
Total	101.42	99.06	99.34	100.93	99.31	99.86	99.37	99.98
Fo (mol%)	58.1	81.8	71.7	73.4	66.1	79.3	59.5	81.9

Each column is an average of 6-14 points analyzed per grain.

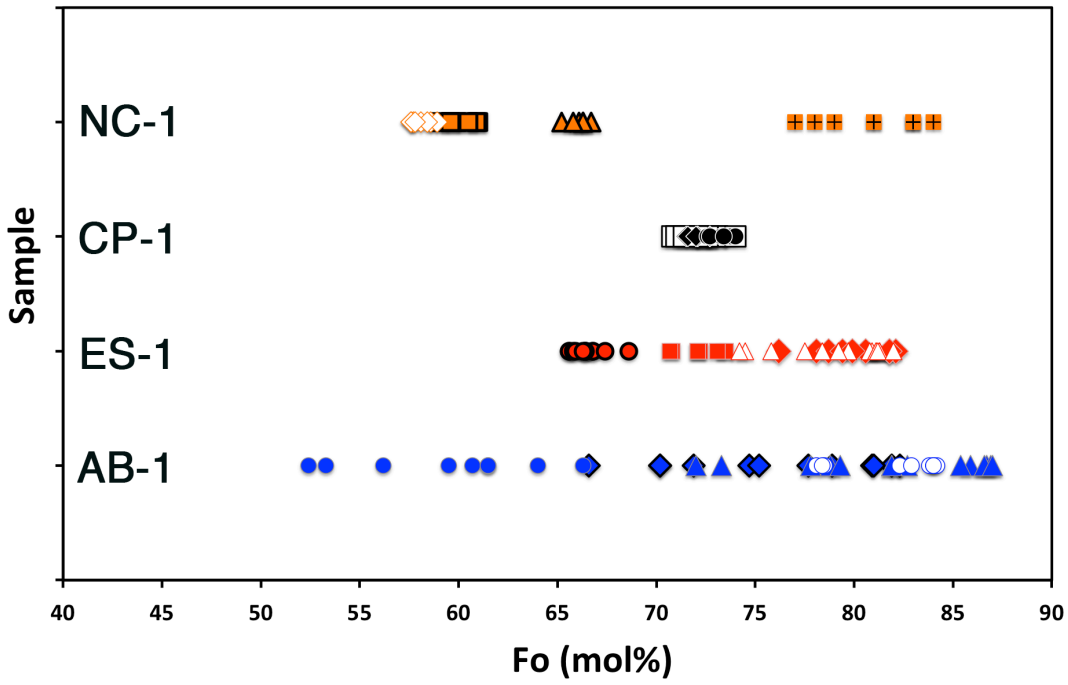

Figure 11. Forsterite (Fo) variation diagram for four samples from dike system 2. Within each sample line, each symbol type represents analyses of a single grain, and each plotted point represents one analyzed point.

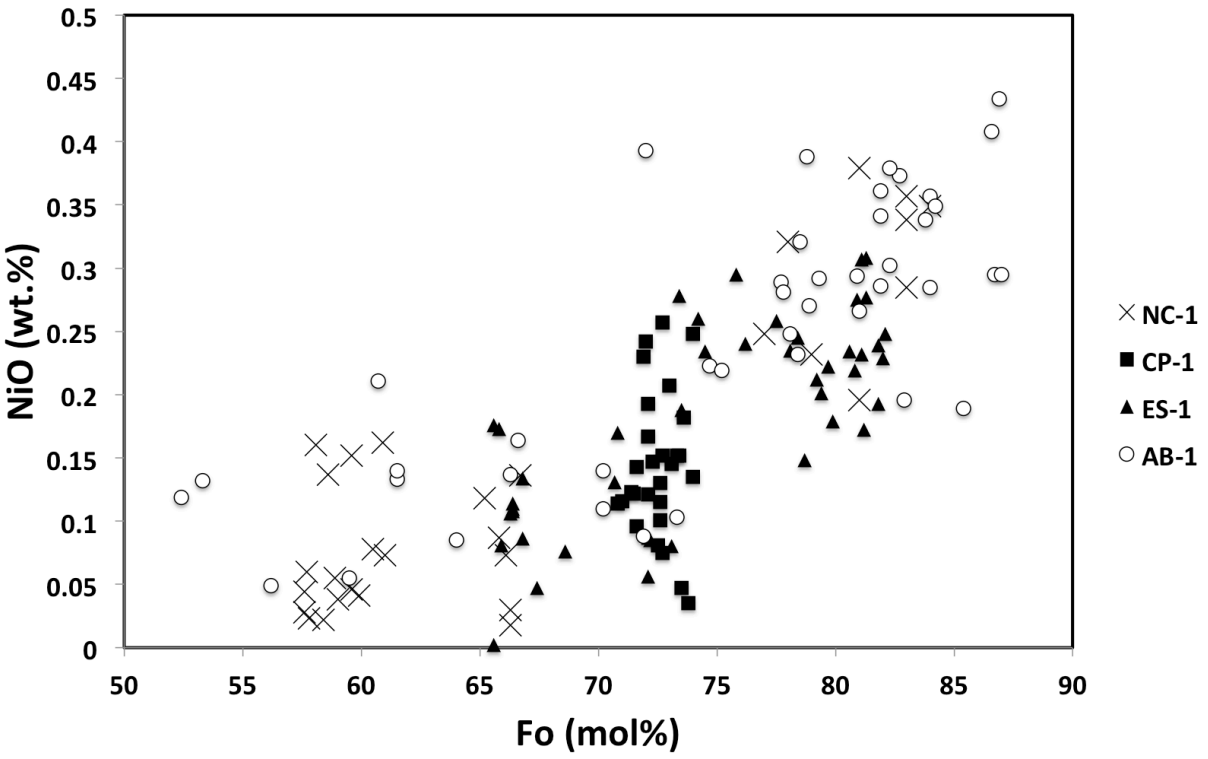

Figure 12. Forsterite (Fo) versus NiO diagram for olivines in four samples of dike system 2. Each symbol type represents point analyses on 3-4 grains in each sample.

Table 6. The most Fo-rich portions of olivines in four samples of dike system 2.

	NC-1	CP-1	ES-1	AB-1
SiO_2	39.2	38.1	38.5	37.9
FeO	15.2	22.7	17.0	12.8
MnO	0.27	0.47	0.34	0.14
MgO	45.4	36.1	43.7	47.8
CaO	0.32	0.15	0.33	0.39
NiO	0.35	0.14	0.25	0.41
Total	100.8	97.67	100.09	99.55
Fo	84.2	74.0	82.1	86.9
$K_D^{Fe/Mg}$	0.33	0.83	0.53	0.35

$K_D^{Fe/Mg}$ represents the partitioning coefficient established for the most Mg-rich composition with respect to its host sample FeO/MgO.
Each column is an analysis of a single point.

Fe-Ti oxide minerals

Average representative Fe-Ti oxide compositions are in Table 7, and FeO versus TiO_2 point analyses are plotted in Figure 13. All samples have Fe-Ti oxides only as matrix grains that are in intergranular to subophitic textures with clinopyroxene, plagioclase laths and olivine (Figure 2-E and F).

Dike system 1 oxides are titaniferous magnetites that form a compositional overlapping continuum of FeO negatively correlating with TiO_2 (Figure 13), where ulvospinel (Usp) molecule ranges from ~26 to 67 mol% (Table 7). Sample HN-1 additionally has grains that are part titaniferous magnetite and part ferrian-ilmenite (Figure 13), for which the average TiO_2 is ~30 wt.% and average hematite (Hem) molecule is ~41 mol% (Table 7).

Dike system 2 samples have titaniferous magnetite that is distinct from that in dike system 1 by lower FeO relative to TiO_2 (Figure 13). The lesser FeO is made up for by slightly higher Al_2O_3 and MgO in dike system 2 Fe-Ti oxide minerals compared to those in dike system 1 (Table 7). The Usp in these minerals is ~20 to 45 mol% (Table 7). Two samples have ilmenite coexisting with titaniferous magnetite, where the Hem molecule is ~10 to 14 mol% (Table 7; Figure 13). This affords the opportunity to apply a two-oxide geothermometer and oxygen barometer (e.g., Ghiorso and Evans, 2008). The equilibrium temperatures calculated are 740°C and 910°C at oxygen fugacities of 10^{-15} and 10^{-12}, respectively (Table 7) for samples NC-1 and CP-1. These values are ~ 0.1 to 0.3 log units above the NNO oxidation buffer and represent relatively oxidizing conditions. The lower

equilibrium temperature in sample NC-1 appears to be consistent with its higher whole rock FeO/MgO compared to CP-1 (Table 2), because a lower equilibrium temperature is likely to occur in a relatively evolved magma.

In the study of Callegaro et al. (2013), samples have Fe-Ti oxide minerals that are Cr-spinel (20-36 wt.% Cr_2O_3), Ti-magnetite (11-22 wt.% TiO_2) and ilmenite (46-48 wt.% TiO_2). Compared to Callegaro et al. (2013) samples, my dike samples have wider TiO_2 (and Usp) range for Ti-magnetite (TiO_2 ~5 to 35 wt.%) but similar ilmenite TiO_2 range (~45 to 50 wt.%) (Figure 13). However, due to the lack of FeO-abundance data in Callegaro et al. (2013), no direct comparison of oxide compositions can be made to my study.

Table 7. Average compositions of representative titaniferous magnetite (Mt), ilmenite (Ilm) and ferrian-ilmenite (Fe-ilm) in samples from two diabase dike systems in central North Carolina.

	Dike system 1					
	HN-1		KT-1		CL-1	
	Fe-ilm	Mt	Mt	Mt	Mt	Mt
TiO_2	30.1	11.6	20.8	24.1	11.1	16.9
Al_2O_3	0.62	1.5	1.4	1.6	1.4	1.2
Cr_2O_3	<0.01	0.04	<0.01	0.04	<0.01	0.10
FeO	63.3	78.8	71.6	72.4	80.4	78.3
MnO	0.74	0.38	0.43	0.57	0.49	0.48
MgO	0.17	0.17	0.12	0.38	0.52	0.03
Sum	94.96	92.48	94.23	99.09	93.89	97.01
Recalculated FeO and Fe_2O_3						
FeO	26.0	40.1	48.7	52.6	39.5	46.3
Fe_2O_3	41.4	43.0	25.5	22.0	45.5	35.6
Total	99.04	96.83	96.82	101.34	98.48	100.61
mol% endmembers						
Usp	-	34.1	61.3	67.6	31.0	48.0
Hem	40.8	-	-	-	-	-

	Dike system 2						
	NC-1		CP-1		ES-1	AB-1	
	Ilm	Mt	Ilm	Mt	Ilm*	Mt	Mt
TiO_2	48.3	7.1	44.7	12.2	46.5	14.8	14.8
Al_2O_3	0.18	3.6	0.19	2.5	<0.01	2.1	2.3
Cr_2O_3	<0.01	<0.01	0.04	0.07	<0.01	0.06	0.01
FeO	48.3	79.5	46.0	70.4	46.7	69.5	70.4

Table 7. Continued

MnO	0.62	0.33	0.28	0.38	4.9	1.3	1.4
MgO	2.3	0.41	3.63	2.7	0.16	0.47	0.52
Sum	99.64	90.92	94.84	88.25	98.11	88.23	89.43
Recalculated FeO and Fe_2O_3							
FeO	38.7	35.2	33.5	35.3	36.6	40.0	40.3
Fe_2O_3	10.6	49.3	13.9	39.1	11.2	32.8	33.6
Total	100.76	95.85	96.22	92.23	99.22	91.57	92.85
mol% endmembers							
Usp	-	20.6	-	31.9	-	44.9	44.1
Hem	9.9	-	13.5	-	10.8	-	-
T°C	740		910				
$\log_{10} fO_2$	10^{-15}		10^{-12}				

Each column is the average of 5 to 7 points analyzed on a single grain. *ES-1 ilmenite composition represents a single point analysis.
Usp = mol% ulvospinel
Hem = mol% hematite
T°C is the lowest temperature for Fe-Ti exchange

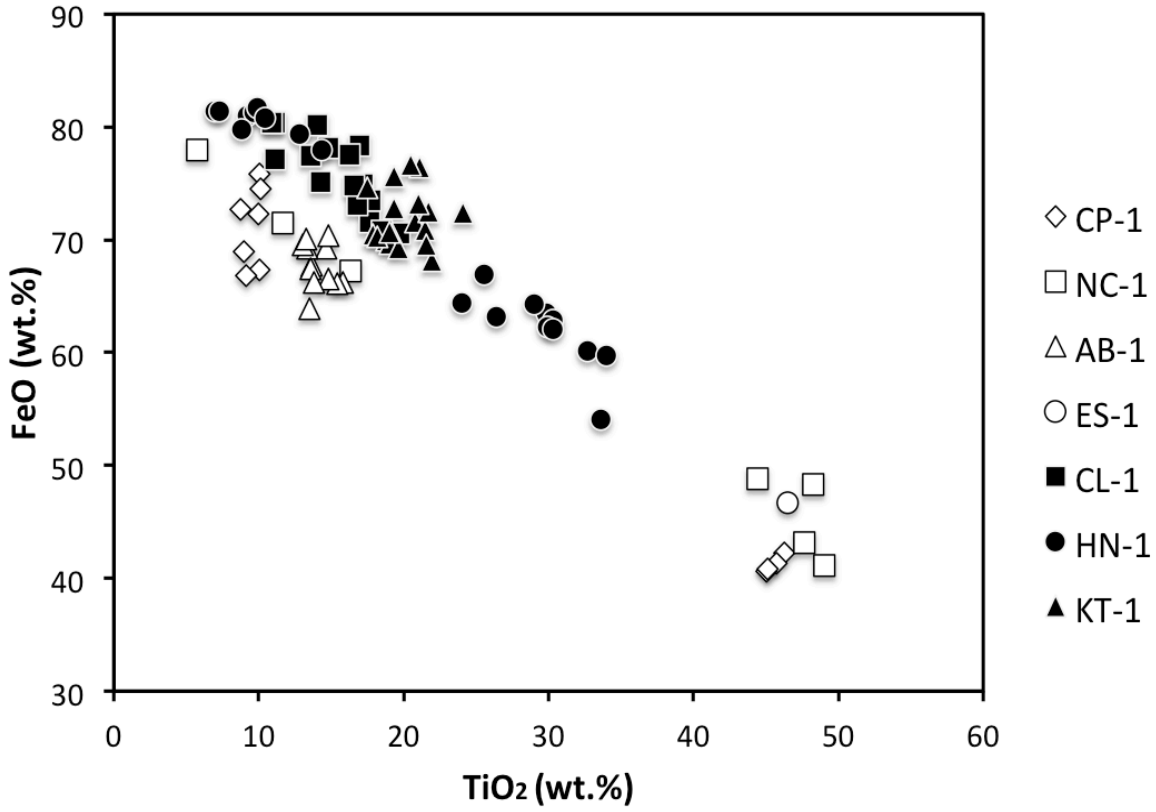

Figure 13. TiO_2 versus total Fe as FeO in Fe-Ti oxide minerals plotted as point-analyses. Each symbol represents an analyzed point. Closed symbols represent analyzed points for dike system 1 samples, and open symbols represent analyzed points for dike system 2 samples.

DISCUSSION

Based on the major and trace element abundances and mineral compositions for the two neighboring dike systems, there are many similar characteristics among samples within each dike system, and notable differences between the two dike systems (e.g., dike system 1 samples are much more evolved than dike system 2 samples, and have plagioclase phenocrysts). The similar and different compositional and mineralogical characteristics of the two dike systems pose several petrologic problems to examine and address. These include (1) how the samples within each dike system are petrologically related to one another; (2) how the two dike systems are related to each other; (3) what role, if any, did crustal contamination play in the magmatic compositions of each system; (4) what trace element characteristics can be identified for the parent material for each dike system; and, on a regional scale, (5) whether either dike system can be part of the magmatic systems identified by previous workers for regional CAMP dikes across North Carolina. It is also necessary to address why Ca-rich plagioclase phenocrysts (xenocrysts) are present in the most evolved dikes.

Therefore, I address these petrologic problems by: (1) using mass balancing, Rayleigh fractionation, MELTS software and mineral compositions to evaluate fractionation relationships among samples within each dike system and between the two dike systems; (2) examining the abundances of major and trace elements for indications of continental crust input into the dike compositions; (3) using trace element abundance ratios to determine source-area relationships between the two dikes systems and trace element

heterogeneity in their sources; (4) using trace element abundance ratios to evaluate whether CAMP samples from the broader North Carolina region share source areas with that of either dike system 1 or dike system 2, and to evaluate trace element heterogeneity in the source(s) for North Carolina CAMP dikes; and (5) modeling the magma reservoir conditions for the highly evolved dike rocks containing high-An plagioclase phenocrysts (glomerocrysts).

Fractional Crystallization

As presented in Figures 4 and 5, the two dike systems fall into two distinct MgO ranges (dike system 1, ~7.8 to 3.3 wt.%; dike system 2, ~13.7 to 9.1 wt.%; Table 2). There are negative correlations of most major elements with MgO across the relatively large MgO ranges that suggest fractional crystallization relationships within each dike system. For example, in dike system 1, TiO_2, K_2O, Al_2O_3, P_2O_5 and Na_2O all inversely correlate with MgO (Figure 5). There are also some highly incompatible trace elements in dike system 1 samples, such as Sr, Nb, Zr and Hf, that negatively correlate with MgO (Figure 6). In dike system 2, SiO_2, CaO, TiO_2, Na_2O and K_2O inversely correlate with MgO to also suggest fractional crystallization relationships within this dike system (Figure 5). There are also weak negative correlations between MgO and some highly incompatible trace elements, such as Sr and La (Figure 6) in dike system 2.

Moreover, a MgO versus Al_2O_3/CaO diagram (Figure 14) suggests fractional crystallization with respect to plagioclase and clinopyroxene removal. In dike system 1, as MgO decreases, the Al_2O_3/CaO ratio increases suddenly at MgO ~5.1 wt.%, due to either an

increase in Al_2O_3 or a decrease in CaO, which suggests removal of clinopyroxene relative to plagioclase. However, in dike system 2, as MgO decreases, the increase in Al_2O_3/CaO ratio is weaker, which suggests that the two dike systems had different plagioclase/clinopyroxene fractionation histories.

These major and trace element relationships for the two dike systems provide good reasons to explore whether samples within each dike system are related by fractional crystallization.

Mass Balancing

For major element fractional crystallization modeling, I used linear regression least squares mass balancing to test the following hypotheses: (1) in dike system 1, the highest-MgO sample RV-1 (MgO ~7.8 wt.%) is a parent for the lowest-MgO sample KT-1 (MgO ~3.3 wt.%) and the basaltic andesite sample CL-1 (SiO_2 ~52.1 wt.%; MgO ~4.3 wt.%); (2) in dike system 2, the most primitive sample ES-1 (MgO ~13.7 wt.%) is a parent for both the most evolved sample NC-1 (MgO ~9.1 wt.%) and a moderately evolved sample CP-1 (MgO ~10 wt.%); and (3) the moderately evolved sample CP-1 is a parent for the most evolved sample NC-1.

For dike system 1, Table 8 shows that sample RV-1 (MgO ~7.8 wt.%) can crystallize 26% plagioclase, 17.3% clinopyroxene and 16.3% orthopyroxene to yield sample KT-1 (MgO ~3.3 wt.%) as 40.3% residual liquid (Table 8). These mineral compositions are the average mineral compositions analyzed by electron microprobe in sample RV-1 (see mineral

compositions section). This model provides a good mathematical fit as suggested by the low sum of the squares of 0.33 (Table 8).

A second mass balancing calculation (Table 8) shows that sample RV-1 can crystallize 25.2% plagioclase, 17.5% clinopyroxene, 13.7% orthopyroxene, and 0.7% magnetite to yield the basaltic andesite sample CL-1 as 42.8% residual liquid (Table 8). This model provides a better fit to the data with sum of squares of 0.07 (Table 8). This model shows calculated results similar to those for the first model but includes a trace amount of magnetite in the crystallization products.

For both models, considerable orthopyroxene and clinopyroxene are calculated, which differs from the modal mineralogy (Table 1), where orthopyroxene and clinopyroxene are present only as matrix grains ~ 0.1 mm and ~ 0.5-1 mm in size, respectively (Table 1), and not as phenocrysts. These results show only that a magma composition similar to RV-1 can mathematically yield low MgO compositions similar to KT-1 and CL-1. If clinopyroxene and orthopyroxene had crystallized from RV-1, they would have required relatively high pressure. For example, orthopyroxene requires 1800-900 MPa to crystallize at temperature of 1350-1095 °C, and clinopyroxene can require even higher pressure (e.g., ~2700-1500 MPa) (Green et al., 1967; Bender et al., 1978; Blatter et al., 2013). Therefore, if RV-1 composition could crystallize orthopyroxene and clinopyroxene to yield low-MgO liquids (e.g., CL-1 and KT-1) as the models suggest, this would occur at middle to lower crustal pressures.

Even though RV-1 can be parental to KT-1 and CL-1, it is also low in MgO (~7.8 wt.%) relative to other CAMP rocks (e.g., MgO ~10.1 wt.% in Martins et al. (2008); MgO

~13.9 wt.% in Callegaro et al. (2013)). Therefore RV-1 could have been derived from a more primitive magma. To explore this origin for RV-1, a primitive sample (C-1) with MgO ~13.9 wt.% was chosen from Callegaro et al. (2013) as a candidate parent for a mass balancing calculation. Its composition is shown in Table 11. The calculation shows that sample C-1 (MgO ~13.9 wt.%) can crystallize 7.9% plagioclase, 9.8% clinopyroxene and 13.9% olivine to yield sample RV-1 (MgO ~ 7.8 wt.%) as 68.4% residual liquid (Table 11). This model provides a good mathematical fit as suggested by the low sum of the squares of 0.36 (Table 14). Therefore, this model is consistent with RV-1 being already evolved from a primitive parent magma.

Dike system 2 shows slightly positive correlation of Ni and Cr with MgO, suggesting possible olivine and clinopyroxene fractionation from a primitive parent, such as ES-1 (MgO ~13.7 wt.%) (Figure 6). Even though samples from dike system 2 are aphyric, whereas mass balancing modeling typically requires crystallization of phenocrysts, it is insightful to use the mass balance calculation to test if any fractional crystallization relationship can explain the compositional characteristics within the dike system.

Mass balancing calculation suggests ~21.1% crystallization (plagioclase, ~3.6%; clinopyroxene, ~4.4%; olivine, ~12.5%; magnetite, ~0.6%) occurred to create the most evolved sample NC-1 (MgO ~9.1 wt.%) from the parent ES-1 (Table 9). The sum of squares is 0.33 for this model (Table 9).

To explore the relationship throughout dike system 2, the moderately evolved sample CP-1 (10 wt.%) is also introduced into the calculation as a daughter of ES-1, and also as a parent for NC-1. When CP-1 is the daughter of ES-1, CP-1 represents 76.8% liquid

remaining after ES-1 crystallized 2.7% plagioclase, 1.2% clinopyroxene, 7.1% orthopyroxene and 12.1% olivine with a fit of 0.13 sum of squares (Table 9). This model shows calculated crystallization percentage similar to the first model (first model, ~78.9%, second model, ~76.8%). There are some differences, however, such as clinopyroxene compositions (e.g. Mg# ~78.8 for the first model, Mg# ~64.4 for the second model), and the first model includes a trace amount of magnetite crystallization, whereas the second model includes orthopyroxene crystallization.

When CP-1 (MgO ~10 wt.%) is used as the parent for NC-1 (MgO ~9.1 wt.%), the mass balancing model shows 24.5% plagioclase, 6.8% clinopyroxene and 9.4% olivine crystallization leaving 59.3% residual liquid (Table 10). The sum of squares for this model is 0.59 (Table 10).

All three models for dike system 2 show a considerable amount of phenocrysts crystallized. However, given that the samples are aphyric, the mass balancing calculation results do not exactly represent the modes of the parents.

In summary, mass balancing calculations provide reasonable models for relationships of fractional crystallization among samples within each dike system based on major element abundances. But because phenocrysts are not present in all the samples (except plagioclase phenocrysts in dike system 1 samples), I can say only that fractional crystallization relationships are capable of explaining the evolution of magma with similar chemical compositions. Each of the evolved (e.g., MgO <10 wt.%) samples appears to be a product of crystallization of clinopyroxene-, orthopyroxene- and olivine-phyric parent rocks not observed at the surface.

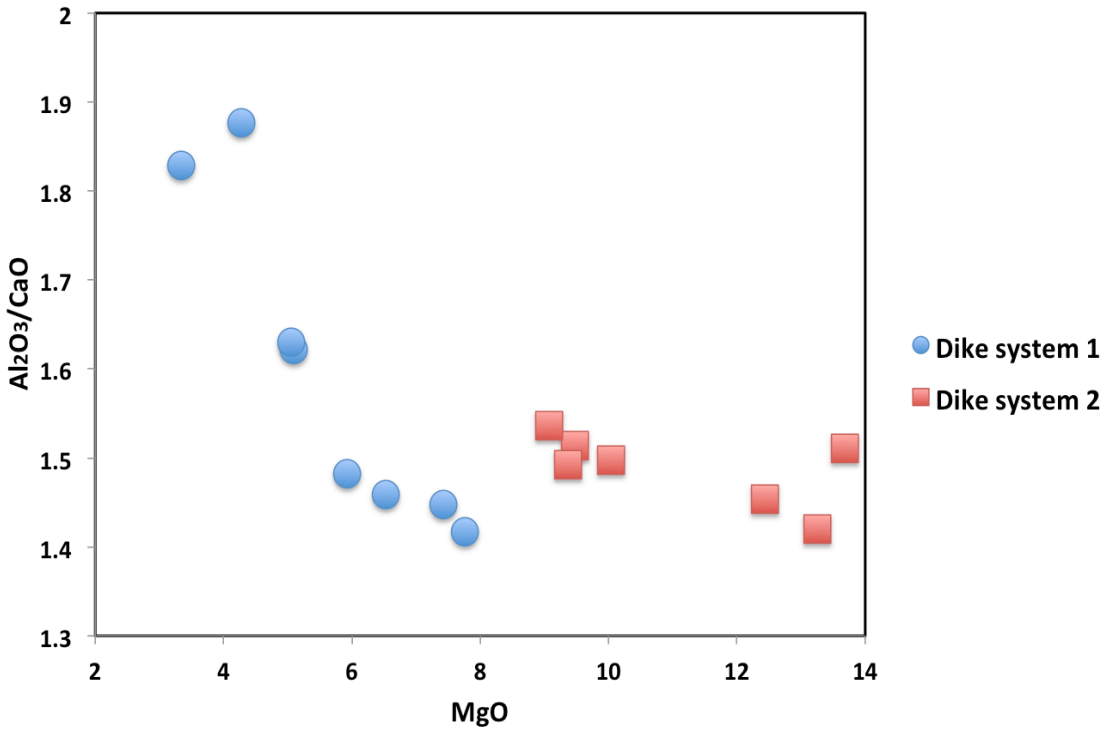

Figure 14. MgO vs. Al_2O_3/CaO plot suggesting two different fractional crystallization paths for the two dike systems based on different ratios of crystallizing plagioclase (relatively high Al) and clinopyroxene (relatively high Ca).

Table 8. Least squares mass balancing to relate most primitive sample RV-1 as parent to most evolved tholeiitic basalt sample KT-1 and to tholeiitic basaltic andesite sample CL-1 in dike system 1. Listed are the actual parent and calculated parent compositions, and the mineral abundances (in %) calculated for fractional crystallization relationships.

	Actual RV-1 parent composition	Calculated hypothetical parent composition to yield daughter (evolved) compositions	
		KT-1	CL-1
SiO_2	50.70	50.48	50.75
TiO_2	0.62	0.57	0.69
Al_2O_3	16.60	16.74	16.65
FeO	8.95	9.36	8.99
MnO	0.17	0.19	0.19
MgO	7.80	7.86	7.84
CaO	11.7	11.94	11.73
Na_2O	2.00	1.82	1.91
K_2O	0.31	0.27	0.53
From RV-1 parent, these phases crystallize in these percentages:			
Plag $An_{78.5}$		26.0	25.2
Cpx Mg#72.9		17.3	17.5
Opx Mg#69.8		16.3	13.7
Mt		-	0.70
Residual (liquid)		40.3	42.8
Σr^2		0.33	0.07

Table 9. Least squares mass balancing to relate most primitive sample ES-1 as parent to most evolved sample NC-1 and to medium-MgO composition sample CP-1 in dike system 2. Listed are the actual parent and calculated parent compositions, and the mineral abundances (in %) calculated for fractional crystallization relationships.

	Actual ES-1 parent composition	Calculated hypothetical parent composition to yield daughter (evolved) compositions	
		NC-1	CP-1
SiO_2	46.30	46.52	46.29
TiO_2	0.47	0.64	0.41
Al_2O_3	14.90	14.91	14.94
FeO	11.18	11.31	12.50
MnO	0.18	0.19	0.23
MgO	13.68	13.68	13.62
CaO	9.86	9.78	9.89
Na_2O	1.84	1.73	1.51
K_2O	0.22	0.25	0.16
From ES-1 parent, these phases crystallize in these percentages:			
Plag $An_{78.3}$		3.6	2.7
Cpx Mg#78.8		4.4	-
Cpx Mg#64.4		-	1.2
Opx Mg#60.7		-	7.1
Olv $Fo_{79.3}$		12.5	12.1
Mt		0.60	-
Residual (liquid)		78.9	76.8
Σr^2		0.33	0.13

Table 10. Least squares mass balancing to relate medium-MgO composition sample CP-1 as parent to most evolved sample NC-1 in dike system 2. Listed are the actual parent and calculated parent compositions, and the mineral abundances (in %) calculated for fractional crystallization relationships.

	Actual CP-1 parent composition	Calculated hypothetical parent composition to yield daughter (evolved) composition
		NC-1
SiO_2	47.12	47.46
TiO_2	0.49	0.46
Al_2O_3	18.19	18.41
FeO	8.44	8.82
MnO	0.14	0.14
MgO	10.04	10.17
CaO	12.15	12.34
Na_2O	1.95	1.87
K_2O	0.21	0.16
From CP-1 parent, these phases crystallize in these percentages:		
Plag $An_{74.9}$		24.5
Cpx Mg#81.9		6.8
Olv $Fo_{73.4}$		9.4
Residual (liquid)		59.4
Σr^2		0.59

Table 11. Least squares mass balancing to relate primitive sample C-1 (Callegaro et al., 2013) as parent to relatively evolved sample RV-1 in dike system 1. Listed are the actual parent and calculated parent compositions, and the mineral abundances (in %) calculated for fractional crystallization relationship.

	Actual C-1 parent composition	Calculated hypothetical parent composition to yield daughter (evolved) composition
		RV-1
SiO_2	48.41	48.86
TiO_2	0.52	0.46
Al_2O_3	14.15	14.25
FeO	8.56	8.82
MnO	0.17	0.18
MgO	13.86	13.96
CaO	10.09	10.09
Na_2O	1.65	1.41
K_2O	0.35	0.38
From CP-1 parent, these phases crystallize in these percentages:		
Plag $An_{78.3}$		7.9
Cpx Mg#78.84		9.8
Olv $Fo_{79.3}$		13.9
Residual (liquid)		68.4
Σr^2		0.36

Rayleigh fractionation calculations

To explore fractionation relationships between samples within each dike system based on their trace element abundances, Rayleigh fractional crystallization models were applied. The fractional crystallization models were calculated using the Rayleigh fractionation equation:

$$\frac{C_l}{C_o} = F^{(D-1)}$$

where C_l is the concentration in the melt after fractionation, C_o is the concentration in the melt before fractionation, F is the remaining melt fraction, and D is the bulk distribution coefficient for the minerals separated from basaltic melt. Published distribution coefficient values vary based on particular studies and experimental conditions. I used acceptable K_D values from the Geochemical Earth Reference Model (GERM) partition coefficient database (https://earthref.org/KDD/). Five fractional crystallization models are calculated based on the five mass balancing calculation models for major elements (i.e., crystallizing phases in percentages calculated from mass balancing are used with corresponding D values for Rayleigh fractionation calculations). Results are in Tables 12, 13 and 14.

To make results easier to examine, actual and calculated trace element abundances are normalized to parent trace element abundances for each model and plotted in Figures 15, 16 and 17. By using the mineral phases from the mass balancing calculations, all models show normalized values for actual and calculated daughters' trace elements that are similar. The normalization ratios differ by factors of only 0.7 to 1.6 (actual/calculated), except when ES-1 is the parent for CP-1 daughter (normalization ratios ~2 to 3). For this last relationship, a trace amount of accessory minerals (i.e., zircon and titanite) have to be added to get better results. When adding to the calculation 0.4 vol% titanite and 0.03 vol%

zircon, actual and calculated CP-1 trace element abundances provide a better fit (Figure 16b). This method is considered acceptable, because these accessory minerals can be sometimes present in basaltic magma (e.g., Hinton and Upton, 1991; Evans and Hanson, 1993).

In summary, Rayleigh fractionation calculations for trace element abundances provide additional support for fractional crystallization relating samples within each dike system.

Table 12. Rayleigh fractionation calculation[1] using (1) RV-1 as C_o and KT-1 as C_l, (2) RV-1 as C_o and CL-1 as C_l. All abundances are in ppm.

		KT-1 (F = 40.3%)		CL-1 (F = 42.8%)	
	C_o (RV-1)	C_l (calculated)	C_l (actual)	C_l (calculated)	C_l (actual)
Rb	9.8	17.3	13.6	22.8	33.8
Ba	91	151	152	193	218
Nb	2.2	5.4	4.7	5.1	8.3
La	4.8	8.7	8.5	10.4	13.9
Sr	134	208	251	154	215
Zr	42.6	102	86.8	95.5	114
Hf	1.2	2.1	2.4	1.9	3.1
Y	20.5	41.7	27.4	39.6	31.8
Sc	42.1	33	33.3	32.9	35.2

Table 13. Rayleigh fractionation calculation[1] using (1) ES-1 as C_o and NC-1 as C_l, (2) ES-1 as C_o and CP-1 as C_l. All abundances are in ppm.

		NC-1 (F = 78.9%)		CP-1 (F = 76.8%)	
	C_o (ES-1)	C_l (calculated)	C_l (actual)	C_l (calculated)	C_l (actual)
Rb	2.3	5.8	4.5	2.3	2.9
Ba	163	189	138	163	181
Nb	1.5	1.9	2.2	1.5	1.1
La	4.1	5.1	5.2	4.0	3.1
Sr	92	154	160	92	115
Zr	38.9	48.8	43.1	38.9	32.3
Hf	1.1	1.0	1.1	1.1	0.91
Y	16.1	19.7	21.9	16.1	15.3
Sc	34.9	38.9	38.5	34.9	39.1

[1] Raleigh fractionation equation: $\frac{Cl}{Co} = F^{(D-1)}$

C_l = resultant concentration in the melt after fractionation
C_o = concentration in the melt before fractionation
F = remaining melt fraction
D = bulk distribution coefficient for the minerals separated

Table 14. Rayleigh fractionation calculation[1] using CP-1 as C_o and NC-1 as C_l. All abundances are in ppm.

		NC-1 (F = 59.3%)	
	C_o (CP-1)	C_l (calculated)	C_l (actual)
Rb	2.6	4.4	4.5
Ba	91	138	138
Nb	1.3	2.1	2.2
La	3.1	4.9	5.2
Sr	135	157	160
Zr	31.2	42.6	43.1
Hf	0.91	1.5	1.1
Y	15.3	20.5	21.9
Sc	37.3	37.7	38.5

[1] Raleigh fractionation equation: $\frac{Cl}{Co} = F^{(D-1)}$

C_l = resultant concentration in the melt after fractionation

C_o = concentration in the melt before fractionation

F = remaining melt fraction

D = bulk distribution coefficient for the minerals separated

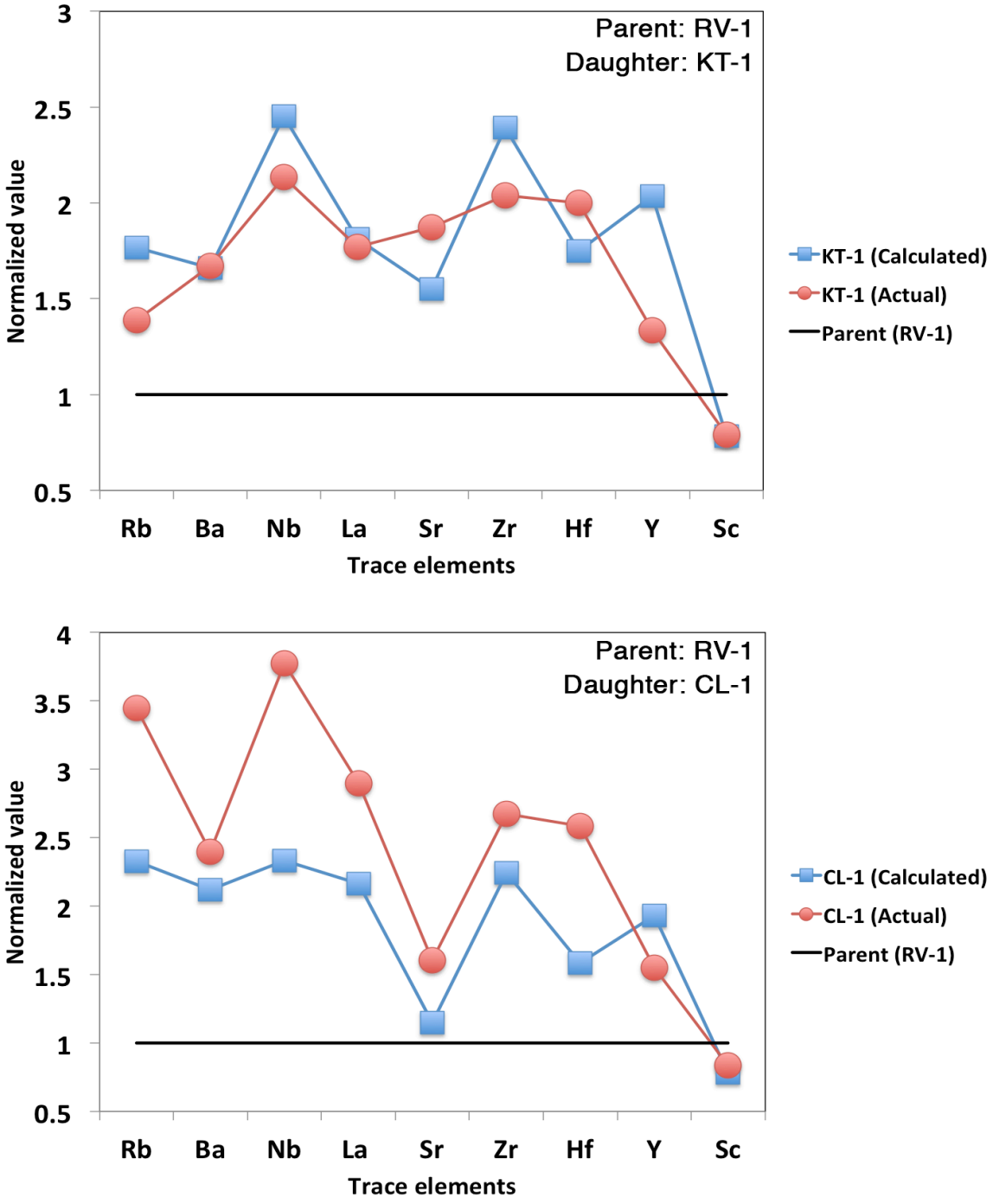

Figure 15. Diagrams show comparison of actual and calculated daughters (KT-1 and CL-1) trace element abundances. Trace element abundances are normalized to those of the parent RV-1.

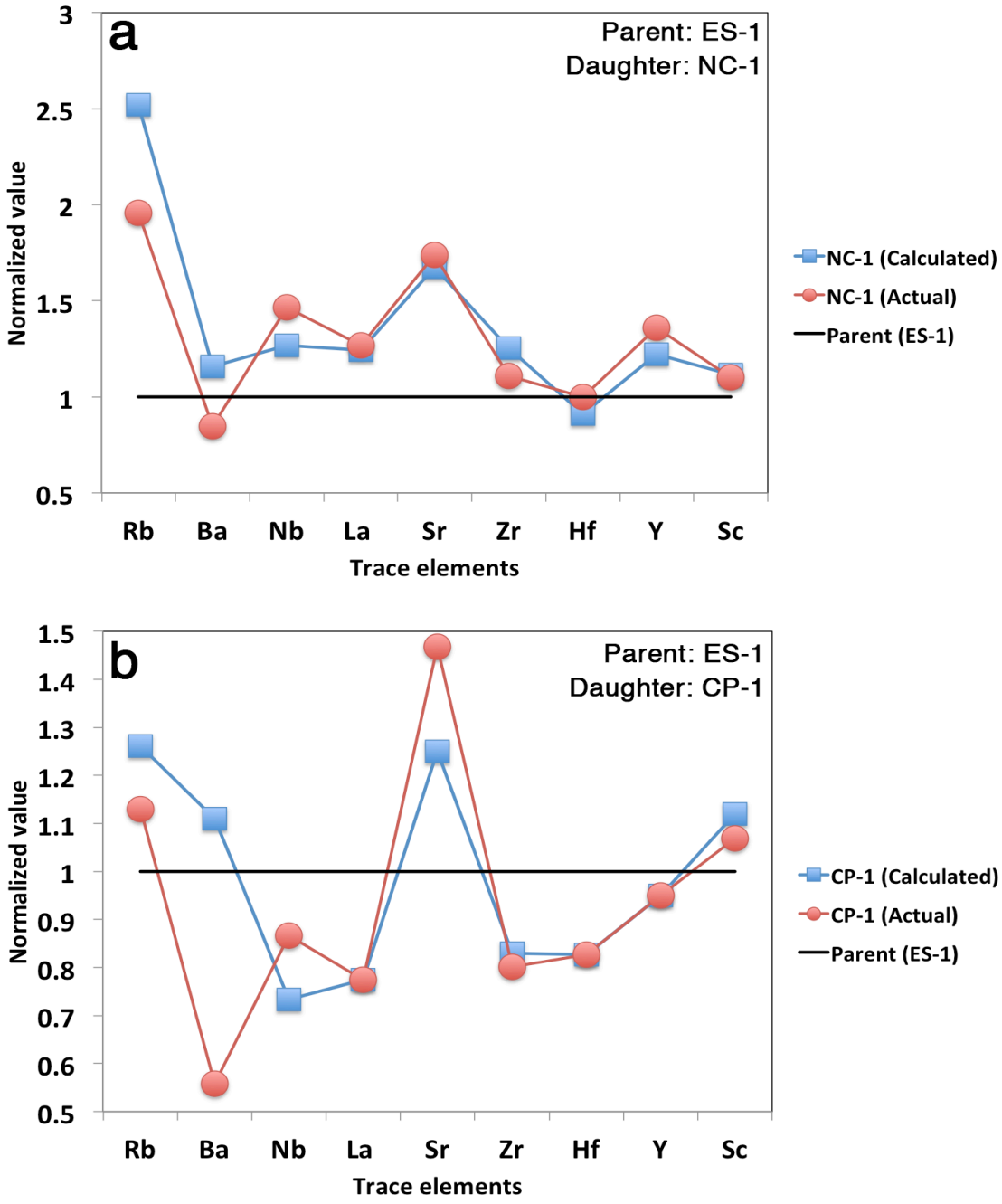

Figure 16. Diagrams show comparison of actual and calculated daughters (NC-1 and CP-1) trace element abundances. Trace element abundances are normalized to those of the parent ES-1.

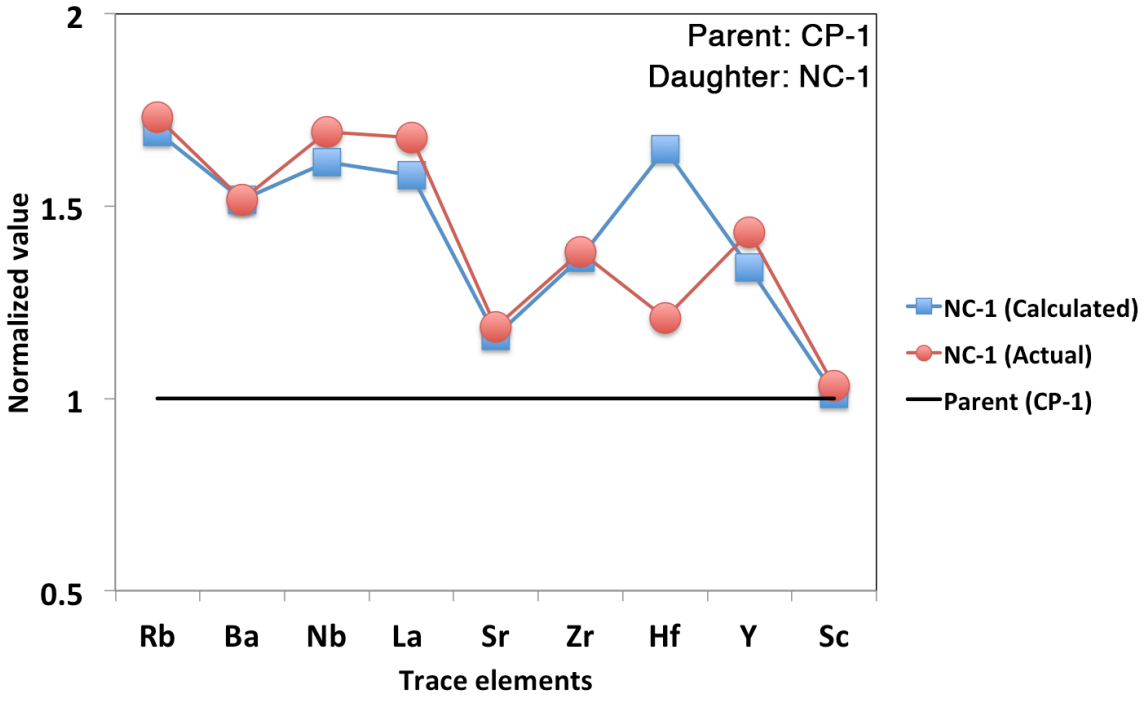

Figure 17. Diagram shows comparison of actual and calculated daughter (NC-1) trace element abundances. Trace element abundances are normalized to those of the parent CP-1.

MELTS modeling

Mass balancing does not evaluate fractional crystallization of basalt in terms of temperature, pressure, or oxygen fugacity. Therefore, as another evaluation of fractional crystallization that applies these magma parameters, I used MELTS (Ghiorso and Sack, 1995; Asimow and Ghiorso, 1998) to model liquids differentiated from the magma compositions used as parents in the mass balancing models for crystallization of each dike system. Pressures between 10 and 1000 MPa and redox conditions from FMQ+1 to FMQ-2 were tested in order to reach more detailed information about crystallization. In general, oxygen fugacities between FMQ-2 (slightly reducing) and FMQ+1 (slightly oxidizing) are reasonable to consider for basalt crystallization (Mallmann and O'Neill, 2007; Mayfield et al., 2011). Results for MELTS modeling are in Tables 15, 16, 17 and 18.

Two parent-daughter models were applied for dike system 1: (1) RV-1 (MgO ~7.8 wt.%) as parent and CL-1 (MgO ~4.3 wt.%) as daughter; and (2) RV-1 as parent and KT-1 (MgO ~3.3 wt.%) as daughter. Results are in Table 15.

When differentiating RV-1 composition containing 1 wt.% H_2O, daughter melt CL-1 can be produced at 500 MPa under redox condition of FMQ-2. The MELTS modeling shows that when the liquid differentiated from RV-1 reached MgO concentration approximating that of CL-1 (~4.3 wt.%), calculated abundances for other major elements are similar to those of CL-1 (Table 15). Crystallization temperature in the model decreased ~125°C from the liquidus temperature of 1228°C to the CL-1 MgO concentration at 1103°C. Total crystallization is 50.7% plagioclase, clinopyroxene and olivine (Table 15), compared to the

mass balancing calculation of 57.1% crystallization of plagioclase, clinopyroxene, orthopyroxene and magnetite (Table 8).

When using RV-1 to produce daughter KT-1, MELTS modeling produced reasonable results also at 500 MPa but at more oxidizing condition of FMQ, and only after adding 3 wt.% H_2O to the parent composition (Table 15). The calculated melt composition is similar to the actual KT-1 composition after ~140°C of crystallization from the liquidus temperature of 1183°C to KT-1 MgO composition at 1043°C. Liquidus and crystallization temperatures for this model are lower than those for the previous model due to the addition of higher H_2O to the parent composition. The model shows 33.7% crystallization of plagioclase, clinopyroxene and olivine (table 15), whereas the mass balancing shows twice the percentage of crystallizing phases, 59.6% plagioclase, clinopyroxene and orthopyroxene (Table 8). The high H_2O content (3 wt.%) in this model suggests that fractionation to produce acceptable results requires a very wet melt. However, such hydrous conditions are not apparent from the loss-on-ignition (LOI) of the samples that are 0.3-0.6 wt.% H_2O in dike system 1 (Table 2).

As presented in the mass balancing calculation (Table 14), the evolved RV-1 used in the MELTS modeling (above) can itself be derived from a hypothetical primitive CAMP dike composition (C-1 of Callegaro et al. (2013); MgO ~13.9 wt.%). To test this relationship in terms of magmatic conditions such as temperature, pressure and oxygen fugacities, another MELTS model was created (Table 16). MELTS produced reasonable results also at 500 MPa and FMQ-2 (as in the first model for RV-1 as parent), and after 0.5 wt.% H_2O was added to the parental composition (Table 16). A daughter composition similar to the actual RV-1 composition occurs after 20.6% crystallization of plagioclase and olivine (Table 16).

However, the mass balancing calculation shows a greater percentage of crystallization that includes clinopyroxene: 31.6% plagioclase, olivine and clinopyroxene (Table 14). Crystallization temperatures in the model decreased ~130°C from a high liquidus temperature of 1335°C to the RV-1 MgO concentration at 1205°C, which is close to the RV-1 liquidus of 1228°C (above; Table 15). This is consistent with RV-1 having been derived from a primitive high-MgO (~13.9 wt.%) parental melt such as ES-1, the most primitive sample in the neighboring dike system 2.

In these three MELTS models, olivine crystallization is involved, which is different from the mass balancing calculation and the modal mineralogy where there is no olivine in dike system 1 samples (Tables 1 and 8). As discussed in the mass balancing calculations, plagioclase and clinopyroxene can crystallize in relatively high pressures. Olivine can also crystallize under high pressures, and usually crystallizes prior to clinopyroxene and plagioclase (e.g., Helz, 2009). Olivine may therefore have segregated before dike system 1 magma was emplaced.

Three MELTS models were applied to samples of dike system 2: (1) ES-1 (MgO ~13.7 wt.%) as parent and CP-1 (MgO ~10 wt.%) as daughter; (2) ES-1 as parent and NC-1 (MgO ~9.1 wt.%) as daughter; and (3) CP-1 as parent and NC-1 as daughter. Results are in Tables 17 and 18.

When using ES-1 as a parent for dike system 2 samples CP-1 and NC-1, MELTS produced reasonable results only at very low crustal pressures, such as 10 and 20 MPa (Table 17). The best results for ES-1 to produce daughter CP-1 were at 10 MPa under redox condition of FMQ with 0.5 wt.% H_2O added to the parent. The MELTS modeling shows

that after the temperature decreased ~70°C from a liquidus of 1289°C to the CP-1 MgO concentration at 1219°C, the daughter liquid reached MgO concentration approximating that of CP-1 (~10 wt.%), and that the calculated abundances for other major elements are similar to actual concentrations in CP-1 (Table 17).

When using ES-1 to produce daughter NC-1, the best result was produced at 20 MPa under more reducing redox condition of FMQ-2 and also with 0.5 wt.% H_2O added to the parent. The MELTS modeling shows results similar to those for the first model, for which temperature decreased ~70°C from a liquidus of 1285°C to the NC-1 MgO concentration (~9.1 wt.%) at 1215°C, and calculated abundances for other major elements are similar to actual concentrations in NC-1 (Table 17). For these two models for ES-1, only olivine fractionation is involved (10.3% and 12.6%, respectively; Table 17), which coincides with olivine being the major phase in the mass balancing calculations (model 1 ~12.1%; model 2 ~12.5%; Table 10).

When using CP-1 to produce daughter NC-1, the best result was reached at a pressure of 100 MPa, higher than in the ES-1 parent model, but under the same redox condition of FMQ and 0.5 wt.% H_2O, similar to the first ES-1 model (Table 18). The MELTS modeling shows that after temperature decreased ~30°C from a liquidus temperature of 1220°C to the NC-1 MgO concentration (~9.1 wt.%) at 1190°C, calculated abundances for other major elements are similar to actual concentrations in NC-1 (Table 18). Phases crystallized are similar to those from the mass balancing calculation, with plagioclase being the major phase along with lesser clinopyroxene and olivine (Tables 12 and 18). However, the crystallization

percentage in the MELTS model (21.3%) is half of that in the mass balancing calculation, ~40.7% (Tables 12 and 18).

In summary, both mass balancing and MELTS modeling suggest that fractional crystallization can account for the compositional variations within each dike system. However, there are some differences between the results from mass balancing and MELTS. For example, for the same parent-daughter relationships, some mass balancing and MELTS models produced different crystallizing phases and crystallization percentages that differ by factors up to 2 (e.g., CP-1 to NC-1; 40.7% and 21.3%; Table 19). Moreover, phenocrysts crystallized in both mass balancing and MELTS models are not present in any samples, except plagioclase phenocrysts in dike system 1 samples, thereby leading to the inference that mafic minerals remained at depth in high-MgO parental magmas. Finally, it appears that both mass balancing and MELTS, when used for major element modeling, can only mathematically explain compositional variations during fractionation, but each calculates different percentages of crystallization.

MELTS models present notable differences for the conditions of crystallization in dike systems 1 and 2, such as much higher pressures, more reducing oxygen fugacities and higher water contents (Tables 15 and 16) in dike system 1 compared to near-surface pressures for the more MgO-rich dike system 2 samples (Tables 17 and 18). The inference can be made, then, that the olivine-dominated fractionation of olivine-normative magmas (dike system 2) transcended nearly the entire crustal thickness, whereas the quartz-normative magmas (dike system 1) underwent fractionation at mid-crustal levels under comparatively more hydrous conditions.

Table 15. MELTS modeling for fractional crystallization of parent RV-1 (MgO ~7.76 wt.%) to daughter CL-1 (MgO ~4.28 wt.%) and KT-1 (MgO ~3.34 wt.%) under conditions with varying pressure and fO_2. Phases crystallized from the parent melts are presented as percentages of the magma system along with compositions for RV-1 and two calculated residual daughter melts.

	Parent	Daughters			
	RV-1	CL-1 (calculated) FMQ-2; 1103°C 1 wt.% H_2O (500 MPa) liquidus T: 1228°C	CL-1 (actual)	KT-1 (calculated) FMQ-2; 1043°C 3 wt.% H_2O (500 MPa) liquidus T: 1183°C	KT-1 (actual)
SiO_2	50.51	52.63%	52.12%	50.73%	50.51%
TiO_2	0.62	0.89	1.05	0.51	1.21
Al_2O_3	16.58	16.48	17.94	18.84	18.40
FeO	8.95	11.76	9.14	9.46	11.13
MnO	0.17	0.06	0.16	0.08	0.16
MgO	7.76	4.17	4.28	3.48	3.34
CaO	11.70	8.50	9.56	9.21	10.06
Na_2O	2.01	2.64	3.00	2.63	2.89
K_2O	0.31	0.55	1.17	0.44	0.63
Fractionated phases (%)					
Pl		22.26 An_{75}		6.78 An_{84}	
Cpx		20.53 Mg#85		19.30 Mg#74	
Olv		7.92 Fo_{68}		7.62 Fo_{69}	

Table 16. MELTS modeling for fractional crystallization of parent C-1 (MgO ~13.56 wt.%, from Callegaro et al., 2013) to daughter RV-1 (MgO ~7.76 wt.%). Phases crystallized from the parent melt are presented as percentages of the magma system along with compositions for C-1 and calculated residual daughter melt.

	Parent	Daughter	
	C-1	RV-1 (calculated) FMQ-2; 1205°C 0.5 wt.% H_2O (500 MPa) liquidus T: 1335°C	RV-1 (actual)
SiO_2	48.41%	50.52%	50.65%
TiO_2	0.52	0.66	0.62
Al_2O_3	14.15	16.84	16.58
FeO	8.56	9.12	8.95
MnO	0.17	0.03	0.17
MgO	13.86	7.36	7.76
CaO	10.09	12.13	11.70
Na_2O	1.65	2.03	2.01
K_2O	0.35	0.44	0.31
Fractionated phases (%)			
Pl		2.34 An_{84}	
Olv		18.26 Fo_{82}	

Table 17. MELTS modeling for fractional crystallization of parent ES-1 (MgO ~13.68 wt.%) to daughter CP-1 (MgO ~ 10.04 wt.%) and NC-1 (MgO ~9.08 wt.%) under conditions with varying pressure and fO_2. Phases crystallized from the parent melts are presented as percentages of the magma system along with compositions for ES-1 and two calculated residual daughter melts.

	Parent	Daughters			
	ES-1	CP-1 (calculated) FMQ; 1219°C 0.5 wt.% H_2O (10 MPa) liquidus T: 1289°C	CP-1 (actual)	NC-1 (calculated) FMQ-2; 1215°C 0.5 wt.% H_2O (20 MPa) liquidus T: 1285°C	NC-1 (actual)
SiO_2	46.30%	47.28%	47.12%	47.58%	47.83%
TiO_2	0.47	0.53	0.49	0.54	0.70
Al_2O_3	14.90	16.65	18.19	17.20	17.19
FeO	11.18	9.55	8.45	11.10	11.44
MnO	0.18	0.18	0.14	0.18	0.17
MgO	13.68	10.05	10.04	9.04	9.08
CaO	9.86	10.98	12.15	11.32	11.19
Na_2O	1.84	2.06	1.95	2.12	2.17
K_2O	0.22	0.25	0.21	0.25	0.31
Fractionated phases (%)					
Olv		10.34 Fo_{82}		12.64 Fo_{81}	

Table 18. MELTS modeling for fractional crystallization of parent CP-1 (MgO ~10.04 wt.%) to daughter NC-1 (MgO ~9.08 wt.%). Phases crystallized from the parent melt are presented as percentages of the magma system along with compositions for CP-1 and calculated residual daughter melt.

	Parent	Daughter	
	CP-1	NC-1 (calculated) FMQ; 1190°C 0.5 wt.% H_2O (100 MPa) liquidus T: 1220°C	NC-1 (actual)
SiO_2	47.12%	47.96%	47.83%
TiO_2	0.49	0.62	0.70
Al_2O_3	18.19	16.66	17.19
FeO	8.44	9.94	11.44
MnO	0.14	0.16	0.17
MgO	10.04	9.14	9.08
CaO	12.15	12.00	11.19
Na_2O	1.95	2.20	2.17
K_2O	0.21	0.26	0.31
Fractionated phases (%)			
Pl		14.87 An_{86}	
Cpx		0.61 Mg#89	
Olv		5.81 Fo_{87}	

Table 19. Comparisons of results from fractional crystallization relationships calculated by mass balancing and MELTS. All abundances are in %.

	Mass Balancing		MELTS	
Dike system 1				
RV-1 / KT-1	Plag $An_{78.5}$	26	Plag An_{84}	6.8
	Cpx Mg#72.9	17.3	Cpx Mg#74	19.3
	OpxMg#69.8	16.3	Olv Fo_{69}	7.6
	Crystallization	59.6	Crystallization	33.7
RV-1 / CL-1	Plag $An_{78.5}$	25.2	Plag An_{75}	22.3
	Cpx Mg#72.9	17.5	Cpx Mg#85	20.5
	OpxMg#69.8	13.7	Olv Fo_{68}	7.9
	Mt	0.7		
	Crystallization	57.1	Crystallization	50.7
C-1 / RV-1	Plag $An_{78.3}$	7.9	Plag An_{84}	2.3
	Cpx Mg#78.8	9.8	Olv Fo_{82}	18.3
	Olv $Fo_{79.3}$	13.9		
	Crystallization	31.6	Crystallization	20.6
Dike system 2				
ES-1 / CP-1	Plag $An_{78.3}$	2.7	Olv Fo_{82}	10.3
	Cpx Mg#64.4	1.2		
	Opx Mg#60.7	7.1		
	Olv $Fo_{79.3}$	12.1		
	Crystallization	23.1	Crystallization	10.3
ES-1 / NC-1	Plag $An_{78.3}$	3.6	Olv Fo_{81}	12.6
	Cpx Mg#78.8	4.4		
	Olv $Fo_{79.3}$	12.5		
	Mt	0.6		
	Crystallization	21.1	Crystallization	12.6
CP-1 / NC-1	Plag $An_{74.9}$	24.5	Plag An_{86}	14.9
	Cpx Mg#81.9	6.8	Cpx Mg#89	0.6
	Olv $Fo_{73.4}$	9.4	Olv Fo_{87}	5.8
	Crystallization	40.7	Crystallization	21.3

Relationship between the two dike systems

To explore if the two dike systems are related to each other by fractionation of the high-MgO dike system 2 samples to yield the highly evolved dike system 1 samples, a MgO vs. Al_2O_3/CaO variation diagram is plotted (Fig. 14). This relationship is sensitive to the crystallization of clinopyroxene and plagioclase, two minerals that both mass balancing and MELTS demonstrate were part of dike system 1 fractionation history.

The mass balancing modelings for dike system 2 show minor amounts of plagioclase and clinopyroxene crystallization (Table 19). The MELTS modelings, however, show essentially no involvement of either plagioclase or clinopyroxene crystallization (Table 19). The low Al_2O_3/CaO slope formed by dike system 2 samples (Figure 14) confirms that fractionation to decrease MgO was essentially unaffected by clinopyroxene and plagioclase crystallization.

The mass balancing results for dike system 1 show more plagioclase crystallizing from, for example, RV-1, than clinopyroxene during fractionation (Table 19). In contrast, the fractionation results from one MELTS model show that the crystallized plagioclase/clinopyroxene percentage ratios are <1 (Table 19). In addition, the steep Al_2O_3/CaO slope formed by dike system 1 samples (Figure 14) suggests that clinopyroxene crystallized in greater abundance than plagioclase over the ~8 to 3 wt.% range in MgO. This does not agree with the mass balancing results (Table 19), but rather is consistent with the MELTS results where more clinopyroxene crystallized relative to plagioclase (Table 19).

In addition to the discrepancies between the Al_2O_3/CaO ratios, mass balancing and

MELTS modeling noted above, the Al_2O_3/CaO ratio plot for each dike system does not offer direct information about whether the two systems represent a continuum of fractionation. On the other hand, the gap in Al_2O_3/CaO at about 8-9 wt.% MgO suggests no relationship between the two dike systems because the gap breaks any continuum in Al_2O_3/CaO that may have connected them by continual changes in Al_2O_3/CaO during fractionation of one magma system. It is possible that the gap (drop in Al_2O_3/CaO between the two systems; Figure 14) resulted from a sudden crystallization and segregation of plagioclase from a magma having 8-9 wt.% MgO, then followed by much greater crystallization of clinopyroxene over plagioclase to increase the Al_2O_3/CaO ratio. However, the mass balancing results suggest greater crystallization of plagioclase over clinopyroxene in the range of MgO ~8-3 wt.% (Table 19). Therefore, there is too much uncertainty to resolve fractionation between the two systems when using Al_2O_3/CaO along with mass balancing and MELTS calculations. A comparison of trace element abundance ratios for the two systems can give another perspective on whether or not they represent the same magma system.

To examine the relationship between the two dike systems in terms of trace elements, selected trace element ratios are plotted in Figures 18-A to D. As shown in these figures, the two dike systems have distinct plotting fields. In Figures 18-A, both dike systems are in clusters far from each other. Figures 18-B, C and D show the two dike systems are in two distinct groups; however, within each group, ratios spread out to form trends, which indicates that there are processes that occurred during crystallization modified these trace element characteristics. In general, the compositional gaps present in these figures (Figures

17-A, B, C and D) suggest that the two dike systems are unlikely to have the same source, as no ratios overlap.

Selected trace elements abundances and ratios are also plotted versus two differentiation indicators, MgO and Zr (Figures 18-E to L). Similar to trace element ratio plots in Figures 18-A to D, these plots show the two dike systems fall into two distinct groups, which suggests they are not likely to be related. However, in Figures 18-E, F, G, H, K and L, samples of dike system 2 form two trends instead of one. For example, in trace element ratios versus MgO plots (e.g., Figures 18-E to H), dike system 2 shows two groupings, as samples with MgO ~9.1 to 10 wt.% fall in one cluster, and samples with MgO ~12.4 to 13.7 wt.% fall in another. This gap in MgO content might be due to the limitation of sampling size. In trace element ratios versus Zr plots (e.g., Figures 18-K and L), dike system 2 also shows two groupings, as samples with Zr ~43 to 54 ppm (MgO ~9.1 to 9.5 wt.%) form one pattern, and samples with Zr ~31.2 to 42.3 ppm (MgO ~10 to 13.7 wt.%) form another. These groupings are for plots involving Th, and the analytical accuracy of Th could be questionable because it is in very low abundances (~0.2 to 0.4 ppm) and therefore extra sensitive to analytical precision.

By and large, there are enough differences in trace element ratios between the two dike systems to conclude that their mantle sources had different trace element characteristics, and so they are unlikely to be related.

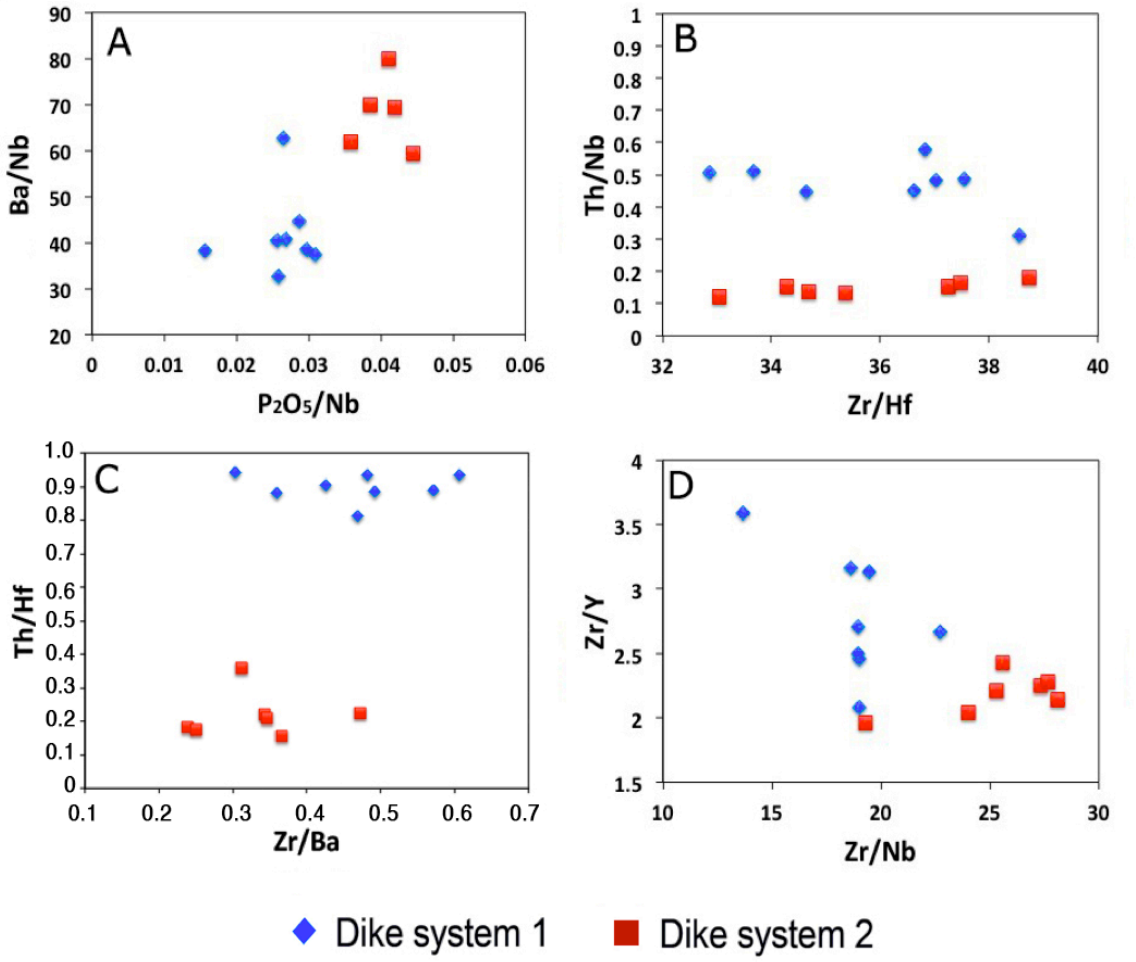

Figure 18. Selected trace element abundance ratio plots for two diabase dike systems to demonstrate that they had sources that differed in trace element characteristics.

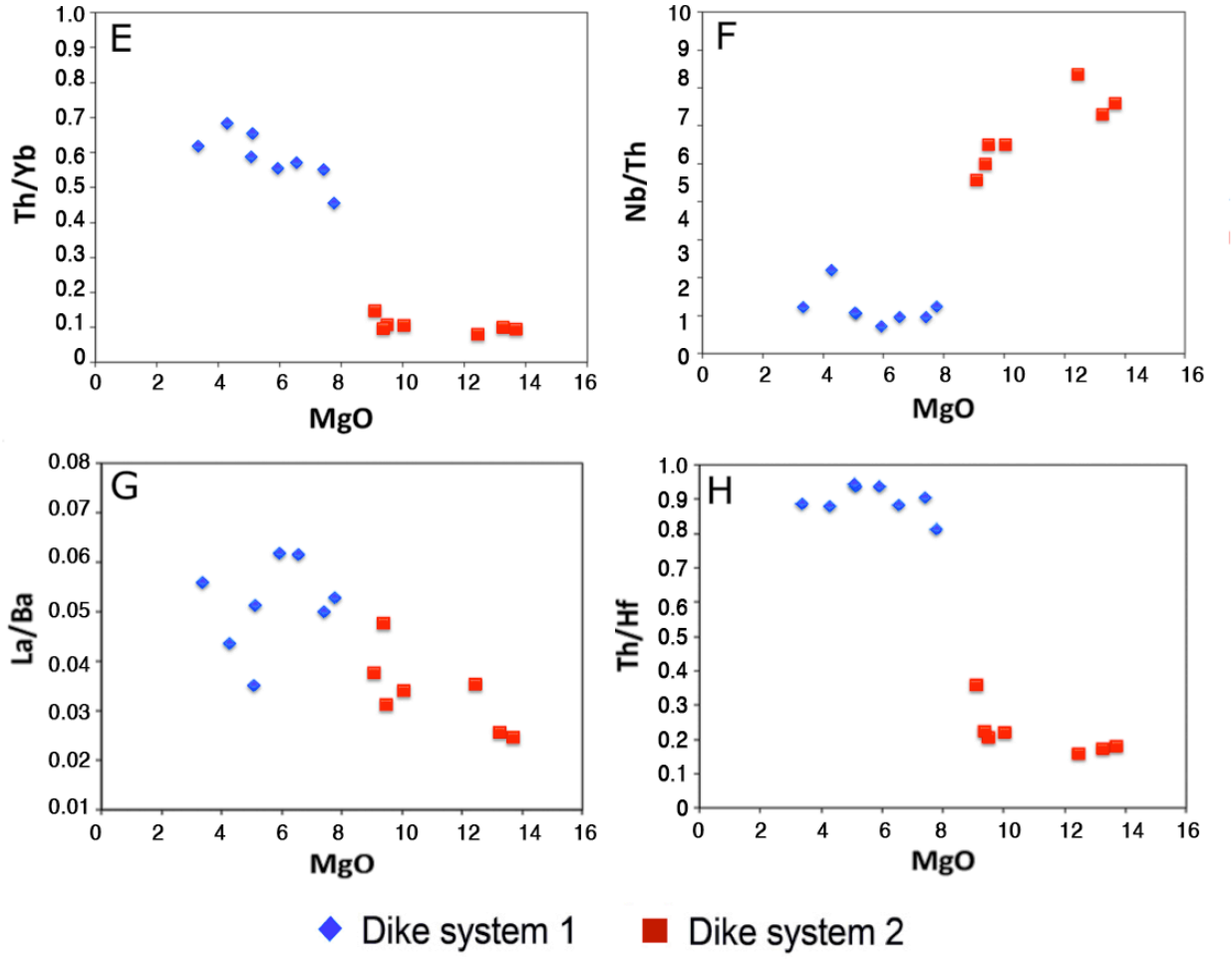

Figure 18 (continued). Selected trace element abundance ratios versus MgO plots for two diabase dike systems to demonstrate that they had sources that differed in trace element characteristics.

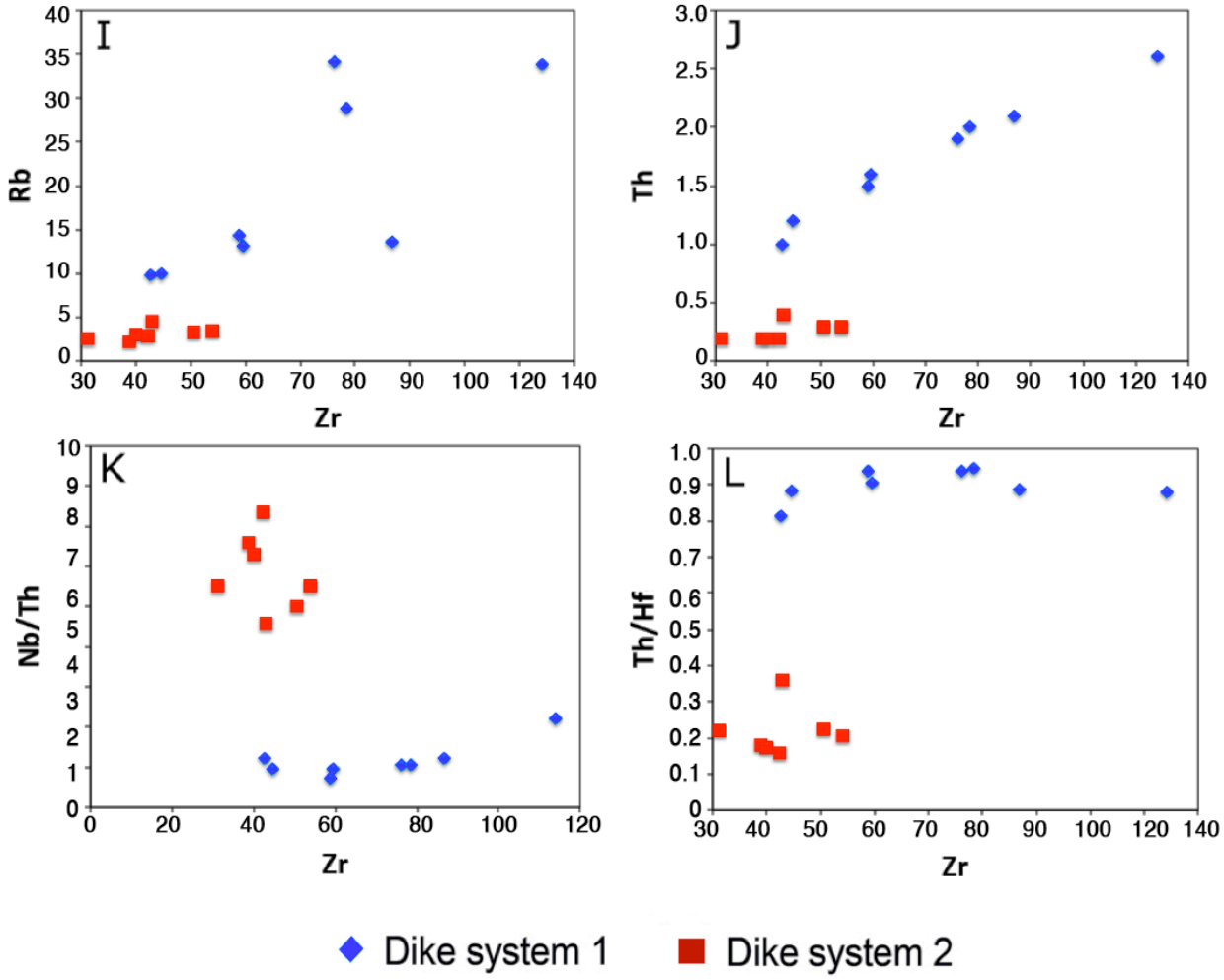

Figure 18 (continued). Selected trace element abundance and ratios versus Zr plots for two diabase dike systems to demonstrate that they had sources that differed in trace element characteristics.

Crustal contamination

Because the intruding magmas for these two dike systems passed through continental crust, there is the possibility that they were contaminated by crustal material. Certain elements of the compositions of the dikes can help determine if they were contaminated. For example, dike system 2 has relatively low SiO_2 (~46.3 to 47.8 wt.%) and high MgO (~9.1 to 13.7 wt.%). In comparison, upper continental crust is much higher in SiO_2 (e.g., ~66.6 wt.%; Rudnick and Gao, 2003) and lower in MgO (~2.48 wt.%; Rudnick and Gao, 2003). Furthermore, dike system 2 has low abundances of LILE such as K, Rb, Ba, light REE and Th (Table 1; Figures 4 and 5) compared to the high abundances in the upper crust (e.g., Rudnick and Gao, 2003). These low LILE abundances along with low SiO_2 and high MgO suggest that magmas represented by dike system 2 are unlikely to have been contaminated by crustal components.

In contrast, relatively high SiO_2 (~50.5 to 52.1 wt.%) in dike system 1 samples could represent contamination by crustal granitic rocks, as has been interpreted for some continental flood basalts that have SiO_2 greater than 50 wt.% (e.g., Turner et al., 1994). To examine this possibility, selected crustal elements such as Rb, Th, K, La, U and Pb are plotted versus SiO_2 in Figure 19. There is no clear correlation between these elements and increasing SiO_2 among dike system 1 samples (Figure 19), which suggests that the high SiO_2 in dike system 1 samples is unlikely due to contamination by average upper crust composition.

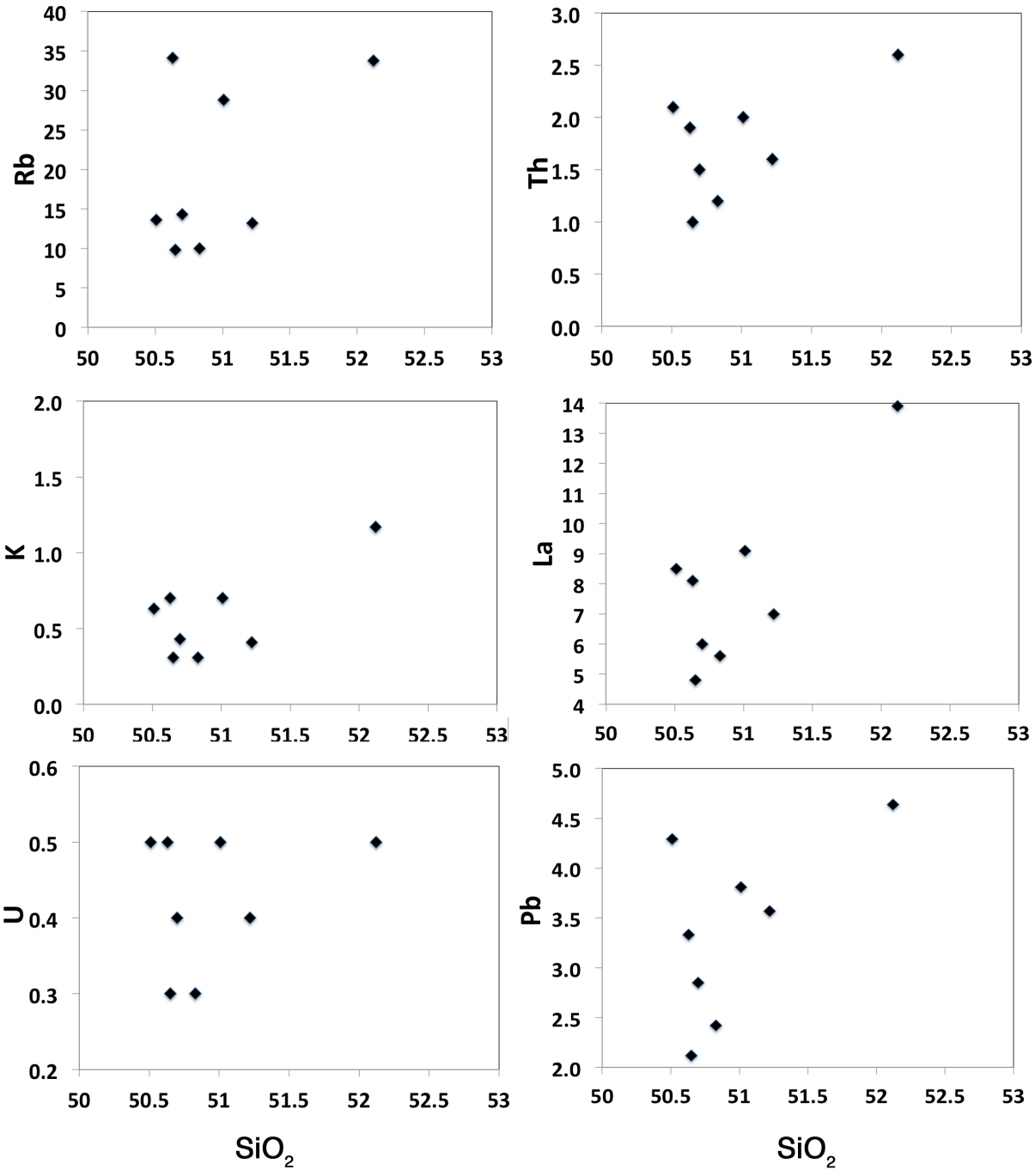

Figure 19. Selected elements enriched in continental crust versus SiO_2 in dike system 1 samples showing no correlation with increasing SiO_2, and therefore no clear case for crustal contamination.

Another perspective on contamination is the possibility of producing dike system 1 by contaminating dike system 2 (shown here to unlikely be contaminated by average continental crust) with the local Rolesville granitic batholith. This late Paleozoic intrusive feature has a ~24 × 80 km northeast trending exposure in eastern North Carolina (e.g., Farrar, 1985; Hibbard et al., 2002). Based on the locations of some dike system 1 samples relative to the Rolesville batholith, it is almost certain that magma related to at least part of dike system 1 ascended through this crustal body.

To evaluate whether dike system 1 samples could be hybrids from dike system 2 magma and Rolesville granitoid rock, I calculated hybrid compositions for mixes between representative Rolesville compositions (e.g., SiO_2 ~68 to 73 wt.%; Kosecki and Fodor, 1997) and dike system 2 samples having various MgO contents, ~13 to 9 wt.%. The best and most reasonable results were achieved by using NC-1, which is at the low end of the dike system 2 MgO range, ~9 wt.%, and a Rolesville sample having 69.7 wt.% SiO_2. Using higher MgO dike samples in the mix produced hybrid compositions that represent unreasonably high amounts of granitoid, >50%.

Table 20 shows how hybrids created from proportions of 85 and 88% NC-1 dike composition mixed with 12 and 15% Rolesville granitoid sample WS8a (Kosecki and Fodor, 1997) compare with some dike system 2 samples. The hybrids have most major and trace element abundances similar to those of some lowest-SiO_2 dike system 1 samples, RV-1 and MB-2 (Table 20). But the hybrids have lower CaO and higher K_2O, Rb, Ba, Sr, Zr and La when compared to actual abundances in dike system 1 samples (Table 20). Some of these elements, however, range widely among Rolesville granitoid compositions (e.g.,

Kosecki and Fodor, 1997), such as La, Ce, Zr and Th, as they can be associated with the accessory minerals zircon, titanite and allanite. On the other hand, it is difficult to explain the higher K_2O and lower CaO in the hybrid compositions relative to actual dike system 1 samples RV-1 and MB-2, although K_2O and CaO would be sensitive to the modal proportions of orthoclase in the granitoid endmember modeled. In summary, it appears that there are enough similarities between hybrid and dike system 1 compositions and adequate explanations for some of the elemental differences to not rule out the possibility that dike system 1 samples are expressions of olivine-normative dike system 2 magma having incorporated ~10 to 15% of Rolesville granitoid.

In support of this model, there is at least one extensive account of a similar percentage of crustal assimilation affecting CAMP dike compositions, leading to relatively low-MgO compositions. Namely, Cebria et al. (2003) studied the Messejana-Plasencia dike in Spain and Portugal, the longest (~530 km) and most northern CAMP dike known. By using $^{87}Sr/^{86}Sr$ ratios vs MgO, Cebria et al. (2003) concluded that the lowest-MgO Messejana-Plasencia dike samples had histories indicating crustal contamination of primitive dike magma compositions. In their case, they identified lower crust felsic granulites as the contaminants. The granulite assimilation was likely <10% and it occurred during <30% fractional crystallization of primitive dike magma. In view of this isotope-based study and the percentage of assimilation believed to create low-MgO dike compositions, I am open to a comparable assimilation accounting for the quartz-normative dikes in my study, as quantified in Table 20.

To better understand whether Rolesville assimilation led to the relatively low-MgO dike system 1 compositions, the differences in abundances for certain trace elements between hybrid magmas and dike system 1 samples, such as La, Ce, Zr, and Th (Table 20), must be evaluated in terms of the influence on these elements from accessory minerals in the granitoid endmember. For example, zircon, titanite, and allanite will influence trace element abundances of Zr, Hf, Th, U, La, and Ce. Therefore, trace element abundance ratios for these elements in the hybrids are superimposed on those for dike system 1 and 2 samples. Figure 20 shows that ratios for the hybrid compositions that use elements in the accessory minerals, such as Th/Hf, Zr/Hf, Zr/La, Th/Nb, and the REE slope represented by La/Yb, do not overlap these ratios for dike system 1 samples (Figure 19). The differences are great enough to leave doubt that dike system 1 compositions are the results of dike system 2 magmas having assimilated local Rolesville granitoid rock.

Table 20. Hybrid compositions calculated by mixing representative Rolesville batholith compositions with a dike system 2 composi to compare with major and trace element compositions of some dike system 1 samples.

	Dike 2	Rolesville batholith	Lowest-SiO_2 dike 1 samples			Hybrids	
	NC-1	WS8a[1]	RV-1	MB-2	KT-1	12%WS8a + 88%NC-1	15%WS8a + 85%NC-1
SiO_2	47.83	69.70	50.65	50.83	50.51	50.45	51.11
TiO_2	0.70	0.42	0.62	0.68	1.21	0.67	0.66
Al_2O_3	17.19	16.19	16.58	17.32	18.4	17.08	17.05
Fe_2O_3	11.44	1.97	9.94	9.86	12.36	10.33	10.05
MnO	0.17	0.03	0.17	0.17	0.16	0.15	0.15
MgO	9.08	0.62	7.76	6.53	3.34	8.06	7.81
CaO	11.19	2.01	11.70	11.87	10.06	10.09	9.81
Na_2O	2.17	4.91	2.01	2.11	2.89	2.50	2.58
K_2O	0.31	3.97	0.31	0.31	0.63	0.75	0.86
P_2O_5	0.08	0.13	0.06	0.07	0.12	0.09	0.09
Rb	4.5	172	9.8	10.0	13.6	25	29.6
Sr	160	713	134	139	251	226	243
Ba	138	1239	91	91	152	270	303
Zr	43	211	42.6	44.7	86.8	63	68

Table 20. Continued

La	5.2	40.6	4.8	5.6	8.5	9.4	10.5
Ce	11	90.8	10.9	12.45	13.6	20.6	23.0
Th	0.4	17.5	1.0	1.2	2.1	2.5	3.0
Hf	1.1	5.2	1.2	1.36	2.37	1.6	1.7
Nb	2.2	8	2.2	2.4	4.7	2.9	3.1
Sc	38.5	2.9	42.1	39.7	33.3	34.2	33.2
Y	21.9	16	20.5	17.9	27.4	21.2	21.0
U	0.03	3.4	0.3	0.3	0.5	0.43	0.54

[1] Composition of sample WS8a is from Kosecki and Fodor (1997).

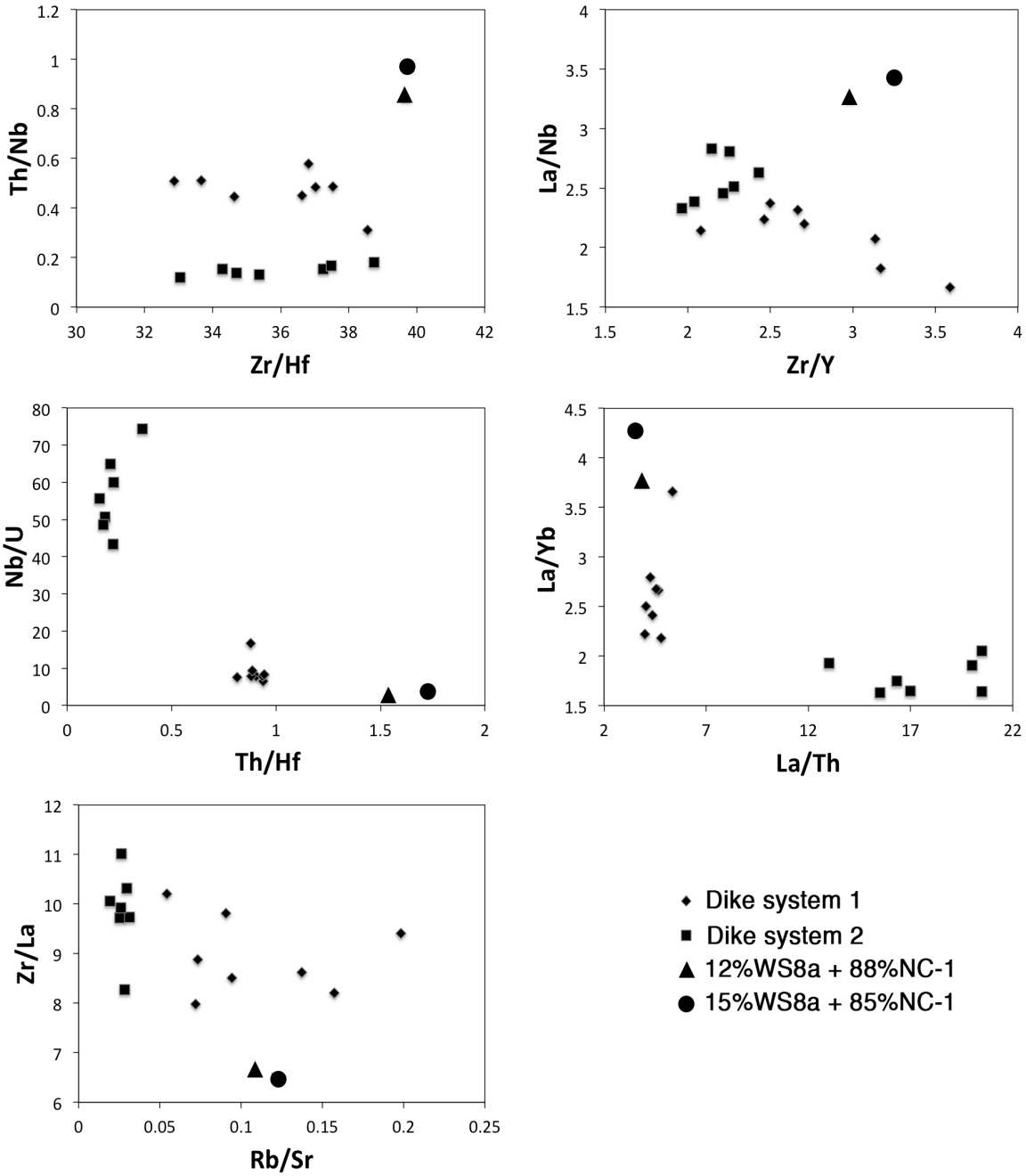

Figure 20. Selected trace element-ratio plots for the two diabase dike systems and calculated hybrid compositions suggest that dike system 1 samples are unlikely the products of dike system 2 assimilating Rolesville batholith.

Origin of high-Ca plagioclase in evolved dike system 1 samples

One characteristic of dike system 1 to address is the seemingly incompatibility of calcic plagioclase (An_{92-70}) that occurs as glomerocrysts in the low-MgO samples (MgO ~7.8 to 3.3 wt.%). One possible explanation for their presence requires particular magmatic conditions. It is long known that characteristically calcic plagioclase compositions (An_{80-100}) are observed in high-alumina basalts and basaltic andesites (Kuno, 1950; Wager, 1962; Arculus and Wills, 1980; Brophy, 1986; Stolz et al., 1988; Beard and Borgia, 1989; Sisson and Grove, 1993; Panjasawatwong et al., 1995). These high-alumina basalts usually contain ~18 wt.% and higher Al_2O_3 and anorthite phenocrysts, or have plagioclase phenocrysts with anorthitic cores. Barsdell (1988) stated that not until the Al_2O_3 content of the lavas reaches approximately ~19 wt.% does highly calcic plagioclase (An_{93}) start to crystallize. This suggests the role of Al content in the stabilization of anorthitic plagioclase. However, there is no evidence of primitive magma with such high Al_2O_3 in the study region. The modeled parent of dike system 1 samples, for example, C-1, has Al_2O_3 ~14 wt.% (Callegaro et al., 2013), and the most primitive dike system 2 sample, ES-1, has Al_2O_3 ~15 wt.% (Table 2).

Yoder and Kushiro (1969) ascribed calcic plagioclase in basaltic magmas to the presence of H_2O, reasoning that at a given temperature a wet basaltic magma will contain plagioclase more calcic than an identical dry basaltic magma. An experiment by Sisson and Grove (1993) supported this model, suggesting that calcic plagioclase in high-alumina basalts can crystallize from melts with H_2O contents >2 wt.% and likely up to 6 wt.%. However, MELTS calculation (Table 14) suggests that as little as 1 wt.% H_2O in the modeled primitive

sample C-1 will facilitate crystallization of high An plagioclase, An_{84}, as a parent magma for dike system 1 sample RV-1 (~7 wt.% MgO).

Additionally, most studies on high-Ca plagioclase suggest the role of Ca content in controlling the presence of calcic plagioclase (Drake, 1976; Johannes, 1978; Arculus and Wills, 1980; Faloon and Green, 1987; Panjasawatwong et al., 1995), stating that increasing magma Ca# (mol Ca/(Ca+Na)*100) increases An content of crystallizing plagioclase. In contrast, Panjasawatwong et al. (1995) proposed that pressure has a negative effect on plagioclase An content, namely that increasing pressure decreases An content of crystallizing plagioclase.

Two experiments combined these conditions (e.g., H_2O, Ca# and pressure) to produce calcic plagioclase. Panjasawatwong et al. (1995) stated that under pressure of 500-1000 MPa, an anhydrous magma requires at least Ca# >85 to produce plagioclase with An>90. Sisson and Grove (1993) stated that under 200 MPa, a hydrous magma with >2 wt.% H_2O content requires only Ca# ~60 to crystallize plagioclase with An>90.

When applying these conditions to dike system 1 samples, the parental magma (C-1) used in mass balancing and MELTS has Ca# ~87 (Tables 10 and 14), and the best results for producing RV-1 was at 500 MPa. Both the Ca# and pressure are in agreement with the experiment noted above. Modeled parent C-1, therefore, is a reasonable source for providing the An_{90} plagioclase in dike system 1. The MELTS modeling parent crystallizes plagioclase An_{84} at 500 MPa, which is less than the most calcic plagioclase observed in dike system 1, but highly calcic nonetheless.

In summary, the effects of Al_2O_3 and H_2O unlikely account for the production of dike

system 1 calcic plagioclase. On the other hand, Ca content and pressure could have played a role, if the MELTS modeling (Tables 13 and 14) at 500 MPa is considered robust.

A possible scenario to explain high-Ca plagioclase in the low-MgO magmas is that it initially crystallized from a high-MgO (~13 wt.%) melt of the composition used in the mass balancing and MELTS differentiation models (Table 19). A sequence of events began with crystallization of the high-MgO melt in the solidification zone along the base and walls of a slab-shaped reservoir (Figure 21 A, B). After ~20-30% crystallization of olivine, clinopyroxene and plagioclase (based on Table 19), the original melt evolved to ~7 wt.% MgO interstitial liquid in the solidification zone (similar to most primitive samples of dike system 1; Table 2). Over the course of decreasing interstitial melt MgO, the crystallizing plagioclase became normally zoned from ~An_{92} to An_{70} (Figure 9). During the formation of the solidification zone, some of the interstitial melt escaped the reservoir to mix with the original melt, causing it to evolve to <13 wt.% MgO (Figure 21 B). The evolved solidification-zone interstitial liquid, now ~7 wt.% MgO, and the plagioclase, both relatively low in density, rose to concentrate in the upper portion of the solidification zone, leaving behind the olivine and clinopyroxene (Figure 20 C). There, plagioclase phenocrysts coalesced to form glomerocrysts, perhaps aided by synneusis and convective activity in the overlying reservoir melt (Figure 21 D). When fractures occurred in the reservoir walls, the evolved liquid along with plagioclase crystals intruded the fractures to erupt and form a portion of dike system 1 (Figure 21 D). The low-MgO (~7 wt.%) magma with An_{92-70} plagioclase is equivalent to, for example, the compositions of rock samples RV-1, MB-2 and FR-1 and their plagioclase compositions (Figure 9).

The other dike system 1 samples (MgO ~5 to 3 wt.%) have plagioclase ~An_{75-35} (Figure 9). These highly evolved samples could represent differentiation products from MgO ~7 wt.% melt that remained in the reservoir (Fig. 21 D). Namely, about 50% crystallization of plagioclase, clinopyroxene and low-Ca pyroxene (as modeled in Table 19) from the remaining ~7 wt.% MgO interstitial melt yielded residual liquid with MgO ~5 to 3 wt.% (Figure 21 E). These differentiation compositional ranges for the interstitial melt are consistent with yielding plagioclase zoning ~An_{75-35}. As before, plagioclase glomerocrysts formed at the upper portion of the solidification zone (Figure 21 E, F). When additional fractures formed in the reservoir walls, the more evolved liquid along with plagioclase crystals intruded the fractures and crystallized to form another portion of dike system 1 (Figure 21 F). These highly evolved magmas (MgO ~5 to 3 wt.%) along with An_{75-35} plagioclase are equivalent to the low-MgO samples HN-1, CL-1 and KT-1 (Figure 9).

The plagioclase crystals in dike system 1 are present as glomerocrysts rather than as individual phenocrysts, which requires additional examination. Differentiation of high- to moderate-MgO (13-7 wt.%) and then moderate- to low-MgO (7-3 wt.%) magmas attended by buoyancy of plagioclase grains can account for the plagioclase with compositions observed in the dike system 1 samples. Buoyancy that would gather plagioclase crystals near the top of the solidification zone and proximity to overlying convective-sweeping currents could lead to the formation of glomerocrysts (Kouchi et al., 1986; Higgins, 1991; Higgins and Chandrasekharam, 2007). Higgins and Chandrasekharam (2007) proposed a possible crystallization history of plagioclase crystals in convecting continental flood basalt systems, which have compositions similar to the dike system 1 samples. In their model, plagioclase

grains at the bottom of a primitive magma chamber are swept by convecting currents to the top of the magma reservoir, where they accumulate in relatively evolved magma and remain there due to their buoyancy. However, plagioclase occurrence as glomerocrysts may require another process, such as synneusis, "the process of drifting-together and mutual attachment of crystals suspended in a melt", as defined by Vance (1969).

In summary, it is most likely that these calcic plagioclase phenocrysts were crystallized in a slab-shaped magma chamber with primitive magma compositions of high Ca contents (Ca# ~80) under moderate crustal pressures (~500 MPa). The plagioclase grains crystallized and became zoned due to the evolving magma, and were continuously brought up to the top of the solidification zone along with interstitial liquid by buoyancy due to their low density and by convective-sweeping magma currents. Finally, they formed glomerocrysts by the proccess of synneusis (Vance, 1969).

Figure 21. Diagrams show the sequence of dike system 1 magma crystallization in a slab-shaped magma chamber. **A)** The magma chamber initially contained MgO ~13 wt.% melt. **B)** The crystallization of olivine, clinopyroxene and plagioclase formed a solidification zone, mainly along with base and the walls. Crystallization evolved the original 13 wt.% MgO liquid at the base to ~7 wt.% MgO within the solidification zone as interstitial melt. Some of the evolved, low-density interstitial melt escaped the solidification zone to mix with the original melt and evolve it to <13 wt.% MgO. **C)** As the solidification zone developed, the evolved interstitial liquid (MgO now ~7 wt.%) included the plagioclase (low density) as it rose to the top of the solidification zone. **D)** The rising plagioclase grains coalesced to form glomerocrysts, probably due to synneusis attended by convection in the overlying remaining reservoir liquid that swept grains together. Eventually, the evolved liquid along with plagioclase grains and glomerocrysts intruded crustal fractures, migrating away from the reservoir and forming a portion of dike system 1. **E)** Further crystallization of plagioclase, clinopyroxene and low-Ca pyroxene evolves the remaining solidification-zone interstitial liquid from MgO ~7 wt.% to MgO ~5 wt.% and less, and it rose along with plagioclase to the top of the solidification zone. **F)** The plagioclase grains coalesced to form glomerocrysts. Eventually, the highly evolved liquid along with plagioclase grains and glomerocrysts intruded additional crustal fractures to erupt from the reservoir and form another portion of dike system 1. These events (panels D-F) likely repeated to account for the approximately 120-km long dike.

A

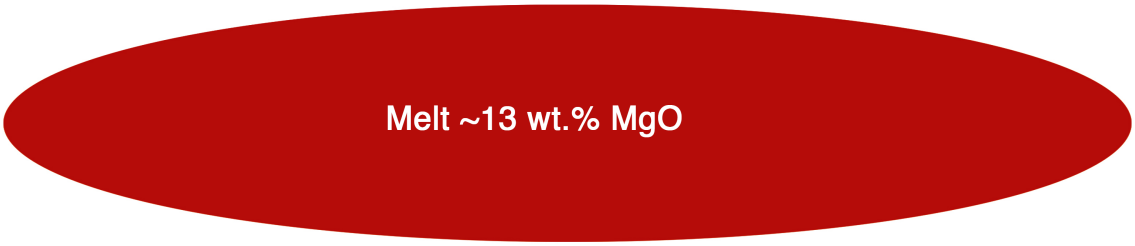

Initial slab-shaped reservoir for dike system 1

B

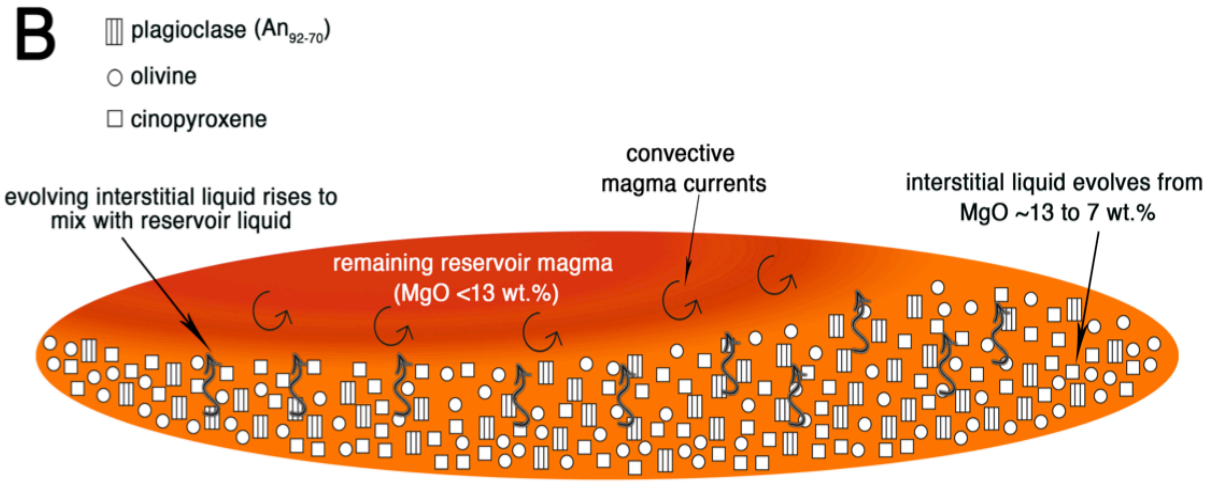

Solidification zone formed by crystallization of plagioclase, clinopyroxene and olivine

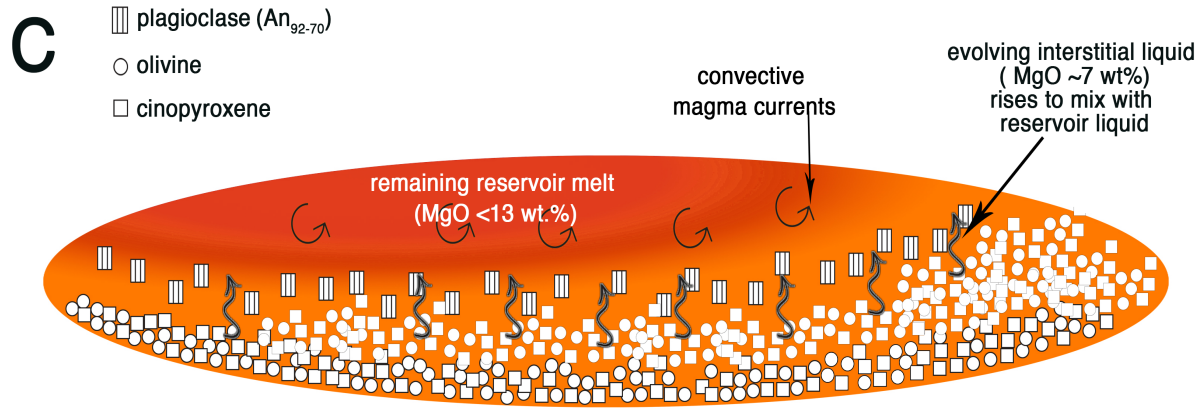

Evolved interstitial liquid (MgO ~7 wt.%) and plagioclase rise to top of the solidification zone due to their low density

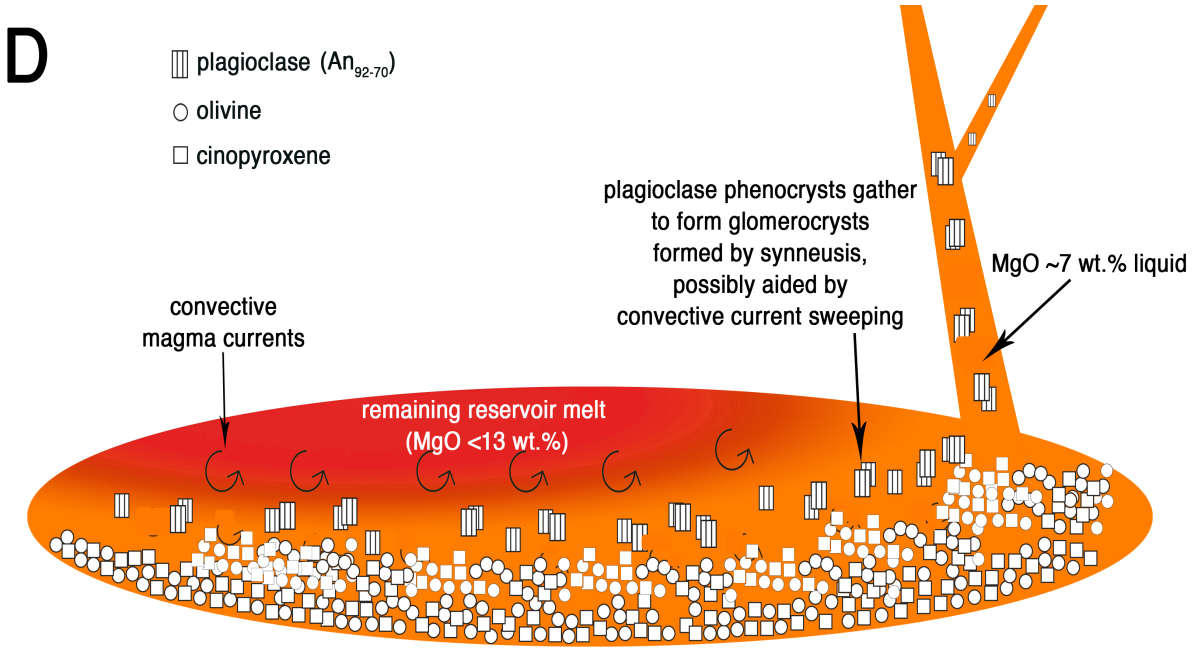

Evolved liquid along with plagioclase crystals and glomerocrysts escape through fractures to erupt as dike system 1

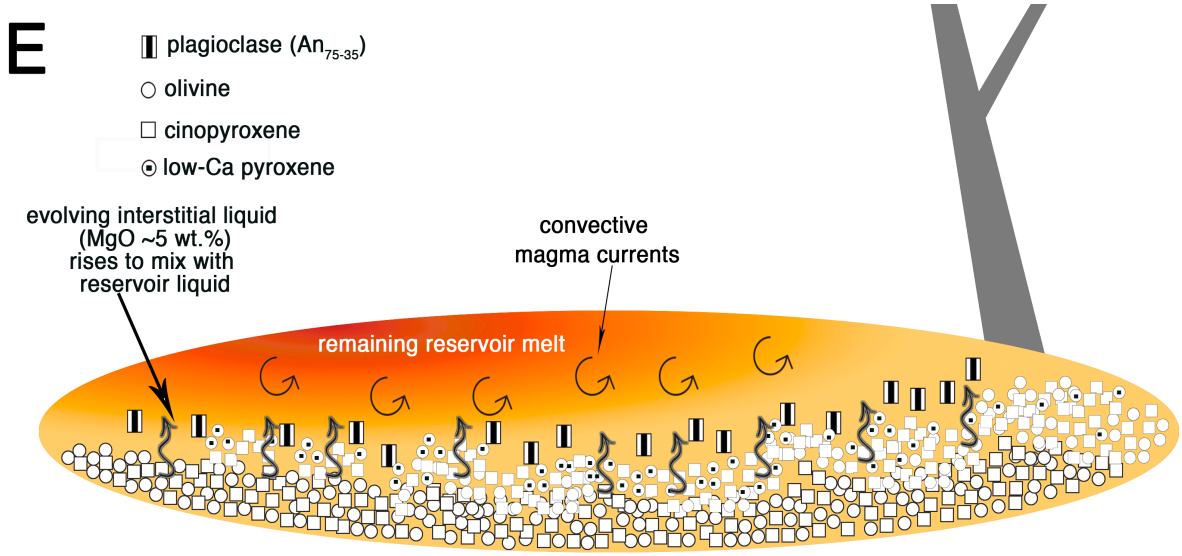

Interstitial liquid evolved from MgO ~7 to 5 wt.%
and rose to the top of the solidification zone along with plagioclase
due to their low density

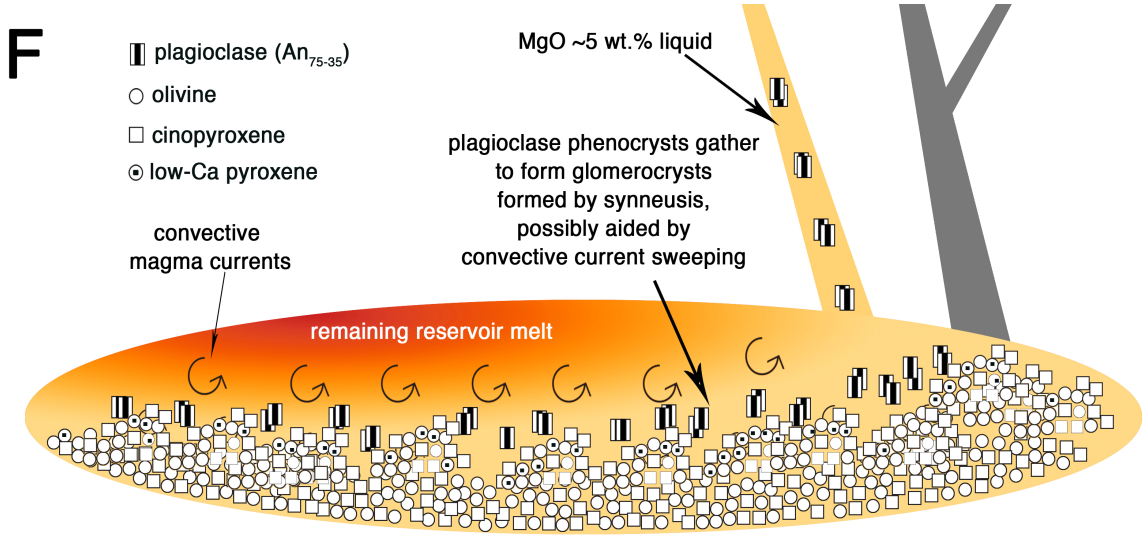

Highly evolved liquid along with plagioclase crystals and glomerocrysts
escape through fractures to erupt as another portion of dike system 1

Source area comparison for two dike systems and dike samples in broader North Carolina region

As presented in the Results section, samples from Callegaro et al. (2013) have a wide range of compositions. For example, the MgO variation diagrams (Figures 4 and 5) show that their MgO abundances range from ~14 to 5 wt.%, and SiO_2 is ~53 to 46 wt.% over this MgO range. Their major element abundances largely overlap those for dike system 2, but only partly overlap those for dike system 1. Similarly, trace element abundances for Callegaro et al. (2013) samples also largely overlap those for dike system 2 but rarely overlap dike system 1. These compositional characteristics, therefore, provide reasons to use trace element abundance ratios to evaluate whether Callegaro et al. (2013) samples share source areas common to those for either dike system 1 or dike system 2, and to evaluate trace element heterogeneity in the source rock for North Carolina CAMP dikes.

Selected trace element abundance ratios are plotted in Figure 22. Only a few samples from Callegaro et al. (2013) overlap those for dike system 2, such as P_2O_5/Nb (Figure 22-C), Ba/Nb (Figure 22-C), Th/Hf (Figures 22-A and D), Th/Nb (Figure 19-E), and Zr/Y (Figure 22-F). The other ratios show good overlapping between samples from Callegaro et al. (2013) and dike system 2, such as Zr/Ba (Figure 22-D), Zr/Hf (Figure 22-E), and Zr/Nb (Figure 22-F). However, for most of the ratios, only one sample from Callegaro et al. (2013) overlaps the fields of dike system 1, such as Th/Hf (Figures 19A and D), Nb/Th (Figure 22-B), P_2O_5/Nb (Figure 22-C), and Th/Nb (Figure 22-E). Some ratios also show good overlapping between samples from Callegaro et al. (2013) and dike system 1, such as Ba/Nb (Figure 22-C), Zr/Ba

(Figure 22-D), and Zr/Hf (Figure 22-E). Overall, Callegaro et al. (2013) samples form large compositional fields of trace element abundance ratios that both overlap and fall outside fields of dike system 1 and 2.

Callegaro et al. (2013) collected from a larger sampling area than represented by dike systems 1 and 2, which correlates with yielding a wider range in trace element ratios (Figure 22). In general, dike system 1 samples have less similarity in trace element abundance ratios with the samples of Callegaro et al. (2013) than dike system 2 samples do. This suggests that the source for dike system 2 is more closely related to that for samples of Callegaro et al. (2013) than to the source for dike system 1 samples.

If trace element ratios reflect subcontinental lithospheric mantle source areas, then the scattered patterns for Callegaro et al. (2013) samples could suggest substantial trace-element heterogeneity over their sampling area, ~100 km wide, east to west. Source heterogeneity is also suggested for the much smaller scale of ~40 km between the two dike systems in the present study, as their trace element abundance ratios for the two dike systems do not overlap (Figures 18 and 22). But the near similarity of trace element abundance ratios within each dike system is consistent with each having had its particular source. In summary, it appears that samples from dike system 2 were derived from a source that is in part the same as that for some Callegaro et al. (2013) samples, whereas samples from dike system 1 originated from a source not associated with that for Callegaro et al. (2013) samples.

Figure 22. Selected trace element abundance ratios for dike systems 1 and 2, and for samples from Callegaro et al. (2013) suggest that the two dike systems are not related to the same source, and that samples within each dike system are related to a single lithospheric source. Also, based on these ratios, the source for some dike system 2 samples may be part of the same source material that yielded some Callegaro et al. (2013) samples.

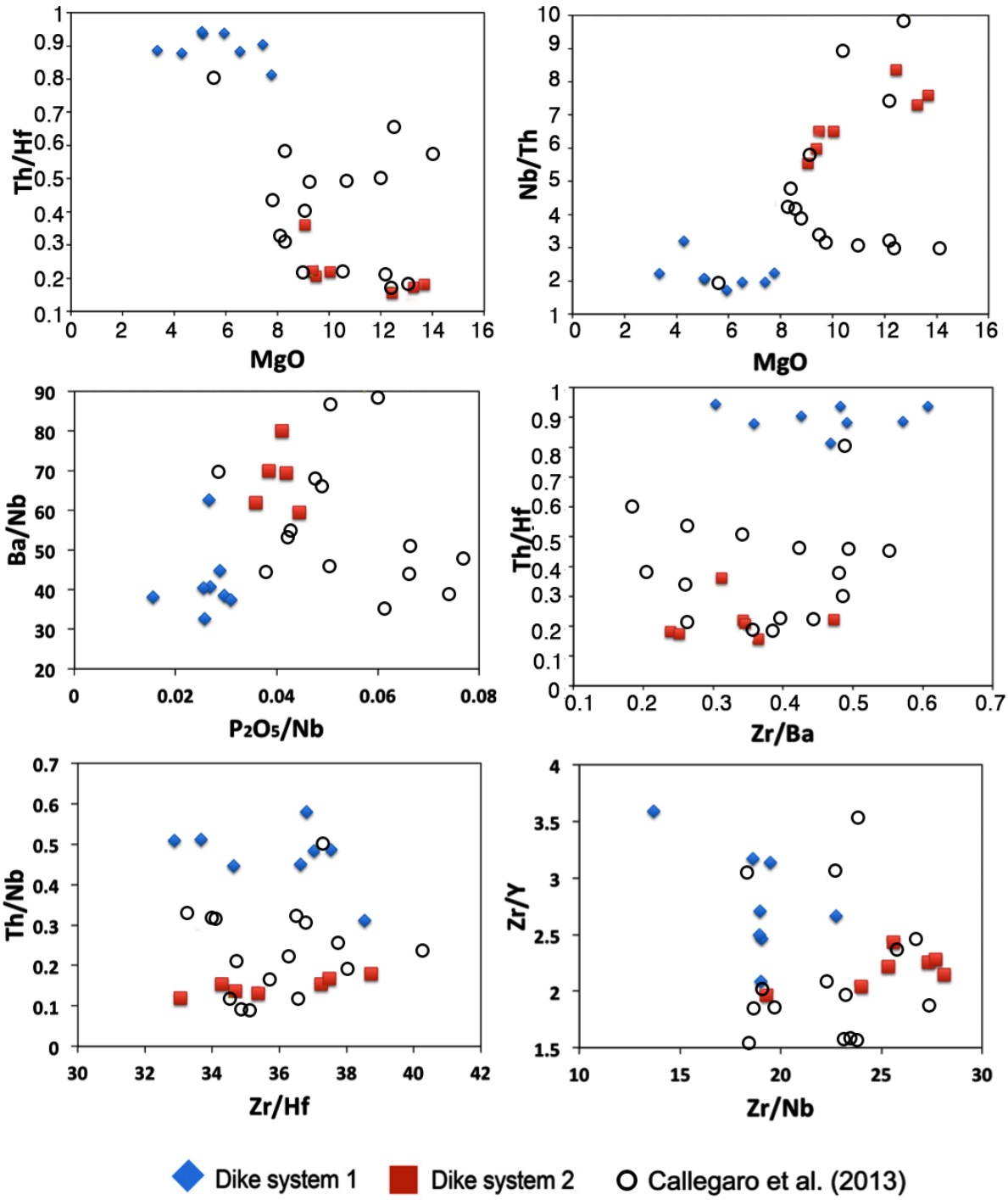
Th/Hf
MgO
Nb/Th
MgO
Ba/Nb
P2O5/Nb
Th/Hf
Zr/Ba
Th/Nb
Zr/Hf
Zr/Y
Zr/Nb
Dike system 1
Dike system 2
Callegaro et al. (2013)

CONCLUSIONS

1) The two N-S trending tholeiitic dike systems, ~90 and 45 km long and ~40 km apart, are located in central North Carolina. Dike system 1 and 2 are respectively distinguished by higher and lower SiO_2 and total alkalis, quartz- and olivine-normative mineralogy, rare earth element patterns that are LREE enriched and close to flat, and by textures that are plagioclase-phyric and aphyric.

2) The absence of positive correlations between SiO_2 and incompatible elements among dike system 1 samples, and the relatively high MgO and low SiO_2 and incompatible element abundances in dike system 2 samples suggest that continental crustal material has not contaminated the magmatic compositions of either dike system. Furthermore, mixing calculations show that dike system 1 (SiO_2 ~51 wt.%) does not represent dike system 2 (SiO_2 ~47 wt.%) magmas that assimilated crustal components. For example, a ~14:86 ratio of typical Rolesville batholith composition (SiO_2 ~69 wt.%) and dike system 2 sample compositions yields ~51wt.% SiO_2 and ~7 wt.% MgO, but not the appropriate CaO, K_2O, and incompatible trace element values to fully resemble dike system 1.

3) Mass balancing calculations and MELTS models demonstrate that fractional crystallization of a parental MgO-rich basalt (~13 wt.%) could account for the compositional ranges among samples in each dike system. The mass balancing shows that crystallization to achieve ~7 wt.% MgO requires removal of ~32% plagioclase, clinopyroxene and olivine, and that ~7 wt.% MgO magma can evolve to ~3 wt.% MgO by ~60% crystallization of

plagioclase, clinopyroxene and orthopyroxene. However, because ferromagnesian phenocrysts are not present in any samples, the mass balancing calculations are only mathematical solutions for fractionation histories where these mafic minerals could have remained in high-MgO parental magmas not observed at the surface.

4) Rayleigh fractional crystallization calculations for trace element abundances (e.g., Rb, La, Sr, Zr, Y) also suggest that samples within each dike system can be related by fractional crystallization because the calculated trace element values are similar to those in dike samples that have evolved compositions (e.g., MgO ~4 to 3 wt.% for dike system 1; MgO ~10 to 9 wt.% for dike system 2). Normalization of the actual and calculated trace element abundances for samples identified as "daughters" to their corresponding parent compositions in each fractional crystallization model shows that the normalization ratios differ by factors of only 0.7 to 1.6 (actual/calculated).

5) An important mineralogical distinction is that some dike system 1 samples have highly calcic plagioclase, ~An_{92-70}, occurring largely as glomerocrysts in rocks that are moderately to highly evolved (MgO ~7 to 4 wt.%). Highly calcic plagioclase in dike system 1 samples could have crystallized from magmas with suitably high Ca# (e.g., ~80; Ca# = mol Ca/(Ca+Na)*100) under intermediate crystallization pressure (e.g., 500 MPa), because these conditions are consistent with producing higher rather than lower An plagioclase.

6) Crystallization of the high-Ca plagioclase is modeled as having initiated along with olivine and clinopyroxene in a slab-shaped reservoir of high-MgO (~13 wt.%) melt. The plagioclase grains became normally zoned (An_{92-70}) in the evolving interstitial liquid of the solidification zone. Due to the relatively low densities of plagioclase and the evolved magma, both rose to the top of the solidification zone, away from clinopyroxene and olivine. The plagioclase grains coalesced into glomerocrysts, perhaps aided by synneusis and by convective activity within overlying remaining reservoir liquid. Eventually, the evolved liquid carrying plagioclase glomerocrysts intruded through crustal fissures to form portions of dike system 1.

7) A comparison of selected trace element abundance ratios (e.g., Ba/Nb, Zr/Hf) for the two dike systems to those for North Carolina CAMP dike samples collected over a large sampling area (~100 km east to west) shows some overlaps that suggest dike system 2 samples were derived from the same subcontinental lithospheric mantle source as some NC CAMP samples. On the other hand, ratios for dike system 1 samples do not overlap NC CAMP samples and therefore had a source independent of those for NC CAMP samples. Scattered compositional fields of the NC CAMP samples suggest substantial trace-element source heterogeneity as represented over their sampling area.

8) On the smaller scale between the two dike systems, trace element abundance ratios (e.g., Ba/Nb, Th/Hf) differ for the two dike systems. The two dike systems are therefore unlikely related to the same source. But the consistency of trace element abundance

ratios within each dike system suggests that samples from each dike system are related to a single subcontinental lithospheric source.

REFERENCES

Arculus, R.J. and Wills, K.J. (1980). The petrology of plutonic blocks and inclusions from the Lesser Antilles island arc. *Journal of Petrology* **21**, 743-799.

Asimow, P.D. and Ghiorso, M.S. (1998). Algorithmic modifications extending MELTS to calculate subsolidus phase relations. *American Mineralogist* **83**, 1127-1132.

Barsdell, M. (1988). Petrology and petrogenesis of clinopyroxene-rich tholeiitic lavas, Merelava volcano, Vanuatu. *Journal of Petrology* **29**, 927-964.

Beard, J.S. and Borgia, A. (1989). Temporal variation of mineralogy and petrology in cognate gabbroic enclaves at Arenal volcano, Costa Rica. *Contributions to Mineralogy and Petrology* **103**, 110-122.

Bender, J.F., Hodges, F.N. and Bence, A.E. (1978). Petrogenesis of basalts from the project FAMOUS area: experimental study from 0 to 15 kbars. *Earth and Planetary Science Letters* **41**, 277-302.

Bertrand, H. (1991). The Mesozoic tholeiitic province of northwest Africa: a volcano-tectonic record of the early opening of Central Atlantic. In Kampunzu, A.B., Lubala, R.T., ed., *Magmatism in Extensional Structural Settings: The Phanerozoic African Plate.* Berlin, Springer-Verlag, 147-188.

Bertrand, H., Dostal, J. and Dupuy, C. (1982). Geochemistry of early Mesozoic tholeiites from Morocco. *Earth and Planetary Science Letters* **58**, 225–239.

Blatter, D.L., Sisson, T.W. and Hankins, W.B. (2013). Crystallization of oxidized, moderately hydrous arc basalt at mid-to lower-crustal pressures: implications for andesite genesis. *Contributions to Mineralogy and Petrology* **166**, 861-886.

Boyd, F.R. and Schairer, J.F. (1964). The System $MgSiO_3$—$CaMgSi_2O_6$. *Journal of Petrology* **5**, 275-309.

Brophy, J.G. (1986). The Cold Bay volcanic center, Aleutian volcanic arc. *Contributions to Mineralogy and Petrology* **93**, 368-380.

Callegaro, S., Marzoli, A., Bertrand, H., Chiaradia, M., Reisberg, L., Meyzen, C., Bellieni, G., Weems, R.E. and Merle, R. (2013). Upper and lower crust recycling in the source of CAMP basaltic dykes from southeastern North America. *Earth and Planetary Science Letters* **376**, 186-199.

Cebriá, J.M., Lopez-Ruiz, J., Doblas, M., Martins, L.T. and Munha, J. (2003). Geochemistry of the early Jurassic Messejana–Plasencia dyke (Portugal–Spain); implications on the origin of the Central Atlantic Magmatic Province. *Journal of Petrology* **44**, 547-568.

Coltice, N., Phillips, B.R., Bertrand, H., Ricard, Y. and Rey, P. (2007). Global warming of the mantle at the origin of flood basalts over supercontinents. *Geology* **35**, 391-394.

Drake, M.J. (1976). Plagioclase-melt equilibria. *Geochimica et Cosmochimica Acta* **40**, 457-465.

Evans, O.C. and Hanson, G.N. (1993). Accessory-mineral fractionation of rare-earth element (REE) abundances in granitoid rocks. *Chemical Geology* **110**, 69-93.

Falloon, T.J. and Green, D.H. (1987). Anhydrous partial melting of MORB pyrolite and other peridotite compositions at 10 kbar: implications for the origin of primitive MORB glasses. *Mineralogy and Petrology* **37**, 181-219.

Farrar, S. (1985). Stratigraphy of the northeastern North Carolina Piedmont, North Carolina. *Southeastern Geology* **25**, 159 – 183.

Ghatak, A. and Basu, A.R. (2012). Central Atlantic Magmatic Province (CAMP): The Palisade sill connection. American Geophysical Union, Fall Meeting 2012, abstract #DI53A-2371.

Ghiorso, M.S. and Evans, B.W. (2008). Thermodynamics of rhombohedral oxide solid solutions and a revision of the Fe-Ti two-oxide geothermometer and oxygen-barometer. *American Journal of Science* **308**, 957-1039.

Ghiorso, M.S. and Sack, R.O. (1995). Chemical mass transfer in magmatic processes IV. A revised and internally consistent thermodynamic model for the interpolation and extrapolation of liquid-solid equilibria in magmatic systems at elevated temperatures and pressures. *Contributions to Mineralogy and Petrology* **119**, 197-212.

Gottfried, D., Annell, C.S. and Byerly, G.R. (1983). Geochemistry and tectonic significance of subsurface basalts near Charleston, South Carolina: Clubhouse Crossroads test holes# 2 and# 3. In G.S. Gohn, ed., *Studies Related to the Charleston, South Carolina, Earthquake of 1886. Tectonic and Seismicit*y, A1-A19. U.S. Geological Survey Professional Paper, no. 1313. Washington, D.C.. Government Printing Office.

Gottfried, D., and Arth, J. G. (1985). Sr and Nd isotope ratios and geochemistry of Mesozoic diabase dikes from Georgia. *EOS Transactions of the American Geophysical Union* **66**, 399.

Green, T.H., Green, D.H. and Ringwood, A.E. (1967). The origin of high-alumina basalts and their relationships to quartz tholeiites and alkali basalts. *Earth and Planetary Science Letters* **2**, 41-51.

Helz, R.T. (2009). Processes active in mafic magma chambers: The example of Kilauea Iki Lava Lake, Hawaii. *Lithos* **111**, 37-46.

Hibbard, J.P., Stoddard, E.F., Secor, D.T. and Dennis, A.J. (2002). The Carolina Zone: overview of Neoproterozoic to Early Paleozoic peri-Gondwanan terranes along the eastern flank of the southern Appalachians. *Earth-Science Reviews* **57**, 299-339.

Higgins, M.D. (1991). The origin of laminated and massive anorthosite, Sept Iles layered intrusion, Quebec, Canada. *Contributions to Mineralogy and Petrology* **106**, 340-354.

Higgins, M.D. and Chandrasekharam, D. (2007). Nature of sub-volcanic magma chambers, Deccan Province, India: evidence from quantitative textural analysis of plagioclase megacrysts in the Giant Plagioclase Basalts. *Journal of Petrology* **48**, 885-900.

Hinton, R.W. and Upton, B.G.J. (1991). The chemistry of zircon: variations within and between large crystals from syenite and alkali basalt xenoliths. *Geochimica et Cosmochimica Acta* **55**, 3287-3302.

Holbrook, W.S. and Kelemen, P.B. (1993). Large igneous province on the US Atlantic margin and implications for magmatism during continental breakup. *Nature* **364,** 433-436.

Husch, J., Sturgis, D. and Bambrick, T. (1984). Mesozoic diabases from west-central New Jersey: Major and trace element geochemistry of whole-rock samples. *Northeastern Geology* **6**, 51-63.

Janney, P.E. and Castillo, P.R. (2001). Geochemistry of the oldest Atlantic oceanic crust suggests mantle plume involvement in the early history of the central Atlantic Ocean. *Earth and Planetary Science Letters* **192**, 291-302.

Johannes, W. (1978). Melting of plagioclase in the system Ab-An-H_2O and Qz-Ab-An-H_2O at P_{H_2O}=5 kbars, an equilibrium problem. *Contributions to Mineralogy and Petrology* **66**, 295-303.

Kosecki, J. and Fodor, R.V. (1997). Petrology, mineralogy and geochemistry of the Rolesville granitic batholith, Eastern Piedmont, North Carolina. *Southeastern Geology* **37**, 91-107.

Kouchi, A., Tsuchiyama, A. and Sunagawa, I. (1986). Effect of stirring on crystallization kinetics of basalt: texture and element partitioning. *Contributions to Mineralogy and Petrology* **93**, 429-438.

Kuno, H. (1950). Petrology of Hakone volcano and the adjacent areas, Japan. *Geological Society of America Bulletin* **61**, 957-1020.

Le Bas, M.J., Le Maitre, R.W., Streckeisen, A. and Zanettin, B. (1986). A chemical classification of volcanic rocks based on the total alkali-silica diagram. *Journal of Petrology* **27**, 745-750.

Lindsley, D.H. (1983). Pyroxene thermometry. *American Mineralogist* **68**, 477-493.

Macdonald, G.A. and Katsura, T. (1964). Chemical composition of Hawaiian lavas. *Journal of Petrology* **5**, 82-133.

Mallmann, G. and O'Neill, H.S.C. (2007). The effect of oxygen fugacity on the partitioning of Re between crystals and silicate melt during mantle melting. *Geochimica et Cosmochimica Acta* **71**, 2837-2857.

Marzoli, A., Jourdan, F., Puffer, J.H., Cuppone, T., Tanner, L.H., Weems, R.E., Bertrand, H., Cirilli, S., Bellieni, G. and De Min, A. (2011). Timing and duration of the Central Atlantic Magmatic Province in the Newark and Culpeper Basins, eastern USA. *Lithos* **122**, 175-188.

Marzoli, A., Renne, P.R., Piccirillo, E.M., Ernesto, M., Bellieni, G. and De Min, A. (1999). Extensive 200-million-year-old Continental Flood Basalts of the Central Atlantic Magmatic Province. *Science*, **284**, 616-618.

Mayfield, A., Bohrson, W.A., Hunt, R. and Creamer, J. (2011). Documenting magma evolution of the Fossa delle Felci (Salina Island, southern Tyrrhenian Sea) volcanic sequence through integration of quantitative modeling and in situ chemical analysis. *Geological Society of America Abstracts with Programs* **43**, 58.

McDonough, W.F. and Sun, S.S. (1995). The composition of the Earth. *Chemical Geology* **120**, 223-253.

McHone, J.G. (2000). Non-plume magmatism and rifting during the opening of the central Atlantic Ocean. *Tectonophysics* **316**, 287-296.

McHone, J.G., Ross, M.E. and Greenough, J.D. (1987). Mesozoic dyke swarms of eastern North America. *Mafic dyke swarms: Geological Association of Canada Special Paper* **34**, 279-288.

Merle, R., Marzoli, A., Bertrand, H., Reisberg, L., Verati, C., Zimmermann, C., Chiaradia, M., Bellieni, G. and Ernesto, M. (2011). $^{40}Ar/^{39}Ar$ ages and Sr–Nd–Pb–Os geochemistry of CAMP tholeiites from Western Maranhão basin (NE Brazil). *Lithos* **122**, 137-151.

North Carolina Geological Survey (1985). Geologic Map of North Carolina. North Carolina Geological Survey, General Geologic Map, scale 1:500000.

Panjasawatwong, Y., Danyushevsky, L.V., Crawford, A.J. and Harris, K.L. (1995). An experimental study of the effects of melt composition on plagioclase-melt equilibria at 5 and 10 kbar: implications for the origin of magmatic high-An plagioclase. *Contributions to Mineralogy and Petrology* **118**, 420-432.

Pegram, W.J. (1990). Development of continental lithospheric mantle as reflected in the chemistry of the Mesozoic Appalachian tholeiites, USA. *Earth and Planetary Science Letters* **97**, 316-331.

Ragland, P.C., Hatcher, R.D. and Whittington, D. (1983). Juxtaposed Mesozoic Diabase Dike Sets From the Carolinas: A Preliminary Assessment. *Geology* **11**, 394-399.

Reising, S.E. and Stoddard, E.F. (2006). An extensive two pyroxene diabase dike in the eastern Piedmont of North Carolina. *Geological Society of America Abstracts with Programs* **38** (3), 8.

Roeder, P.L. and Emslie, R. (1970). Olivine-liquid equilibrium. *Contributions to Mineralogy and Petrology* **29**, 275-289.

Rudnick, R.L. and Gao, S.X. (2003). Composition of the continental crust. In Rudnick, R. L., ed*., The Crust, v. 3,* in Holland, H. D. and Turekian, K. K., ed*., Treatise on Geochemistry.* Oxford, United Kingdom, Elsevier-Pergamon*,* 1–64.

Schlische, R.W., Withjack, M.O. and Olsen, P.E. (2003). Relative timing of CAMP, rifting, continental breakup, and basin inversion: tectonic significance. In: Hanes, W.E., McHone, J.G., Renne, P.R., ed*., The Central Atlantic Magmatic Province: Insights from Fragments of Pangea*. Washington, D.C., American Geophysical Union, 33-60.

Sisson, T.W. and Grove, T.L. (1993). Experimental investigations of the role of H_2O in calc-alkaline differentiation and subduction zone magmatism. *Contributions to Mineralogy and Petrology* **113**, 143-166.

Smith, R.C., Rose, A.W. and Lanning R.M. (1975). Geology and geochemistry of Triassic diabase in Pennsylvania. *Geological Society of America Bulletin* **86**, 943–955

Stolz, A.J., Varne, R., Wheller, G.E., Foden, J.D. and Abbott, M.J. (1988). The geochemistry and petrogenesis of K-rich alkaline volcanics from the Batu Tara volcano, eastern Sunda arc. *Contributions to Mineralogy and Petrology* **98**, 374-389.

Turner, S., Regelous, M., Kelley, S., Hawkesworth, C. and Mantovani, M. (1994). Magmatism and continental break-up in the South Atlantic: high precision ^{40}Ar-^{39}Ar geochronology. *Earth and Planetary Science Letters* **121**, 333-348.

Vance, J.A. (1969). On synneusis. *Contributions to Mineralogy and Petrology* **24**, 7-29.

Verati, C., Bertrand, H. and Féraud, G. (2005). The farthest record of the Central Atlantic Magmatic Province into West Africa craton: Precise $^{40}Ar/^{39}Ar$ dating and geochemistry of Taoudenni basin intrusives (northern Mali). *Earth and Planetary Science Letters* **235**, 391-407.

Wager, L.R. (1962). Igneous cumulates from the 1902 eruption of Soufrière, St. Vincent. *Bulletin of Volcanology* **24**, 93-99.

Warner, R.D., Snipes, D.S., Hughes, S.S., Steiner, J.C., Davis, M.W., Manoogian, P.R. and Schmitt, R.A. (1985). Olivine-normative dolerite dikes from western South Carolina: Mineralogy, chemical composition and petrogenesis. *Contributions to Mineralogy and Petrology* **90**, 386-400.

Warner, R.D., Snipes, D.S., Hughes, S.S., Walker, R.J., Schmitt, R.A. and Steiner, J.C. (1992). Geochemistry and petrology of Mesozoic dikes in South Carolina. *Geological Society of America Special Paper* **268**, 333-346.

Weigand, P.W. and Ragland, P.C. (1970). Geochemistry of Mesozoic dolerite dikes from eastern North America. *Contributions to Mineralogy and Petrology* **29**, 195-214.

Wilson, M. (1997). Thermal evolution of the Central Atlantic passive margins: Continental breakup above a Mesozoic super-plume. *Journal of Geological Society*. **154**, 491-495.

Yoder, H.S. and Kushiro, I. (1969). Melting of a hydrous phase: phlogopite. *American Journal of Science* **267**, 558-582.

Yoder, H.S. and Tilley, C.E. (1962). Origin of basalt magmas: an experimental study of natural and synthetic rock systems. *Journal of Petrology* **3**, 342-532.

APPENDICES

APPENDIX I

Table 21. Latitudes, longitudes and USGS 7.5-minute quadrangles for the locations of samples taken from the two dike systems in central North Carolina.

	Latitude	Longitude	Quadrangle
Dike system 1			
RV-1	35.99215	-78.43774	Rolesville
MB-1	36.42444	-78.35417	Middleburg
MB-2	36.42556	-78.35389	Middleburg
FR-1	36.03774	-78.43564	Franklinton
HN-2	36.28278	-78.39000	Henderson
HN-1	36.28333	-78.38917	Henderson
KT-1	36.14559	-78.40914	Kittrell
CL-1	35.62028	-78.33639	Selma
Dike system 2			
ES-1	35.73694	-78.90000	New Hill
AB-1	35.82972	-78.90528	Green Level
ST-1	35.67278	-78.84278	Apex
CP-1	35.80417	-78.90111	Green Level
SV-1	36.05444	-78.95917	Northwest Durham
NI-1	35.88111	-78.87889	Southwest Durham
NC-1	35.97833	-78.89194	Southwest Durham

APPENDIX II

Topographic maps of each sample location. (Modified after quadrangle maps from USGS)

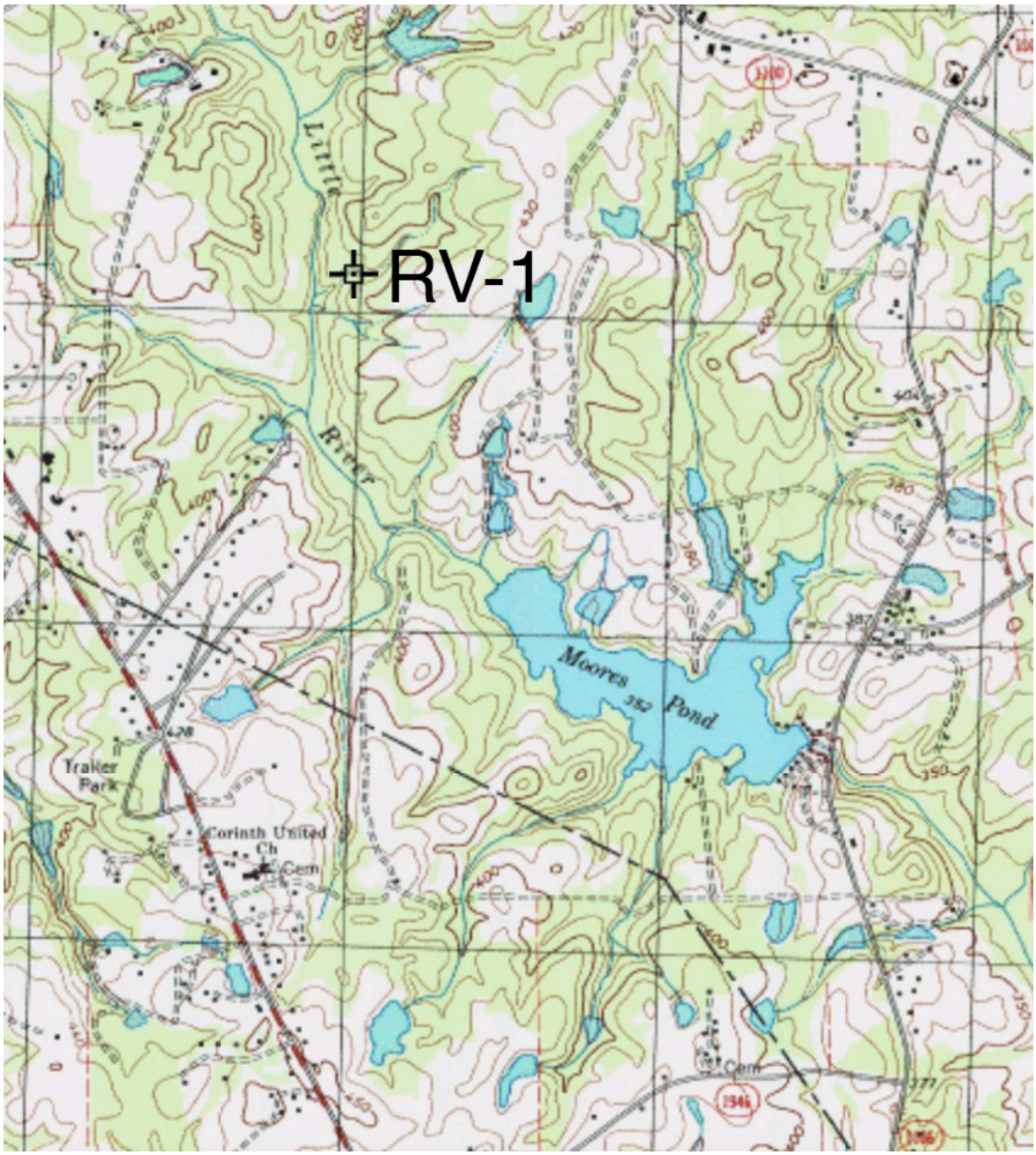

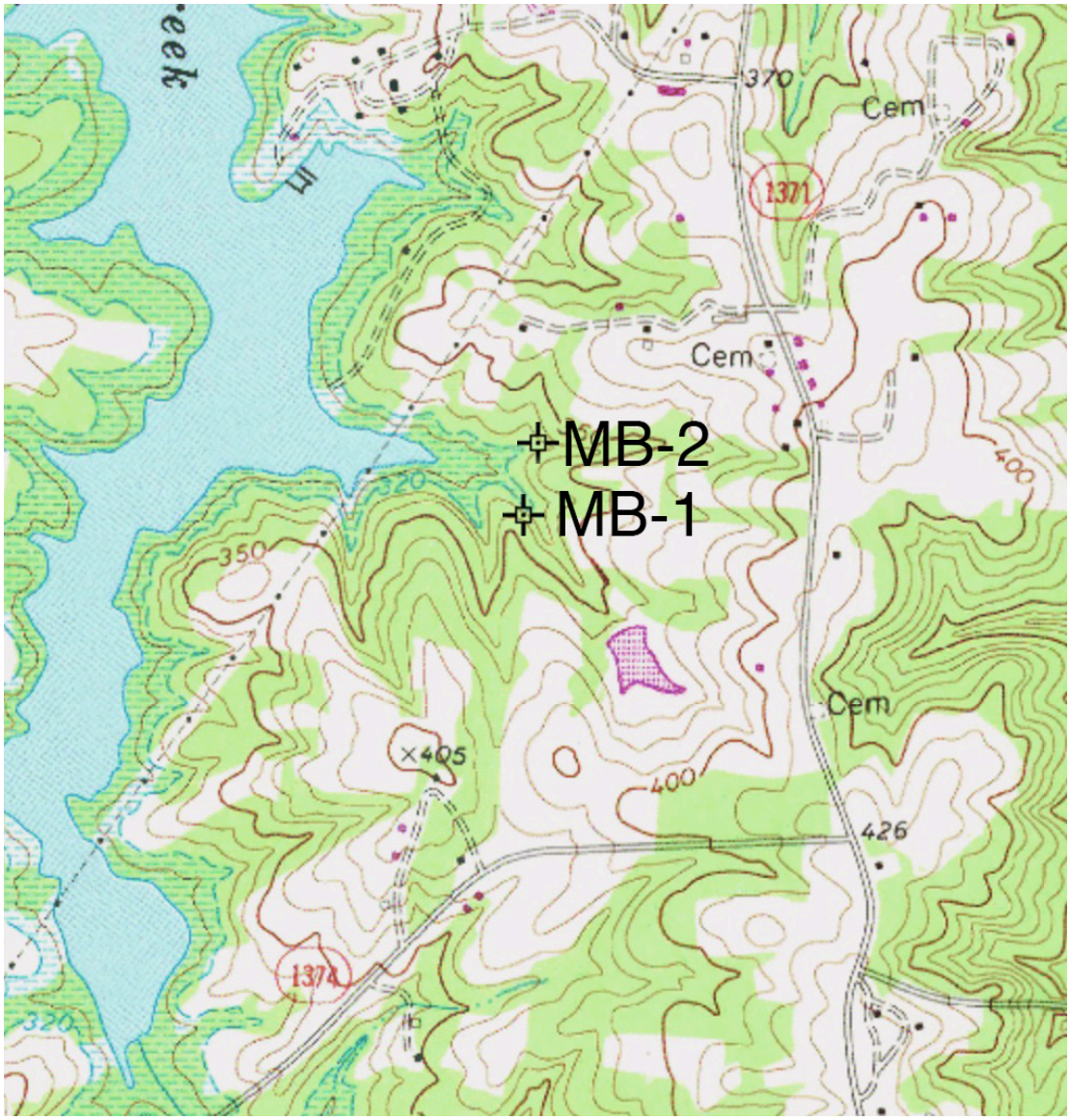
MB-2
MB-1
370
Cem
1371
Cem
400
320
350
Cem
405
400
426
1374
320

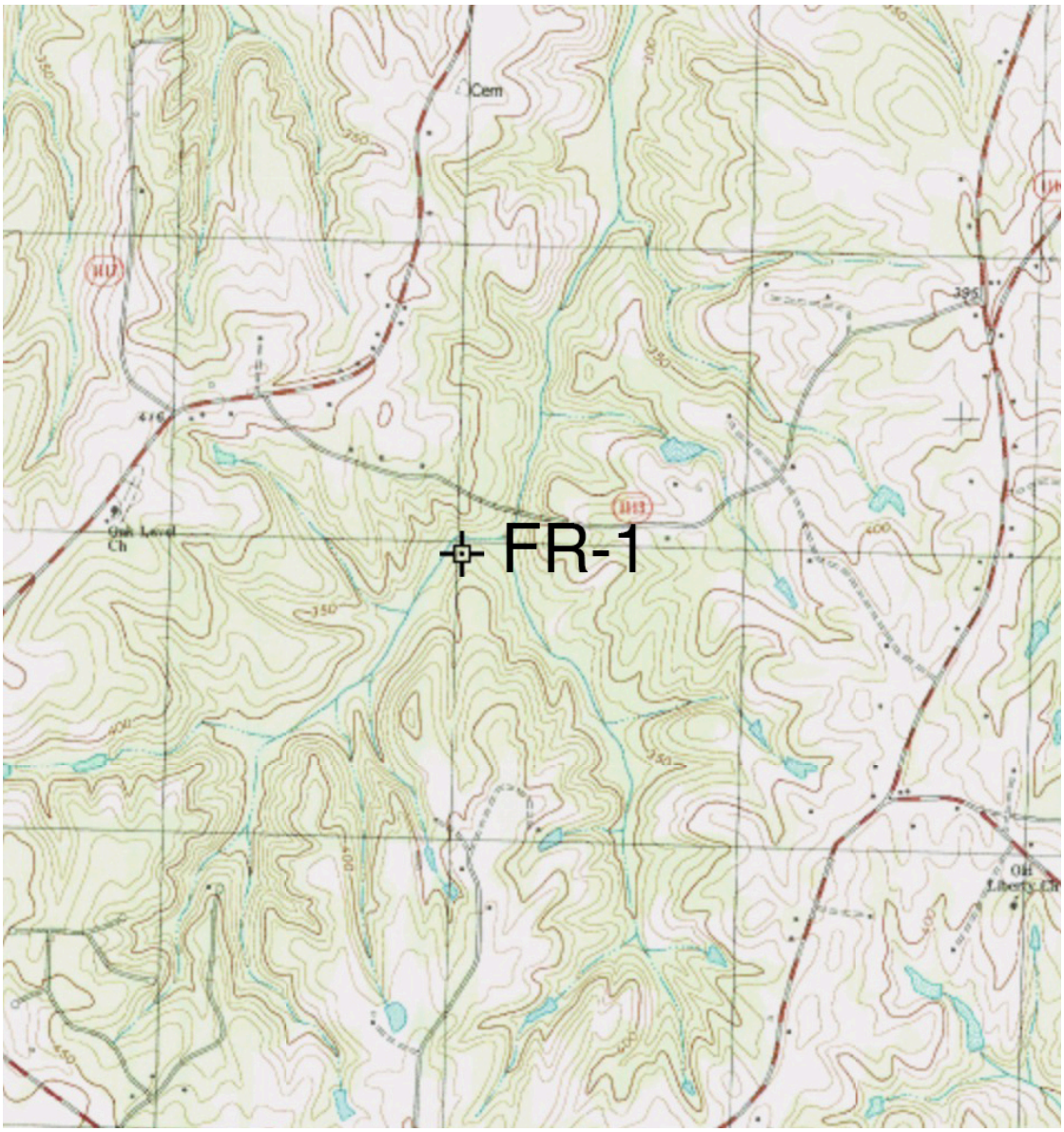
Cem
FR-1

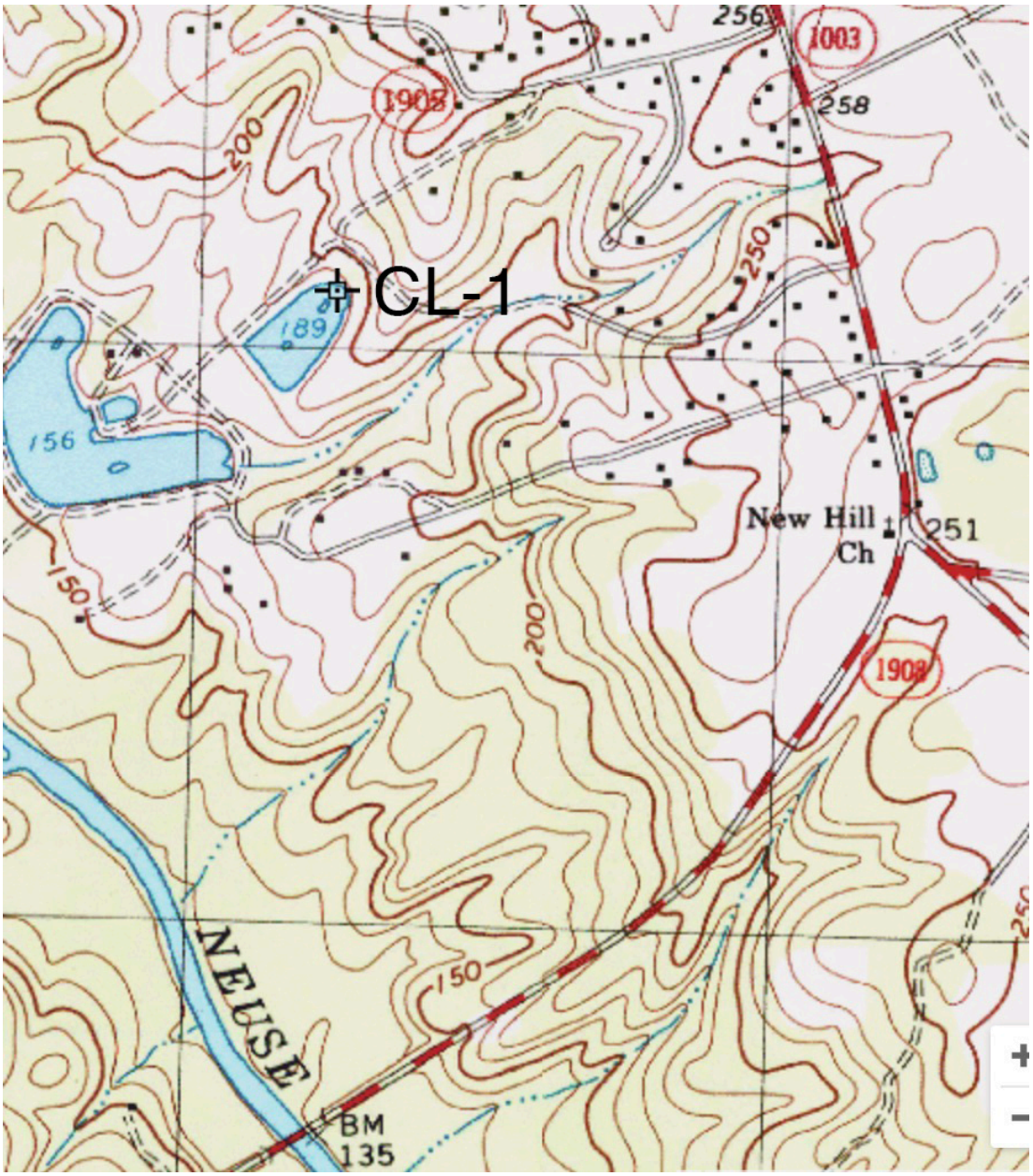
CL-1
New Hill
Ch
251
258
200
250
150
189
156
NEUSE
BM
135
1003
1908

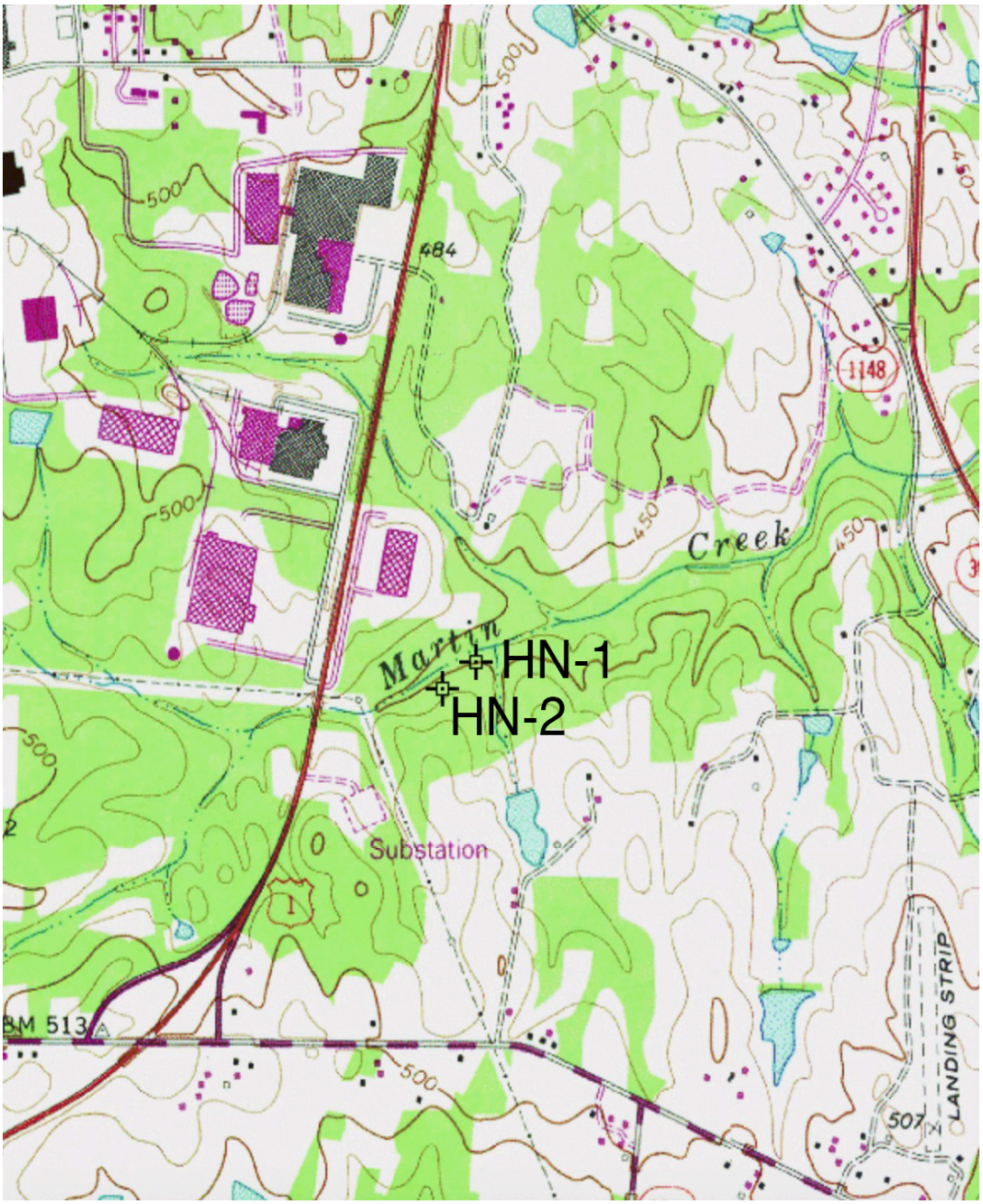
HN-1
HN-2
Martin
Creek
Substation
LANDING STRIP
BM 513
484
1148
500
450
507

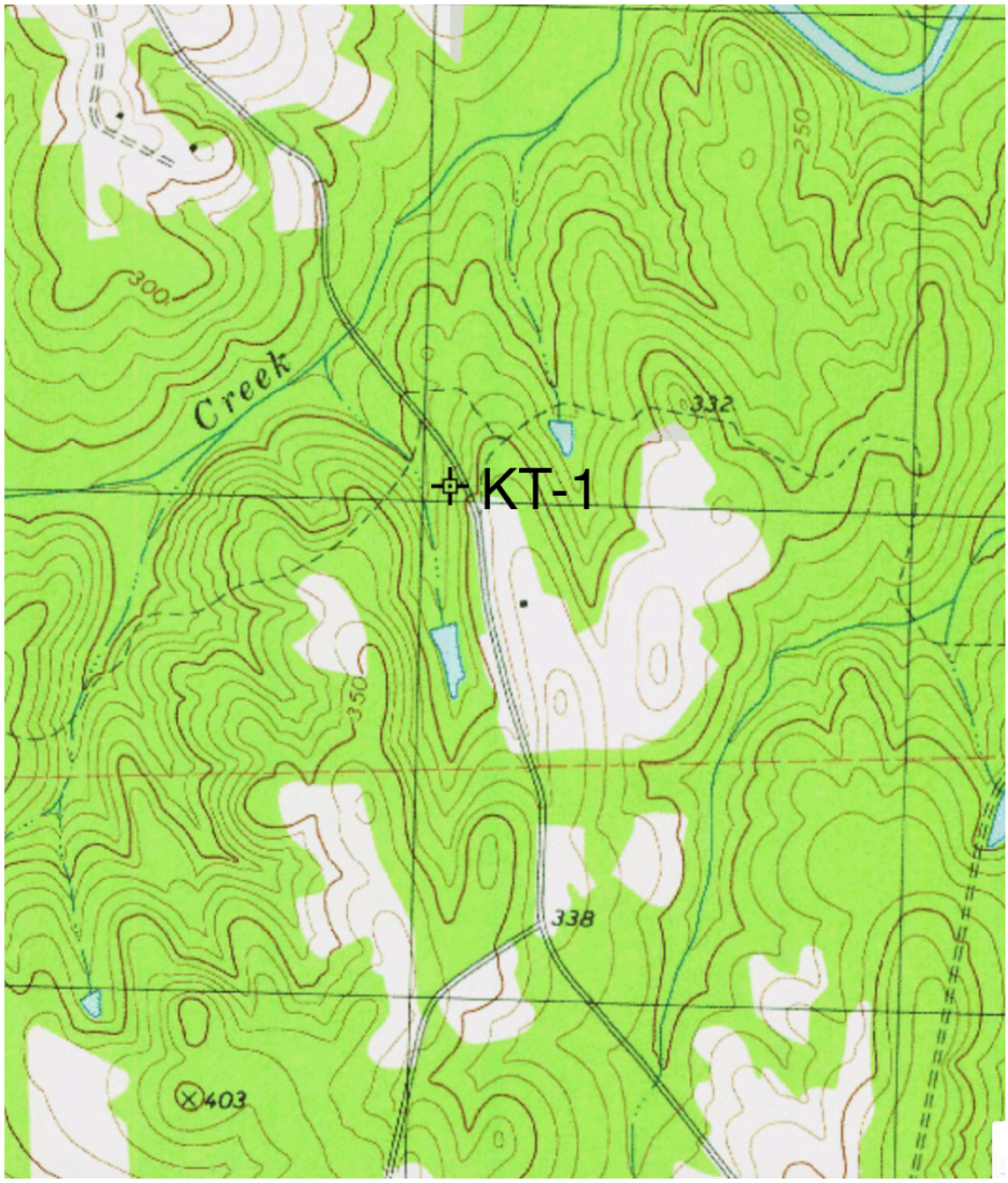
KT-1
Creek
300
250
332
350
338
403

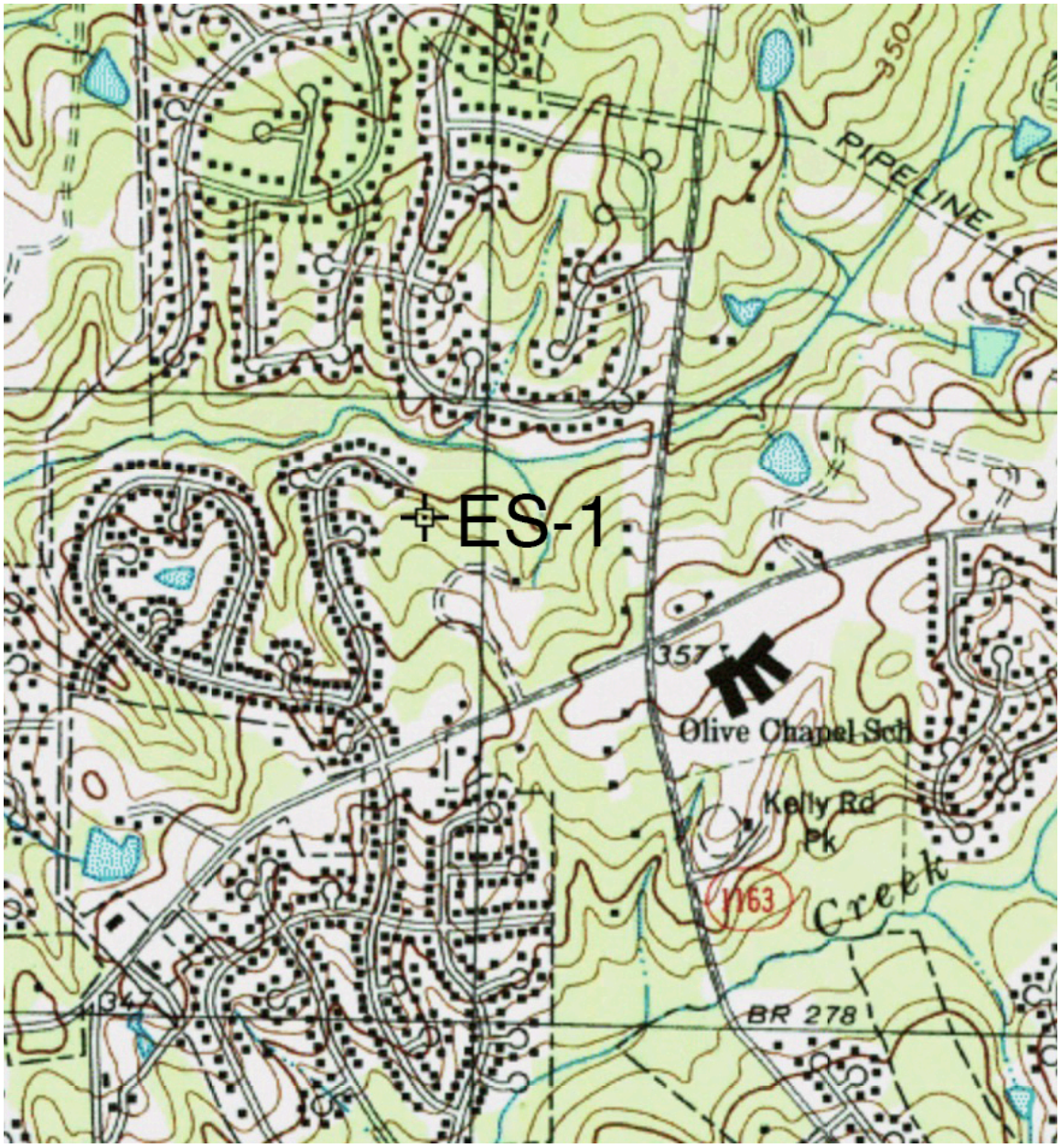
ES-1
PIPELINE
350
357
Olive Chapel Sch
Kelly Rd
Pk
1163
Creek
BR 278

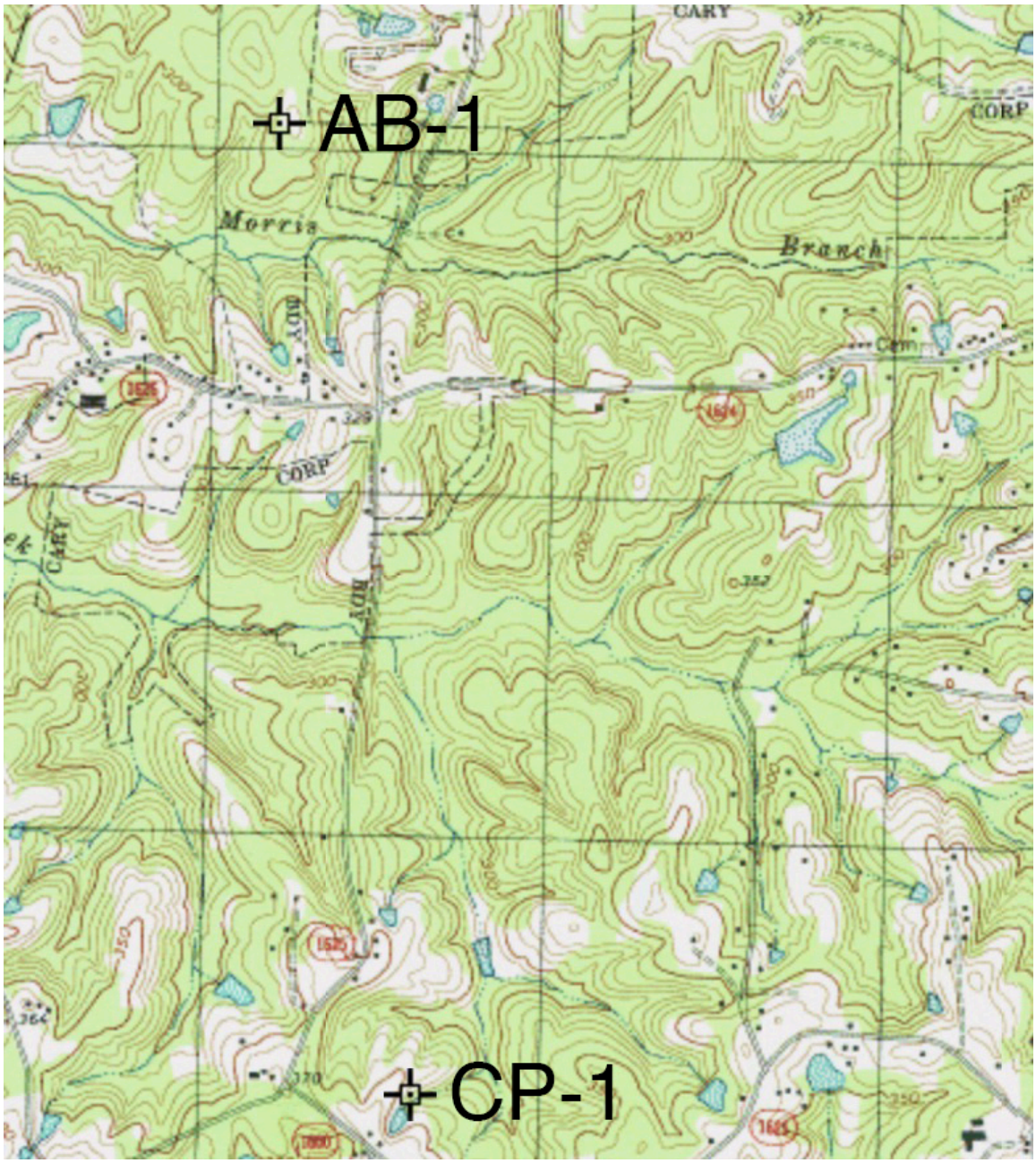
AB-1
CP-1
Morris
Branch
CARY
CORP

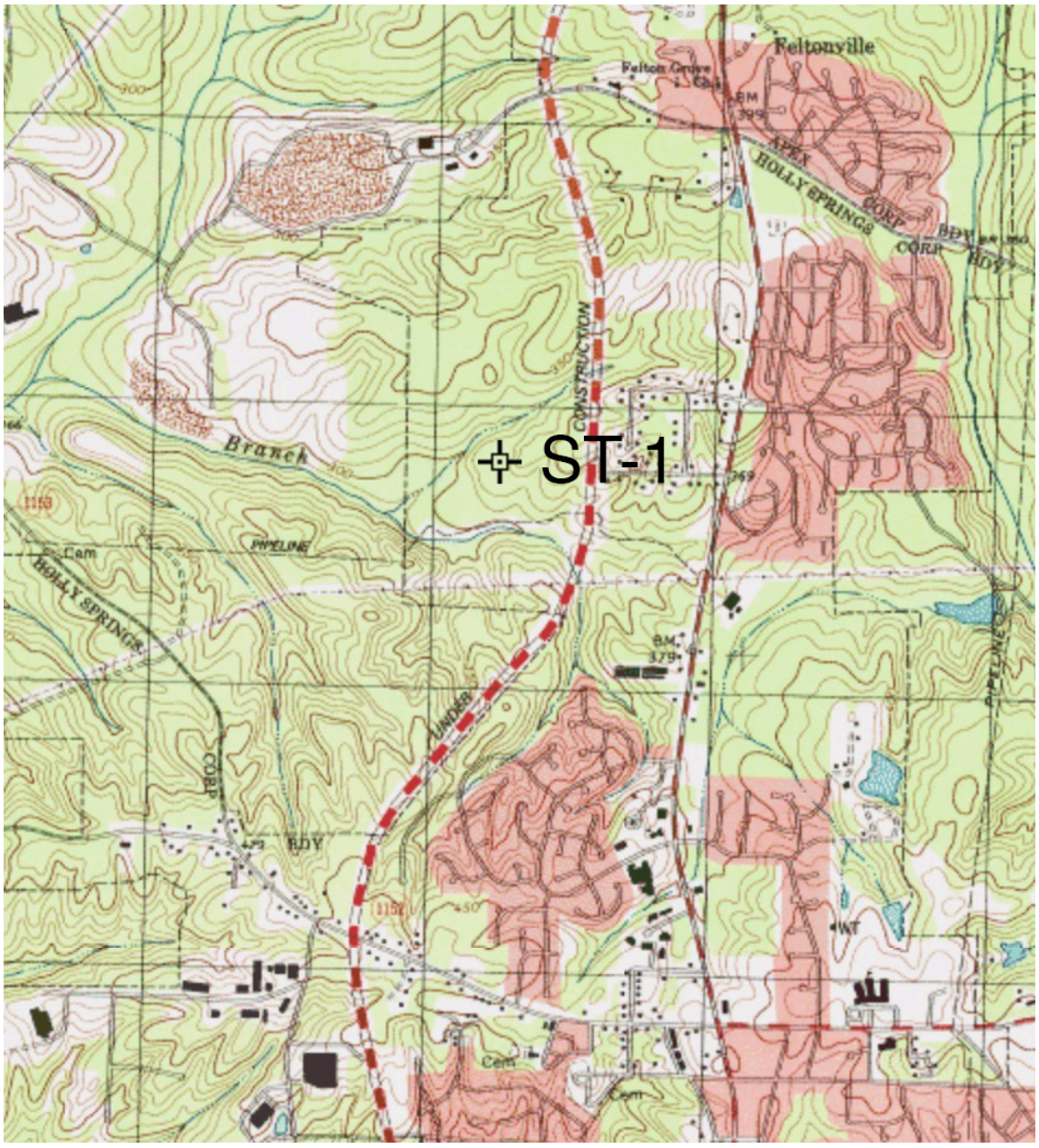
Feltonville
Felton Grove Ch.
BM 395
APEX
HOLLY SPRINGS
CORP
BDY
CONSTRUCTION
ST-1
Branch
PIPELINE
Cem
HOLLY SPRINGS
BM 379
UNDER
CORP
BDY
PIPELINE
INT
Cem
Cem

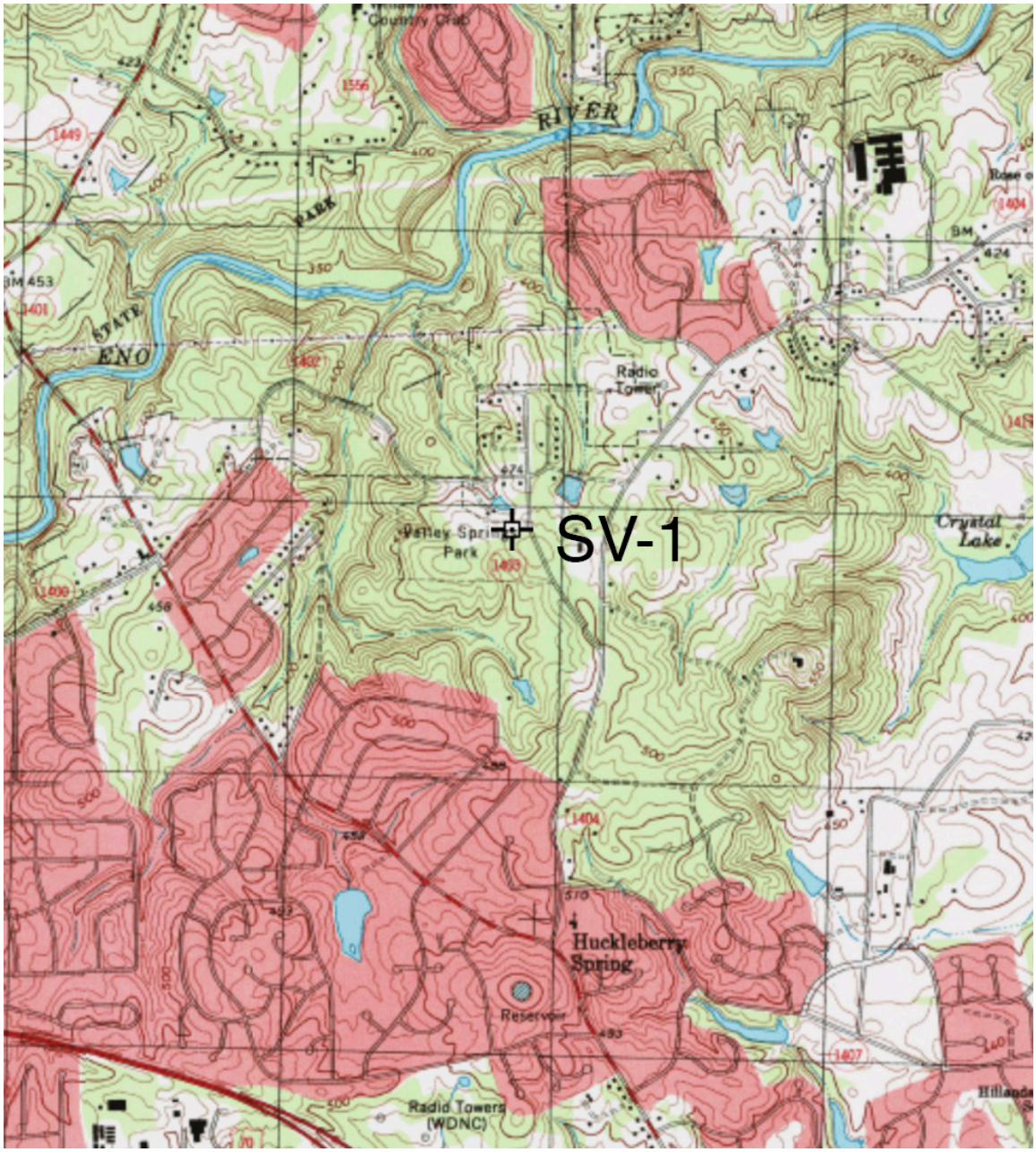
SV-1
RIVER
STATE
PARK
ENO
Radio Tower
Crystal Lake
Huckleberry Spring
Reservoir
Radio Towers (WDNC)

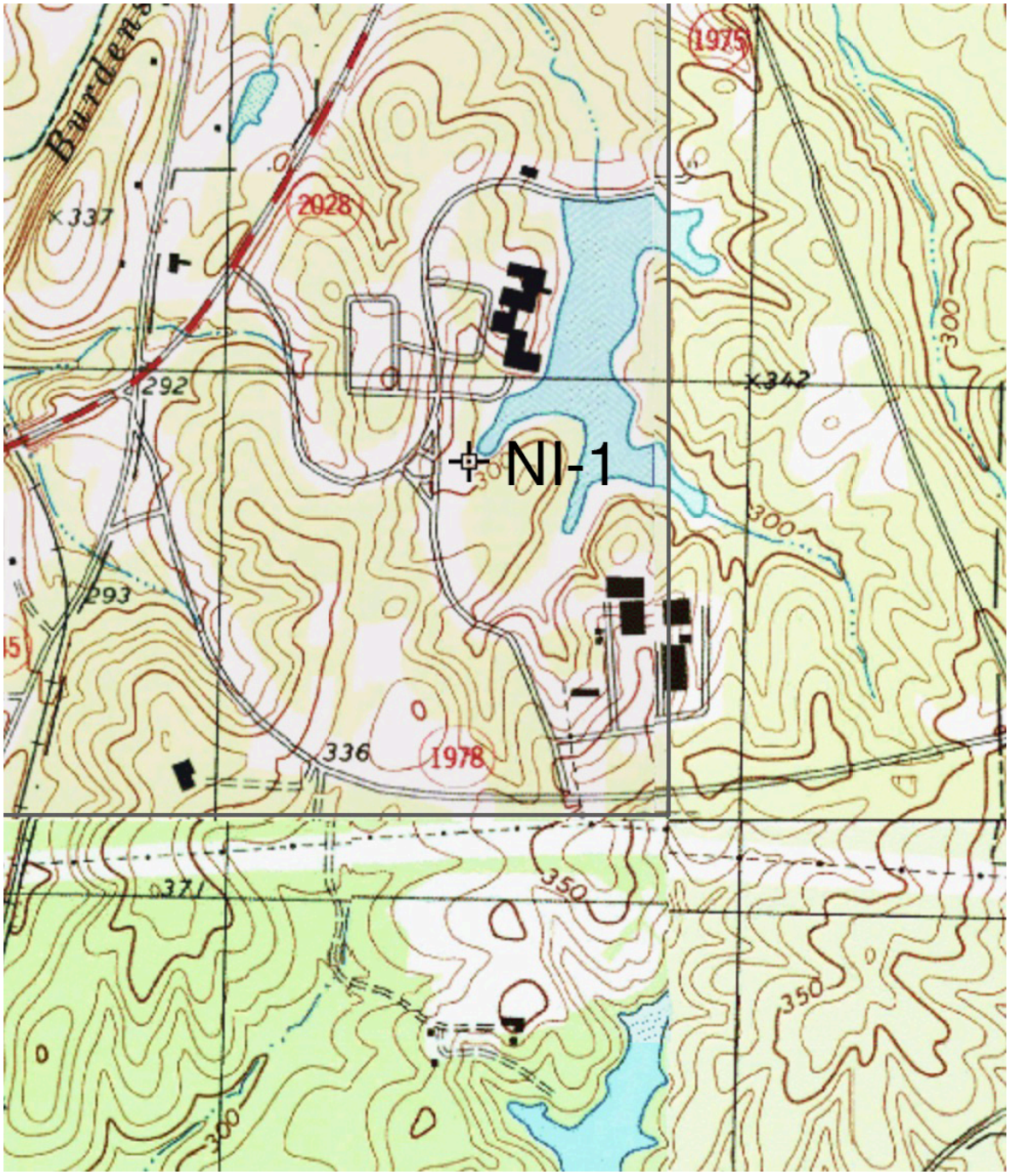
NI-1
1975
2028
337
292
342
300
293
336
1978
371
350
350
300

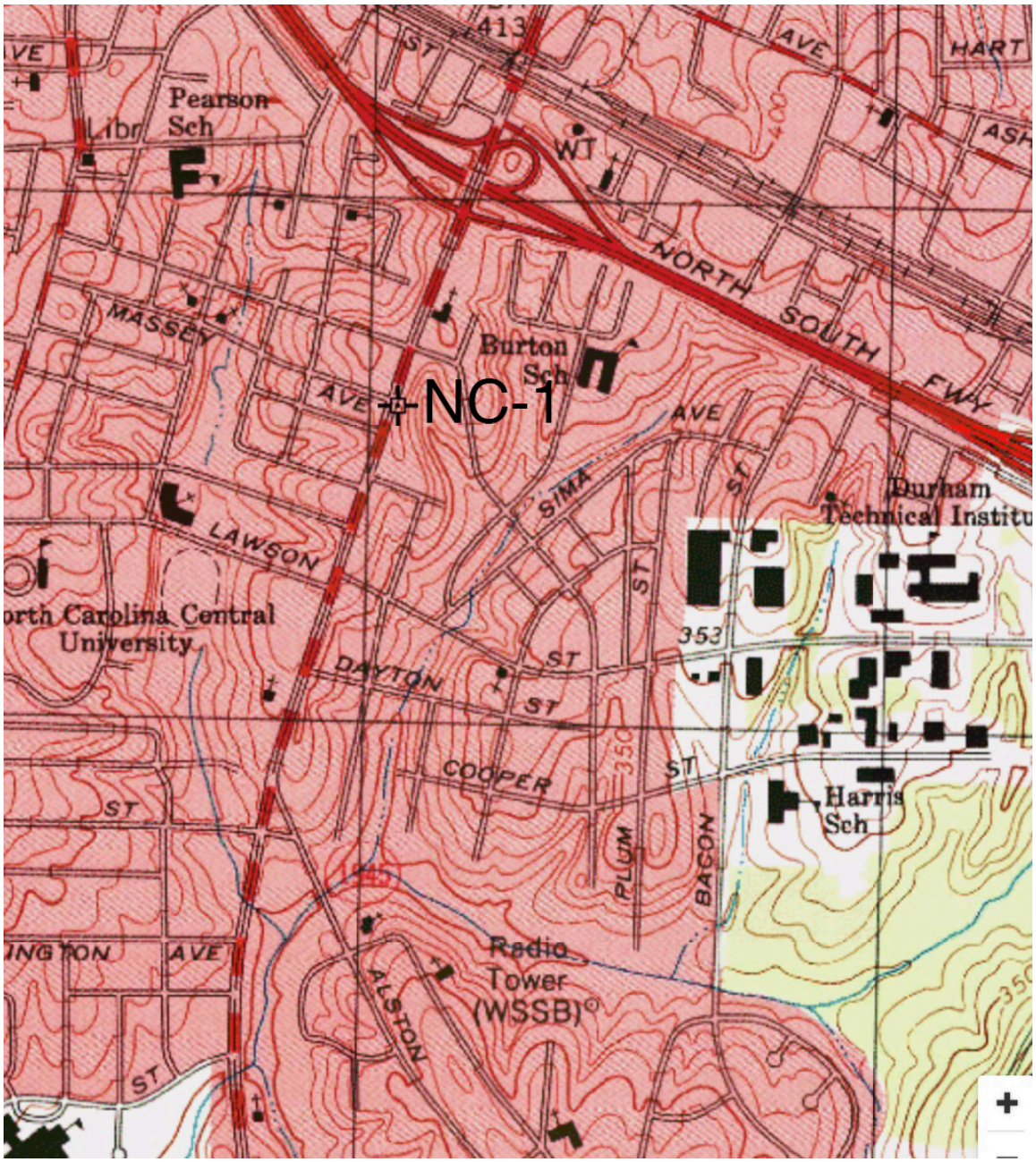
NC-1
Pearson Sch
Libr
WT
NORTH SOUTH FWY
MASSEY AVE
Burton Sch
AVE
SIMA
LAWSON
Durham Technical Institu
orth Carolina Central University
DAYTON ST
ST
COOPER
353
Harris Sch
PLUM
BACON
Radio Tower (WSSB)
ALSTON
AVE
HART
ST